Functional Characterization of Integrated Chemotaxis Pathways and Proteins in the Soil Bacterium, *Azospirillum brasilense*

A Dissertation Presented for the
Doctor of Philosophy
Degree
The University of Tennessee, Knoxville

Jessica Marie Gullett
December 2017

Copyright © 2017 by Jessica M Gullett.
All rights reserved.

DEDICATION

For my nieces, Laura and Rebecca, so that they know anything is possible if they dream big and work hard.

ACKNOWLEDGEMENTS

I cannot even begin to describe how thankful I am to everyone who supported me during my time here at The University of Tennessee. First and foremost, I must thank Dr. Gladys Alexandre, who has shown me endless patience and understanding since my first day in the lab day. She allowed me to take a project and drive it in a direction that interested me, even though it was a new direction for her. Through this, she fostered my scientific creativity and encouraged me to never be afraid to ask questions even if they seem outside my reach. It is not often one gets the privilege of having an advisor also be a mentor, and for this I consider myself lucky.

I must also acknowledge all the members of the Alexandre lab, both past and present, especially Amber Bible, Anastasia Aksenova, and Lindsey O'Neal. We all spent many lunchtimes together throughout the years and these moments together are cherished and will be missed. To the undergraduates who helped me along the way, especially Adam Hubler, I sincerely appreciate your efforts. I feel very fortunate to have several of my undergraduate researchers go above and beyond to help further my projects, and I truly enjoyed our time together.

I am also very fortunate to have a loyal army of Texas friends who have cheered me on through this journey. They have been the recipients of late night phone calls, frantic stress-induced text messages, and have all selflessly lent me an ear when I needed it the most. Thank you all for taking the time to stay connected to me, to encourage me, and to prioritize our friendship even though we are thousands of miles apart. I wouldn't be where I am today without you all.

To my family, where do I even begin? To all my aunts, uncles, cousins, grandparents, and extended family, thank you for your cards, calls, and well-wishes! Mom and Pop, you guys have stood by me even when you had no idea what direction my life was going! Thank you for growing with me and striving to understand what exactly it is that I do! Graduate school and a PhD in Biochemistry certainly wasn't my plan at age seven but it was the right choice for me. This path makes me truly happy. If not for you, I would have missed many holidays and special occasions; you made it possible for me to come home and I am so grateful. To Wes and Ni, thank you for your endless support and understanding. If we totaled up the number of hours we have spent on the phone together discussing life, I am pretty sure we would set some kind of record. These chats have kept me sane and helped me make some tough decisions. Ni, I think we can officially say that not only did I get off the porch but I found the puppy. Most of all, these conversations kept me connected to you all. For this, I am forever indebted to you. One of the hardest things I've ever done was drive away from that small Kansas town, leaving behind a precious little girl who didn't understand. You make me a part of Laura and Rebecca's lives, and I cannot express enough gratitude for this. Now some may laugh but I will also thank the unconditional love I received from my fur baby, Pug Cat. Now, she didn't have a choice to come to graduate school but she made the bad days better and the good days great!

To Will: You have only ever known me as a scientist, meaning you've had plenty of experiences with "science mode", that special time when I transition from normal into a mega-logical, problem-solving, critical thinker who goes a mile a minute. Thank you for accepting that you may be able to take the girl out of the lab, but you can't take the lab out

of the girl! You provide the calm in my life I never knew I needed. Your constant encouragement and faith in me is truly a gift. From the bottom of my heart, I sincerely thank you for teaching me patience and the power of positivity.

This may be a little unusual, but I would also like to thank myself. Seven years ago I took a chance. I left behind everything that was familiar to me and started off in a whole new path in a field that intimidated me. These past seven years have been filled with fear, doubt, and panic at times. They've also shown me that I can do anything I set my mind to; I can rise to any occasion, and I am capable. This experience has taught me to take the big jump even if you don't quite know where you'll land! You just might find out who you really are on the way down.

ABSTRACT

Chemotaxis is the biased movement of cells in a chemical gradient. Most of what we know about chemotaxis comes from work in *Escherichia coli*, which encodes one chemotaxis signaling pathway. However, recent genome sequencing provided evidence that most chemotactic bacteria encode for more than one chemotaxis signaling pathway, but little is known about how these multiple pathways function. In the soil bacterium, *Azospirillum brasilense*, two chemotaxis pathways are used to control motility in response to chemicals. We aim to characterize these pathways and determine whether or not interaction exists between proteins of the two pathways. We find that paralogs of the two chemotaxis pathways can interact to form mixed arrays of signaling clusters. Furthermore, we characterize a specific protein in one of these pathways, CheA1, and find that it is present as two isoforms, unlike canonical CheA proteins. This is made possible by the presence of an additional domain on the N-terminus which is not involved in chemotaxis but instead responsible for a cell length defect in *cheA1* mutants. Characterization of this domain, TMX, reveals that it is present as a single domain protein in Bacteria and Eukarya and predicted to span the membrane seven times. TMX affects the localization of membrane-associated protein, alters membrane properties, and directly controls membrane fluidity in response to temperature shifts. Here, we characterize TMX's role as a universal fluidity sensor in bacteria and point to a possible mechanism of action.

TABLE OF CONTENTS

INTRODUCTION **1**
Bacterial Cellular Membranes **1**
Regulation of the Fatty Acid Biosynthesis (FAB) Pathway **5**
Membrane Response to Abiotic Stressors **6**
Membrane Composition Affects Protein Localization and Function **8**
Membrane Effects on Cellular Behavior **10**
Proteins Involved in Chemotaxis **11**
Chemotaxis in *Azospirillum brasilense* **14**

CHAPTER I Distinct chemotaxis proteins paralogs assemble into chemoreceptor signaling arrays to coordinate signaling output **19**
Abstract **20**
Introduction **21**
Materials and Methods **24**
Strains, Media, and Chemicals 24
Electron Cryotomography 24
Fluorescence Microscopy 26
Western Blot 29
Bacterial Two-Hybrid Assay 30
Results **32**
Cryo-EM Reveals Two Distinct Receptor Arrays in *A. brasilense* 32
Localization of Chemotaxis Proteins Depends on Che1 and Che4 34
Che1 and Che4 Chemotaxis Proteins Interact with Each Other in the Bacterial Two-Hybrid Assay 47
Relative Contribution of CheA4 and CheA1 to Clustering of Chemotaxis Receptors into Polar Arrays 48
Contribution of Che1 and Che4 Proteins, other than CheA Paralogs, in Clustering of Chemotaxis Receptors 56
Discussion **60**

CHAPTER II Distinct domains confer CheA with unique functions in chemotaxis and cell length in *Azospirillum brasilense* SP7 ..... **67**
Abstract **68**
Introduction **69**
Materials and Methods **73**
Strains, Media, and Chemicals 73
Behavioral Assays 73
Mutant Construction 76
Fluorescence Tagging of CheA1 and its Variants 79
Fluorescence Imaging 80
Cell Length Measurements 80
Doubling Time 81
Cell Fractionation 81
Western Blotting 82

Results **85**
Domain Architecture Reveals Unique N-Terminal Fusion to CheA1 85
The Presence of the N-Terminal TMX Domain is Associated with the CheA1-Dependent Cell Length Phenotype but is Dispensable for Chemotaxis 86
CheA1 is Produced as Two Isoforms 94
The CheA1 Isoforms Localize to the Cell Surface and to the Cell Poles 98
Discussion **102**

CHAPTER III TMX: A Universal Regulator of Membrane Fluidity **107**
Abstract **108**
Introduction **108**
Materials and Methods **110**
Membrane Staining 110
Fatty Acid and Phospholipid Analysis 110
DPH Anisotropy 111
Immunolocalization 111
Minimum Inhibitory Concentrations 112
Biofilm Assay 113
Bacterial Two-Hybrid Assay 113
Site-Directed Mutants 116
Results **117**
TMX Affects Membrane Permeability 117
TMX Affects Localization of Membrane Proteins 120
TMX Affects Biofilm Production 120
TMX Involved in Regulating Membrane Fluidity 122
Fluidizing the Membrane Rescues Phenotypes of Δ*tmx*º Mutants 122
Mutating Conserved Residues Affects Membrane Permeability 125
Temperature Provokes Subtle Differences in the Fatty Acid Profiles of Wild Type and the *tmx* Mutant 128
TMX Interacts with FAB Enzymes 135
TMX Site-Directed Mutants Lose Interaction with FAB Enzymes 138
TMX Present in Bacteria and Eukaryotes 138
Discussion **147**

CONCLUSION **154**

REFERENCES **161**

VITA **179**

LIST OF TABLES

Table 1. Names and general functions of enzymes in the fatty acid biosynthesis pathway 2
Table 2. Strains used in chapter 1 25
Table 3. Plasmids used in chapter 1 27
Table 4. Primers used in chapter 1 28
Table 5. Strains and plasmids used in chapter 2 74
cloned into pCR 2.1 TOPO vector (Invitrogen). The putative *cheA1* promoter was 76
Table 6. Primers used in chapter 2 77
Table 7. Strains and plasmids used in chapter 3 114
Table 8. Primers used in chapter 3 115
Table 9. Minimum inhibitory concentrations of antibiotics grown with wild type *E. coli* or the △*tmx*° mutant 119
Table 10. Percentages of fatty acid chains produced by WT *E. coli* and the Δ*tmx*^{o} mutant 132
Table 11. Percentages of long chained fatty acids produced at 28ºC and 37ºC in wild type and Δ*tmx*^{o} in terms of SFAs (top) and UFAs (bottom) 134
Table 12. Percentage of cyclopropane fatty acid produced by wild type and Δ*tmx*^{o} at 28ºC and 37ºC 136
Table 13. Percentages of fatty acids produced by wild type *B. subtilis* and Δ*tmx*$_{bs}$ at 28ºC and 35ºC 143
Table 14. Percentages of C15:0 and C17:0 fatty acids produced by wild type *B. subtilis* (WT) and the mutant, Δ*tmx*$_{bs}$ 144

LIST OF FIGURES

Figure 1. Fatty acid biosynthesis in *E. coli* 3
Figure 2. Effects of temperature on lipid packing 7
Figure 3. Chemotaxis signal transduction in *E. coli* 12
Figure 4. Components of chemotaxis receptor baseplates 13
Figure 5. Domains of CheA in *E. coli* 15
Figure 6. Chemotaxis pathways in *A. brasilense* Sp7 16
Figure 7. Schematic of integration of chemotaxis pathways 18
Figure 8. Schematic representation of BACTH fusions to genes of interest 31
Figure 9. Electron cryotomography of wild type *A. brasilense* 33
Figure 10. Electron cryotomography of *A. brasilense* mutants 35
Figure 11. Localization of CheA1△TMX-YFP and CheA4-YFP in *A. brasilense* 37
Figure 12. Quantification of the localization of cell population of CheA1△TMX-YFP 38
Figure 13. Quantification of fluorescence intensity of CheA1ΔTMX-YFP 39
Figure 14. Quantification of the localization of cell population of CheA4-YFP 41
Figure 15. Quantification of fluorescence intensity of CheA4-YFP 42
Figure 16. Quantification of the localization of cell population of CheY4-YFP 43
Figure 17. Quantification of the localization of cell population of CheW1-YFP 44
Figure 18. Quantification of the localization of cell population of CheW4-YFP 45
Figure 19. Quantification of the localization of cell population of CheY1-YFP 46
Figure 20. BACTH interactions of chemotaxis proteins encoded in the same pathway 49
Figure 21. BACTH interactions of chemotaxis proteins encoded in different pathways 50
Figure 22. Localization of YFP-tagged chemoreceptors in *A. brasilense* 52
Figure 23. Fluorescence intensity of chemoreceptors in *A. brasilense* 53
Figure 24. Distribution of YFP-tagged chemoreceptors in wild type and mutants 54
Figure 25. Analysis of the mislocalization of chemoreceptor clusters in wild type and mutants. 55
Figure 26. Expression levels of YFP-tagged chemoreceptors in mutant backgrounds 57
Figure 27. BACTH of chemotaxis proteins and Tlp1 58
Figure 28. BACTH of chemotaxis proteins and Tlp4a 59
Figure 29. Domain analysis of CheA orthologs in *E. coli* and *A. brasilense* 70
Figure 30. Representation of CheA1 variants constructed for this study 88
Figure 31. Role of CheA1 domains in cell length regulation 89
Figure 32. Expression of CheA1 in *A. brasilense* and mutant derivatives 91
Figure 33. Soft agar assays of chemotaxis domains and swimming speed analysis 93
Figure 34. Western blot of CheA1 whole cell lysates 95
Figure 35. Cell fractionation and western blot analysis of *A. brasilense* Sp7 97
Figure 36. Analysis of fluorescent fusions of CheA1 and variants showing functionality 99
Figure 37. Fluorescence images of CheA1 and its variants in *A. brasilense* 100
Figure 38. Quantification of the localization of the cell population of CheA1 variants 101
Figure 39. Membrane staining of *E. coli* wild type and Δ*tmx^o* mutant cells 118
Figure 40. Immunolocalization of *E. coli* Tsr, CheB, and CheR 121
Figure 41. Biofilm assays of *E. coli* and *B. subtilis* 123
Figure 42. DPH anisotropy of *E. coli* and Δ*tmx^o* mutant bacteria 124
Figure 43. Membrane staining of wild type and Δ*tmx^o* with and without fluidizer 126
Figure 44. Biofilm assay of *E. coli* WT and Δ*tmx^o* with benzyl alcohol 127
Figure 45. Fluorescence intensity of membrane staining of *E. coli* and Δ*tmx^o* site-directed mutants 129
Figure 46. Fatty acid profiles of *E. coli* and the Δ*tmx^o* mutant 131
Figure 47. Percent of total chain lengths of the Δ*tmx^o* mutant relative to wild type 133
Figure 48. BACTH interactions of TMX with FAB enzymes 137
Figure 49. BACTH interactions of TMX mutant (H72F) with FAB enzymes 139
Figure 50. BACTH interactions of TMX mutant (H23F) with FAB enzymes 140
Figure 51. Fatty acid profile of *B. subtilis* and Δ*tmx$_{bs}$* 142

Figure 52. Percent of total chain lengths of the Δ*tmx*$_{bs}$ mutant relative to wild type 145
Figure 53. Percentage of branched chained fatty acids in *B. subtilis* and Δ*tmx*$_{bs}$..... 146
Figure 54. Immunolocalization of *B. subtilis* chemoreceptor McpB 148
Figure 55. Model representation of mixed baseplates of paralogs (top) and an integrated extended receptor array (bottom). 156

INTRODUCTION

Bacterial Cellular Membranes

Bacterial cellular membranes form barriers between the intracellular region of cells and the outside environment. These extremely dynamic structures also function as a medium for numerous chemical reactions (1) as well as a marker for proper protein localization. The major molecules found in membranes are phospholipids (2). In Bacteria and Eukarya, phospholipids consist of two hydrophobic fatty acid chains connected via a glycerol molecule to a hydrophilic polar head group.

To make a membrane, bacteria first synthesize the hydrophobic fatty acid chains, and they do this by utilizing a fatty acid synthesis type II (FAS II) system which contains eight cytosolic enzymes—FabA, B, D, F, G, H, I, and Z (3-7). Their names and functions are listed in Table 1 (Table 1). This system is present in bacteria, plants, parasites (8), and eukaryotic mitochondria (9). The cytoplasm of mammals and some fungi, however, utilize the FAS I system which funnels substrates through one large enzymatic complex to form fatty acids (10). Most of what is known about how bacterial membranes are synthesized comes from the gram-negative bacteria *Escherichia coli*. Fatty acid biosynthesis (FAB) is broken down into three steps: initiation, elongation, and insertion into the membrane (3). The initiation phase requires the beginning substrate, acetyl-coA, which is a product of the glycolytic pathway (Fig. 1) (11, 12), and malonyl-coA which is a product of the reaction of acetyl-coA with the enzyme acetyl-coA carboxylase (AccABCD). Malonyl-coA is then acted upon by FabD (malonyl-CoA:ACP transacylase) to add an Acyl Carrier Protein (ACP) to the malonyl group (3, 13). ACP acts as a tag which indicates that substrate is to

Table 1. Names and general functions of enzymes in the fatty acid biosynthesis pathway

Name		Function
FabA	3-hydroxyacyl-ACP dehydrase	synthesizes first reaction toward unsaturated fatty acids
FabB	3-ketoacyl-ACP synthase	synthesizes unsaturated fatty acids
FabD	malonyl-CoA:ACP transacylase	initiation into fatty acid neogenesis
FabF	3-ketoacyl-ACP synthase	elongation of C16 to C18 fatty acids
FabG	3-ketoacyl-ACP reductase	specific for intermediate chain lengths
FabH	3-ketoacyl-ACP synthase	initiates first cycle of chain elongation
FabI	enoyl-ACP reductase	determines if another round of elongation occurs
FabZ	3-hydroxyacyl-ACP dehydrase	dehydration of 3-hydroxyacyl-ACP intermediates

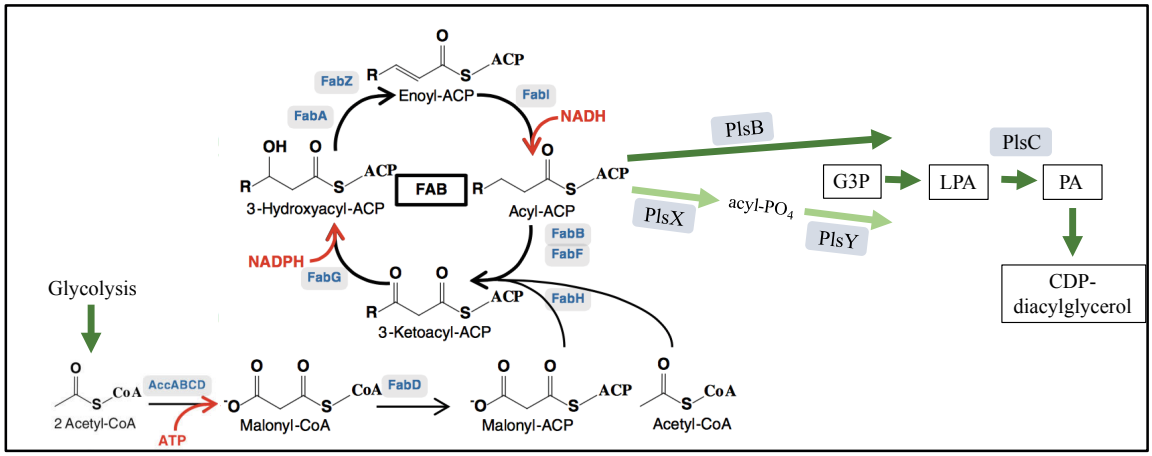

Figure 1. Fatty acid biosynthesis in *E. coli*

Fatty acid biosynthesis (FAB) pathway of *E. coli*. The end product of glycolysis (left) produces the starting product, acetyl-coA, which initiates FAB. The first step is the transformation of acetyl-coA into malonyl-coA via AccABCD. Next, ACP is added to the malonyl moiety via FabD; this produces malonyl-ACP. The growing carbon chain undergoes various modifications by FAB enzymes including condensation (FabH), elongation (FabB or FabF, FabG, FabI, FabZ), dehydration by FabZ, and reduction via FabI. The end product, acyl-ACP can either be put through another round of FAB or inserted into the membrane through either the PlsB or PlsX/PlsY pathway. These enzymes use acyl-ACP and G3P to ultimately form PA which can then produce CDP-diacylglycerol which can be fitted with a phospholipid head group. *Adapted from Cronan and Rock, 2008 and Janßen and Steinbuchel, 2014.*

be utilized in the FAB pathway and therefore is not to be degraded (13). The malonyl-ACP molecule and acetyl-coA are then condensed by FabH (3-ketoacyl-ACP synthase III) which produces acetoacetyl-ACP (Fig. 1) (3). From here, four enzymes—FabB or F, G, I, and Z—elongate the growing carbon chain (3). FabB and FabF are both 3-ketoacyl-ACP synthases and one will act on the acyl-ACP to form 3-ketoacyl-ACP (3). This product is reduced by FabG (3-ketoacyl-ACP reductase), dehydrated by FabZ (3- hydroxyacyl-ACP dehydrase), and further reduced by FabI (enoyl-ACP reductase) to form acyl-ACP (Fig. 1) (3). This product has two fates: either it will be used for another round of elongation or it will be used as a substrate for placement into the phospholipid bilayer. FabI serves a crucial role in the determining which path the acyl-ACP product takes and is, subsequently, the target of many antimicrobials (14). It should be noted that many of these Fab enzymes can perform the same type of reaction, i.e., FabB and FabF both being 3-ketoacyl synthases. However, enzymes such as these have been found to have different substrate specificities (15) and therefore can each independently modify the growing fatty acid chain in different capacities (3). The 3-hydroxydecanoyl-ACP dehydrase, FabA, plays a role in the production of unsaturated fatty acids (UFAs). FabA catalyzes the first dehydration reaction that produces double bonds; however, FabB is necessary to complete the process (3). At the end of elongation and modification, if the acyl-ACP is slated to be put into the membrane, this occurs through interaction of the substrate with either PlsB or the PlsX/PlsYpathway (Fig. 1) (3, 13, 16). In *E. coli* and other alpha- and gamma-proteobacteria, PlsB is the most common route and directly condenses the acyl-ACP with glycerol-3-phosphate (G3P) (3). An alternative pathway for *E. coli* is a two-step process

involving PlsX, which adds a phosphate group, and PlsY, which then condenses it with glycerol-3-phosphate (13, 16, 17). The genes encoding for PlsX and PlsY are conserved and for most bacteria, this is the primary pathway for transferring the acyl group to G3P (3, 16, 17). The product, 1-acyl-G3P (lysophosphatidic acid), is then acetylated via PlsC into phosphatidic acid (PA) (18, 19) which is then converted to the key intermediate in membrane phospholipids, CDP-diacyglycerol (3). In bacteria, most fatty acid chains contain between 12-24 carbons and the polar head groups are usually phosphatidylethanolamine (PE), phosphatidylglycerol (PG), and cardiolipin (CL) (2). The nature of fatty acids and polar head groups vary, conferring the membrane with various biophysical properties.

Regulation of the Fatty Acid Biosynthesis (FAB) Pathway

The FAB pathway is tightly regulated by a variety of mechanisms (20). Perhaps the most well studied form of regulatory control is through transcriptional control of the FAB enzymes through FabR and FadR (13, 21-25) although other forms of regulation exist such as feedback inhibition of intermediate acyl-chains, regulation through the amount of ACP (3), and regulation through the signaling molecule ppGpp which seemingly ties the synthesis of fatty acids to the growth rate of the bacteria (26-28). FabR represses gene expression of the two genes which encode for proteins necessary for synthesizing unsaturated fatty acids, FabA and FabB (3). FadR has a slightly more involved role as it has been shown to both repress and activate genes in the fatty acid synthesis pathway (14, 22-24).

Membrane Response to Abiotic Stressors

Bacteria have evolved the ability to regulate the fatty acid composition of the membrane in response to environmental challenges such as temperature change. They accomplish this through either altering the polar head group attached to the glycerol molecule or through synthesizing lipids with different acyl chain lengths or synthesizing acyl chains with more or less double bonds (29-31). Some studies suggest that changing the hydrophilic head group or changing the length of the acyl chains are not as efficient when a quick response to temperature change is needed (32-34); this leaves controlling the amount of saturated and unsaturated fatty acids as an attractive target for the most efficient control in response to abiotic stressors. Characteristics of the phospholipids alter the membrane fluidity, or the lipid packing order of the phospholipid bilayer (34) which, in turn, allows the cell to adapt to the new environment (35). These characteristics also alter the permeability of the membrane which affects the ability of small molecules to pass into and out of the intracellular space (36). Bilayers which contain few unsaturated fatty acids, can pack closely together and form tight connections while bilayers with numerous unsaturated fatty acids cannot. The double bonds bend the acyl chain and cause neighboring fatty acids to be pushed away (31). As temperature lowers, bacteria increase the amount of unsaturated fatty acids in their membrane, otherwise the membrane will become too rigid (Fig. 2). Conversely, an increase in temperature provokes an increase in saturated fatty acids (31, 37).

In the gram-positive *Bacillus subtilis*, lower temperatures cause the induction of the Des system which is a two-component signaling pathway that encodes a histidine kinase, DesK,

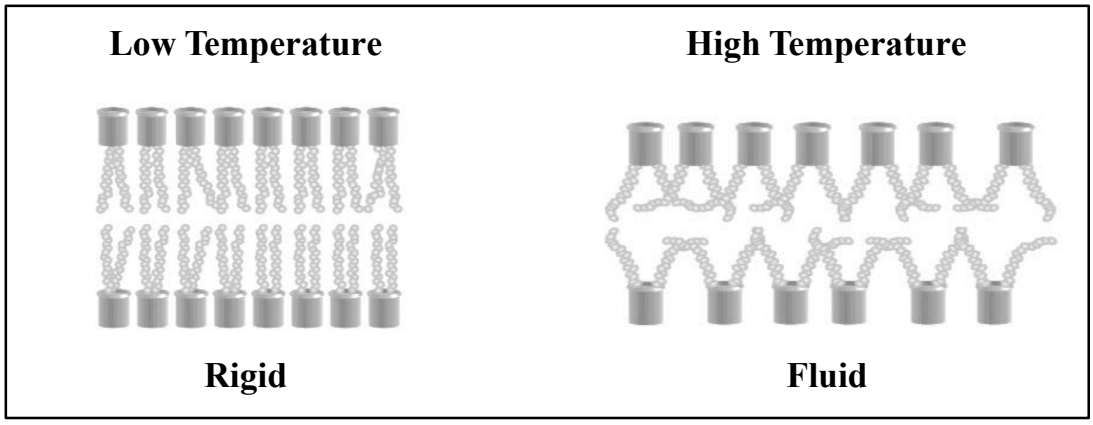

Figure 2. Effects of temperature on lipid packing

Effects of temperature on lipid membrane packing as shown in *E. coli*. As environmental temperature decreases (left), membranes become rigid as shown by an abundance of saturated fatty acids. To combat the increased rigidity that occurs with chilling, bacteria increase the amount of unsaturated fatty acids which increases fluidity. Conversely, at high temperatures the membrane will be fluid and bacteria respond by increasing the amount of saturated fatty acids to decrease the fluidity. *Adapted from Los and Murata, 2004.*

and a response regulator, DesR. The *desK* gene encodes for a desaturase which produces double bonds (38), therefore altering the fluidity of the membrane in response to temperature. Similar systems exist in cyanobacteria (*Synechocystis*), ciliates (*Tetrahymena*), amoeba (*Acanthamoeba*), and fish (39-42). The exact mechanism underlying this response is not well understood but one theory is that the membrane-bound histidine kinase is conformationally altered as the temperature changes and this leads to its autophosphorylation and subsequent phosphotransfer to the response regulator (39). Furthermore, there have been several reports of specific subsets of genes being induced in either colder or warmer temperatures (39, 43). It should also be noted that in *E. coli*, temperature regulates fatty acid biosynthesis as the 3-ketoacyl-ACP synthase, FabF, is temperature-sensitive and is more active at lower temperatures (44, 45). Decreased growth temperatures have also been shown to provoke cells to produce shorter acyl chains (46). Membrane modification is not limited in response to temperature but has been observed in response to changes in pH, osmotic stress, and phosphate starvation (29, 30).

Membrane Composition Affects Protein Localization and Function

Not only does the cellular membrane act as a barrier, it is also the location for several chemical reactions and serves as a marker for protein recruitment. The effect of membrane fluidization of DesK was already mentioned but several other cases of membrane fluidity altering protein function have been noted including in gramicidin channel proteins, a membrane protein which forms a channel that regulates ion permeability (47), in a human neuroblastoma cell line. It is believed that changes in fluidity conformationally change the transmembrane domains of the protein and alter protein function (48). Integral membrane

proteins may be the most affected by changes in the membrane fluidity, but other proteins can be affected as well. For example, there are many cytosolic proteins which utilize specific membrane characteristics to properly localize. Some proteins are attracted to either the concave nature of the membrane or the presence of certain polar elements—such as the anionic phospholipid cardiolipin—which are enriched at the curvature (49). In the Min system in *E. coli*, there is pole-to-pole oscillation of Min proteins which allows for the cell to properly divide in its middle (50). The MinD protein binds at the poles due to its attraction and interaction with specific acidic phospholipids enriched only at the cell poles (51, 52). The binding of MinD to the membrane leads to the recruitment of MinC which is activated only while bound to MinD (50). MinC stops the FtsZ ring from forming and, therefore, cell division from occurring at that site. If MinD cannot bind to the membrane due to changes in its composition, MinC will not accumulate at the cell poles (50). The mislocalization of MinC could disastrously cause FtsZ to localize at the cell poles and form the FtsZ ring in the wrong region of the cell.

Perhaps the most well-known example of membrane-dependent polar localization of proteins involves the chemotaxis signal transduction system and its membrane-bound chemoreceptors. Chemoreceptors cluster into some of the largest networks in bacteria and this clustering and subsequent polar localization is crucial to their function (49). They begin with self-assembly at the division site, which is furthest away from existing clusters, and are pushed to the cell poles. Though there is still some speculation as to how this occurs, recent work has proposed that this push toward the pole is due to interaction of chemoreceptors with the Tol-Pal system (53). This system encodes several proteins, many

of which are embedded in the outer- and inner membrane; they seemingly help the chemoreceptors to localize specifically at the cell poles (53). Though their data show that lipid composition did not affect the ability of chemoreceptors to localize, they only tested chemoreceptor localization in mutants which could either not produce cardiolipin or mutants that could not generate certain anionic phospholipids (53). Testing localization in mutants with altered fatty acid profiles should be performed to more fully investigate this claim. It seems likely that if membrane fluidity were drastically changed, and therefore the lipid packing order, these membrane-bound proteins may undergo conformational changes which alter their ability to function properly and thus localize chemoreceptors.

Membrane Effects on Cellular Behavior

To further understand the important role that cellular membranes have in determining cellular behavior, a closer look can be taken into the chemotaxis system in *E. coli*. It was previously mentioned that membrane-bound chemoreceptors must localize at the cell poles to properly function. In fact, in cells that cannot localize clusters of chemoreceptors to the cell poles, disadvantageous cell behaviors such as increased tumbling and altered cell motility occur (53). Motile bacteria move using runs, linear forward movement, and tumbles, switches in direction. Alternating between runs and tumbles allows a bacterium to be able to stay in a favorable environment or move away from an unfavorable environment. Thus, explaining the dramatic impact that cellular membrane changes have on motility and cell survival. This directed movement of bacteria in chemical gradients is called chemotaxis (54-56).

Proteins Involved in Chemotaxis

Much of what is understood about chemotaxis results from work done in *E. coli*, which possesses a single chemotaxis system (57). When a repellant binds to a membrane-bound chemoreceptor, a conformational change occurs, causing autophosphorylation of the soluble CheA (Fig. 3). Phospho-CheA then promotes changes in swimming direction via phosphotransfer to cytosolic CheY, yielding phospho-CheY with an increased affinity to flagellar motors. Ultimately, the flagellar motor switches the direction of its rotation causing the cell to tumble and change its orientation. The system is reset, causing the tumble to end, through the phosphatase, CheZ (58, 59). Phospho-CheA can also reset chemoreceptors to promote adaptation to background conditions, via phosphotransfer to the CheB methylesterase (Fig. 3) (60, 61). Additionally, receptors can alter their sensitivity through the addition of methyl groups, which are added via CheR. CheR is constitutively expressed and to function appropriately, must localize with receptors; a CheR-docking motif on chemoreceptors has been identified which allows for this interaction (60).

Transmembrane chemoreceptors are present on the inner membrane and organize as a trimer of dimers (Fig. 4) (62-65). At the cytoplasmic tips, chemoreceptors interact with the soluble histidine kinase, CheA, and the adaptor protein CheW, to form a baseplate (63, 66-68). This baseplate, through dimer- and trimerization forms an extended array, which is a series of connected hexagonal baseplates (Fig. 4). This extended array is responsible for signal amplification, which allows cells to respond to concentrations of attractants or repellants anywhere from 10 mM to 3.2 nM (69). All chemoreceptors interact with CheA and CheW through their cytoplasmic tips due to the fact that all chemoreceptors have a

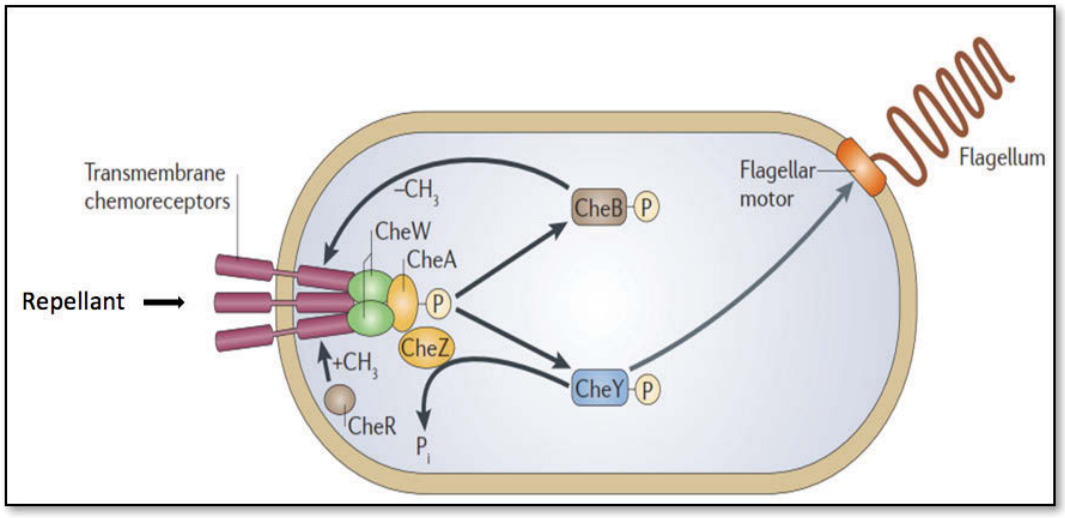

Figure 3. Chemotaxis signal transduction in *E. coli*

Chemotaxis signal transduction as shown in *E. coli*. Upon binding of repellants or a decreasing concentration of attractants, transmembrane chemoreceptors undergo a conformational change which autophosphorylates the histidine kinase, CheA. This prompts a phosphotransfer to CheA's cognate response regulator, CheY. Phosphorylated-CheY then binds to flagellar motor proteins which ultimately causes the motor to switch direction of rotation. This, in turn, causes the bacterium to undergo a "tumble" allowing for a change in swimming direction. The system is then reset via CheZ and the cell ceases to tumble. Also shown, the chemotaxis adaptor protein, CheW, which interacts with CheA at the cytoplasmic tips of chemoreceptors and CheB and CheR which alter the methylation status of receptors, allowing them to alter their sensitivity. *Adapted from Porter et al., 2011.*

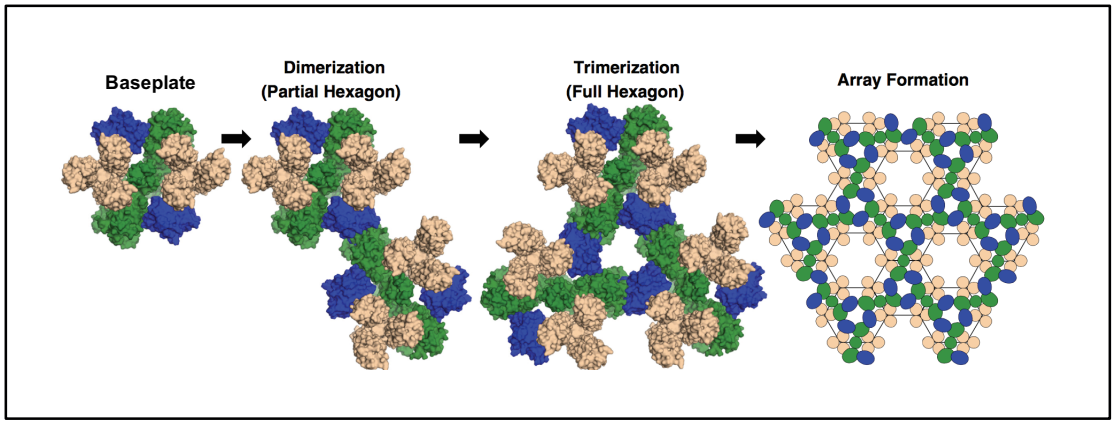

Figure 4. Components of chemotaxis receptor baseplates

Chemoreceptors (tan) form as trimers of dimers and interact at their cytoplasmic tips with CheW (blue) and CheA (green). The baseplate core unit (far left) forms a multimer which ultimately forms a signaling array (far right). This extended array is what propagates the chemotaxis signal up to five orders of magnitude. *Adapted from Falke and Piasta, 2014.*

highly conserved cytoplasmic tip, which is called the cytoplasmic signaling domain (70). Furthest away from the signaling domain is the extracellular ligand-binding domain which is not conserved and allows for the binding of a variety of ligands (71, 72). Also included are an adaptation domain and a HAMP (Histidine kinases, Adenylyl cyclases, Methyl-accepting chemotaxis proteins and Phosphatases) domain which are both located between the extracellular ligand-binding domain and the cytoplasmic signaling domain (73, 74). Chemoreceptors are classified based on length, which can vary due to the amount of heptad repeats—insertions or deletions of seven consecutive amino acids—located in the cytoplasmic portion of receptors (70). Chemoreceptors organize not only as a trimer of dimers but as a trimer of dimers with identical lengths (75).

The soluble histidine kinase, CheA, is the central regulator of chemotaxis. CheA functions as a homodimer, with each monomer containing five domains denoted as P1-P5 (Fig. 5) (68). The ATP-binding domain of CheA (P4) phosphorylates at the conserved histidine residue in the N-terminal phosphorylation domain (P1) (Fig. 5). P2 is a docking site for interaction with CheB and CheY while P3 serves as a dimerization domain. The P5 domain closely resembles and also interacts with the adaptor protein CheW, which couples chemoreceptors to CheA (76).

Chemotaxis in *Azospirillum brasilense*

The complete genome sequences of most motile bacteria indicate the presence of multiple chemotaxis operons, and many of these operons are implicated in the regulation of cellular functions other than flagellar motility (77-82). The alphaproteobacterium *Azospirillum brasilense*'s genome encodes four signal transduction (Che) pathways (Fig. 6) but only two

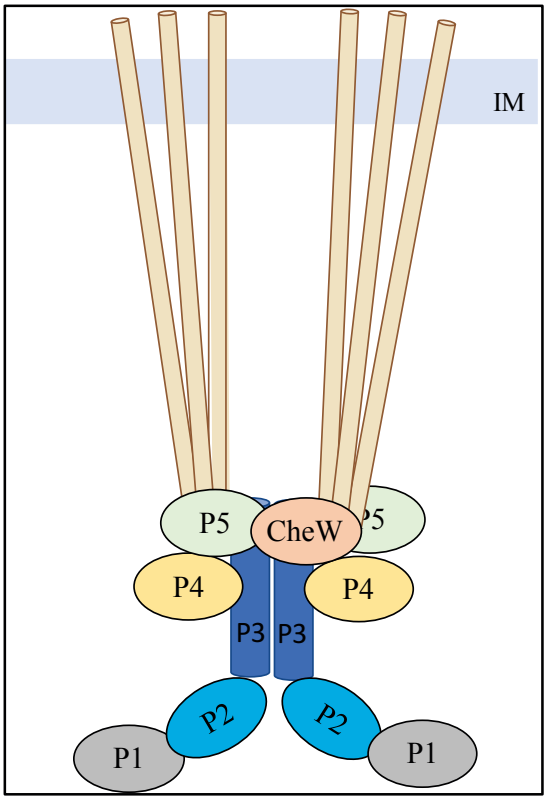

Figure 5. Domains of CheA in *E. coli*

Cartoon schematic of the histidine kinase, CheA, and its multiple domains in *E. coli*. The transmembrane chemoreceptors (tan) extend through the inner membrane (IM) and interact with CheW (orange) and the P5 domains (green) of CheA, which are structurally similar to CheW. The P3 domains (dark blue) are dimerization domains, and the P4 domains (yellow) are the ATP-binding domains. The P2 domains (light blue) are docking sites for CheB and CheY and but are not present in all chemotactic bacteria. The P1 domains (grey) are the phosphorylation domains.

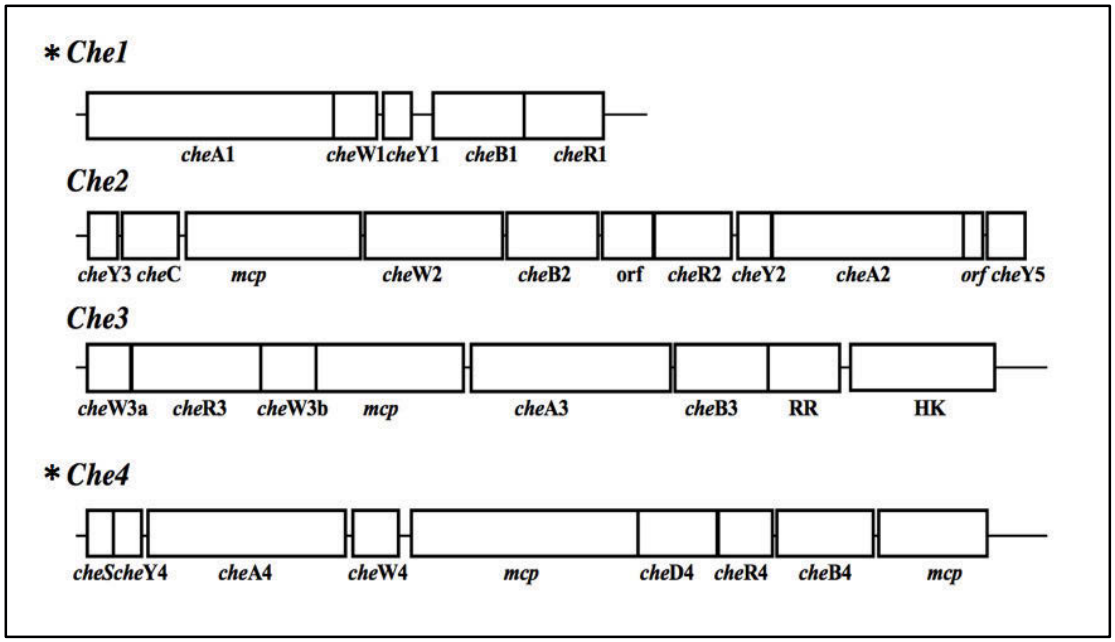

Figure 6. Chemotaxis pathways in *A. brasilense* Sp7

Chemotaxis genes encoded within *A. brasilense* strain Sp7. All genes listed have been characterized by the Alexandre lab or are predicted through homology searches. * denotes pathways that have been experimentally determined to be important in chemotaxis signaling in this strain. *Adapted from Mukherjee et al., 2016.*

of these pathways, Che1 and Che4, regulate chemotaxis (83). The Che4 pathway controls swimming reversal frequency and when deleted, the cells are null for chemotaxis (83). The Che1 pathway controls transient increases in swimming speed and when deleted, the cells are impaired but not null for chemotaxis. Therefore, the Che1 pathway in *A. brasilense* serves a supporting role in chemotaxis. Though it is known that the two pathways, Che1 and Che4, coordinate a single chemotaxis response in *A. brasilense*, it is unknown how the two chemotaxis systems coordinate signaling output to generate the chemotaxis response (Fig. 7). Whether there is any interaction between the proteins of the two pathways has also not been addressed.

Thus, the first project of this dissertation is aimed at understanding if and how two chemotaxis signaling pathways, which both control separate aspects of motility, could coordinate a single chemotaxis response. Another is aimed at characterizing a unique protein within the Che1 chemotaxis pathway in *A. brasilense*. The final project examines a distinct domain, serendipitously found within a protein of the Che1 pathway, and attempts to understand its involvement in the regulating membrane fluidity through interaction with components of the fatty acid biosynthesis pathway.

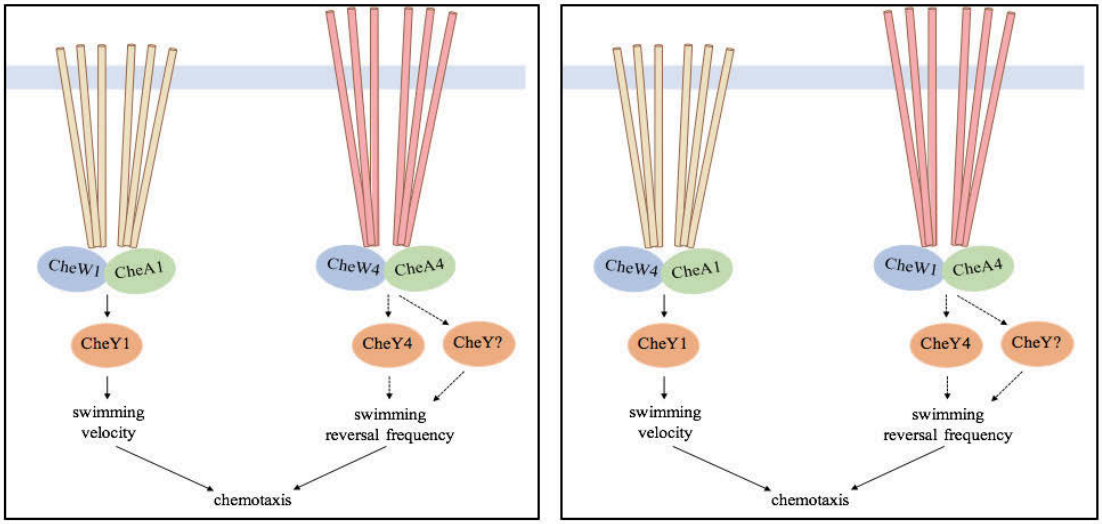

Figure 7. Schematic of integration of chemotaxis pathways

Cartoon demonstrating pathway segregation (left) or pathway interaction (right) of chemotaxis proteins from the Che1 and Che4 signaling pathways in *A. brasilense* strain Sp7. The Che1 pathway controls swimming velocity of cells and the Che4 pathway controls swimming reversal frequency. These two motility parameters are coordinated into a single chemotaxis output. If the two pathways do this without interaction, the proteins encoded in each pathway would only interact with each other and no interaction would exist between paralogs (left panel). If, however, there is interaction of the proteins of the Che1 and Che4 signaling pathways, the proteins of the two pathways may interact with each other (right panel). One such potential interaction is demonstrated here but others may exist.

CHAPTER I
DISTINCT CHEMOTAXIS PROTEINS PARALOGS ASSEMBLE INTO CHEMORECEPTOR SIGNALING ARRAYS TO COORDINATE SIGNALING OUTPUT

Text and figures were taken from the following:

Gullett JM, Aksenova, A, Hubler A, Briegel, A, Kjær, A, Jensen, G, and Alexandre G. 2017. Distinct chemotaxis protein paralogs assemble into chemoreceptor signaling arrays to coordinate signaling output. *Proc Natl Acad of Sci USA*. Manuscript in preparation

Author contributions to this work included: JMG, GA designed research; JMG, AH, AA, AB, AK performed research; JMG, GA, AB analyzed data; JMG, GA, AB wrote the paper.

Abstract

Most chemotactic motile bacteria possess multiple chemotaxis signaling systems, the function of which is typically not fully characterized. Chemotaxis signaling is initiated by chemoreceptors that assemble as large arrays, together with chemotaxis coupling proteins (CheW) and histidine kinase proteins (CheA) which form a baseplate with the cytoplasmic tips of receptors. These arrays, found in the polar regions of bacteria, mediate sensing, signal amplification, and signaling during bacterial chemotaxis responses. Membrane-bound chemoreceptors with different cytoplasmic domain lengths segregate into distinct arrays, as expected for ensuring productive assembly with baseplate proteins. Here, we provide evidence that a bacterium which utilizes two chemotaxis signaling systems, each encoding a complete set of chemotaxis proteins with distinct effects on motility, coordinates its chemotactic responses through the production of two distinct membrane-bound chemoreceptor arrays, each with baseplates comprised of paralogs from the two pathways. Using electron tomography and fluorescence microscopy we show that proper localization of chemotaxis proteins involved in baseplate formation (CheW, CheA) from one chemotaxis system depends on the presence of the proteins from the other chemotaxis system. We also show that the polar localization of membrane-bound chemoreceptors of

different length classes is compromised unless baseplate signaling proteins from both chemotaxis systems are present. Furthermore, chemoreceptors and chemotaxis proteins from each of the chemotaxis signaling system can physically interact with one another, supporting the hypothesis that they mix to form functional chemotaxis signaling baseplates. We propose that integration of chemotaxis signals detected by different chemotaxis systems is facilitated by mixing signaling baseplate proteins into polar chemoreceptor arrays. Given the propensity of chemotaxis systems for horizontal gene transfer, we surmise that this is unlikely a unique mechanism to coordinate signaling from distinct chemotaxis systems.

Introduction

Motile bacteria navigate chemical gradients using chemotaxis to accumulate at locations most favorable for growth. The signal transduction system that controls bacterial chemotaxis has been best characterized in *Escherichia coli* (84). During chemotaxis, chemoreceptors sense and propagate environmental signals via a conserved signal transduction cascade. In *E. coli* chemoreceptors sense changes in concentration gradients and initiate signaling that ultimately affects the direction of rotation of the flagellar motors. In *E. coli*, chemoreceptors are arranged into large clusters at the cell poles (84). Decreased attractant concentration, sensed by chemoreceptors, results in autophosphorylation of the CheA histidine kinase that in turn phosphorylates the CheY response regulator. Phosphorylated CheY interacts with the flagellar motor switch complex causing it to change its direction of rotation. Phosphorylated CheA also phosphorylates the methylesterase, CheB, which then demethylates chemoreceptors and increases their

affinity for attractants. Experimental evidence and mathematical modeling indicate that the stimuli detected by chemoreceptors are greatly amplified at the signaling complex, which indicates that one receptor can interact with multiple histidine kinases (84-86). *E. coli* has five different transmembrane chemoreceptors (84, 87-91) that form mixed clusters and localize to the cell poles along with CheA and CheW proteins to form large patches (85, 92). Cryo-electron microscopy and tomography revealed that these patches are about 250 nm in diameter, localize to the cell poles, and remain mobile within the curvature of the pole while nonpolar patches form at the future division site (63, 64, 92, 93). These patches correspond to hexagonally packed trimers of chemoreceptor dimers linked together by rings of interacting CheA and CheW proteins. These large assemblies of transmembrane chemoreceptors in polar arrays are universal features of chemotaxis found in Bacteria and Archaea. The high degree of cooperativity results from allosteric interactions between chemoreceptors, CheA, and, CheW, and this largely accounts for signal amplification (87). Comparative analysis of the genome sequences of motile bacteria suggested that most species have more than one chemotaxis pathway encoded within their genome and a greater number of receptors (94). Experimental evidence from genetic approaches and cryo-EM analyses also demonstrated that bacteria may express more than one chemoreceptor array segregated into distinct assemblies (62, 63, 65, 75). The C-terminal region of chemoreceptors is conserved and displays an alpha-helical structure. This region mediates the stable assembly of chemoreceptors into trimers of dimers that interact with both CheA and CheW to form the structural unit of the chemotaxis array. Additional comparative sequence analyses identified distinct classes of chemoreceptors that vary in the number of

heptad (H) repeats in the signaling-terminal region (70). This observation strongly suggested that membrane anchored chemoreceptors from different length classes were unlikely to mix within arrays as the length difference would prevent the stable assembly of a CheA-CheW baseplate at the chemoreceptor tips. Further experimental evidence confirmed this assumption and demonstrated that membrane-anchored chemoreceptors of different length classes segregated into distinct chemotaxis signaling arrays (63).

The genome of the nitrogen-fixing soil bacteria, *Azospirillum brasilense*, encodes four chemotaxis (Che) pathways (95). While Che2 and Che3 do not control flagellar motility per se but control other cellular functions ((80); Alexandre lab, unpublished), Che1 and Che4 both affect the pattern of flagellar motility and contribute to the chemotaxis response (83). Signaling output from Che1 modulates transient changes in swimming speed (96), and the signaling output from Che4 controls transient changes in the probability of reversal in the swimming direction (83). Experimental evidence further suggests that the final chemotaxis response of motile *A. brasilense* cells in a gradient depends on coordination of the signaling outputs from both Che1 and Che4 (83, 97, 98). In addition, evidence points to a possible coordination between Che1 and Che4 signaling mediated at the level of chemoreceptor activity (98, 99), but a specific mechanism remains to be elucidated. Here, we characterize the organization of Che1 and Che4 signaling chemotaxis proteins into two chemoreceptor arrays in *A. brasilense* and identify a novel mode of assembly of chemoreceptor arrays components that provides a mechanism for the integration of signaling from Che1 and Che4 into a coordinated output to control chemotaxis.

Materials and Methods

Strains, Media, and Chemicals

The bacterial strains used in this study are listed in Table 2. *A. brasilense* strains were grown on plates at 28°C on minimal media for *A. brasilense* (MMAB) supplemented with 10 mM malate. Liquid cultures were grown by shaking (200 rpm) at 28°C in MMAB supplemented with 10 mM malate and 18.7 mM ammonium chloride. To induce nitrogen fixation, cells were pelleted and washed three times with MMAB (supplemented with 10 mM malate [+C], no nitrogen [-N]), and incubated in 5 mL of MMAB (supplemented with 10 mM malate, no nitrogen) at 28°C without shaking to ensure low aeration for at least 6 hr.

Electron Cryotomography

Azospirillum cultures were grown overnight in 5 mL MMAB + N with 200 μg/mL ampicillin at room temperature without shaking. The culture was spun down for 10 minutes at 3,500 x g, the pellet was resuspended in 5 mL MMAB - N, and spun down again for 10 min at 3,500 g. The pellet was then resuspended in 5 mL MMAB - N with 200 μg/mL ampicillin and left at room temperature (on bench), without shaking, overnight. Cells were prepared on EM grids as described previously (65). Images were collected on either a G2 300 keV filed emission gun microscope or TITAN Krios microscope with lens aberration correction (both FEI company, now part of Thermo Fischer Scientific). Both microscopes were equipped with a GATAN K2 summit counting electron-detector cameras and GATAN imaging filters. Data were collected using the UCSFtomo software, using a cumulative dose of ~ 160 e/A2. Tomograms were constructed either automatically using

Table 2. Strains used in chapter 1

Strains	Relevant Characteristics	Source
Top10	General cloning strain	Invitrogen
BTH101	F$^-$ *cya-99 araD139 galE15 galK16 rpsL1 hsdR2 mcrA1 mcrB1*	Karimova *et al*., 1998 (100)
XL-1 Blue	*recA1 endA1 gyrA96 thi-1 hsdR17 supE44 relA1 lac* [F′ *proAB lacIq Z*Δ*M15* Tn*10* (Tet^r)].	Agilent Technologies
S17.1	*thi endA recA hsdR* with RP4-2Tc::Mu-Km::Tn*7* integrated in chromosome	Simon *et al.,* 1983 (101)

RAPTOR (102), a program embedded in the Jensen lab pipeline and database (103) (47) or imod software package (104).

Fluorescence Microscopy

Gateway cloning (Invitrogen) and the pRH005 vector were used to construct all yellow fluorescence protein (YFP) fusions (105). The pRH005 vector allows cloning of any gene to generate products fused in-frame with YFP at their C-terminus. Most YFP strains used in this study were previously generated in the Alexandre lab (Table 3) (99, 106, 107) using Gateway technology and adhering to manufacturer's protocol. Briefly, genes of interest were amplified using specific Gateway primers (Table 4) and *A. brasilense* strain Sp7 genomic DNA. Five microliters of PCR products were ran on a 0.8% gel for verification of insert and PCR clean-up (Macherey Negel) was performed on the remainder of the PCR product. Resulting PCR products underwent a BP Clonase (Invitrogen) reaction with the pDONR2.1 vector (Invitrogen). Then, this reaction was transformed into Top10 chemically competent cells and plated on LB with kanamycin (50 μg/mL). Colonies from these plates were grown in 5 mL of LB with kanamycin (50 μg/mL), plasmid prepped (Qiagen) and resulting plasmids underwent an LR Reaction (Invitrogen) with the pRH005 plasmid. Resulting reactions were transformed into Top10 competent cells and plated on LB with kanamycin (50 μg/mL). All constructs were grown up in LB with kanamycin, plasmid prepped, and introduced into Sp7 and other strains (Table 2) by biparental mating as described in Hauwaerts *et al*., 2002 (108). One mL of cells grown as described above were pelleted at 5,000 rpm for 2 min. Twenty μL of the pelleted cells were resuspended in MMAB and mounted on a glass slide containing a 100 μL agarose pad (1% LMP agarose

Table 3. Plasmids used in chapter 1

Plasmids	Genotype or relevant characteristics	Reference/source
TOPO 2.1	PCR cloning vector, Km	Invitrogen
pRH005	Gateway-based destination vector expressing proteins fused with YFP at the C-terminus; Km, Cm	Hallez *et al.,* 2007 (105)
pRHTlp1	pRH005 containing a *tlp1* promoter region and ORF; Km, Cm	Russell et al., 2013 (99)
pRHTlp4a	pRH005 containing a *tlp4a* promoter region and ORF; Km, Cm	Alexandre lab, unpublished
pUT18	Derivative of pUC19 plasmid encoding T18 of CyA, Cb	Karimova *et al.,* 1998 (100)
pKNT25	Derivative of pSU40 plasmid encoding T25 of CyA, Km	Karimova *et al.,* 1998 (100)
pUT18C-zip	a derivative of pUT18C in which the leucine zipper of GCN4 is genetically fused in frame to the T18 fragment, Cb	Karimova *et al.,* 1998 (100)
pKT25-zip	a derivative of pKT25 in which the leucine zipper of GCN4 is genetically fused in frame to the T25 fragment, Km	Karimova *et al*., 1998 (100)
pUT18cheA4	pUT18 containing *cheA4*, Cb	Alexandre lab, unpublished
pUT18cheW4	pUT18 containing *cheW4*, Cb	Alexandre lab, unpublished
pUT18tlp1	pUT18 containing *tlp1*, Cb	Alexandre lab, unpublished
pUT18tlp4a	pUT18 containing *tlp4a*, Cb	Alexandre lab, unpublished
pUT18cheA1	pUT18 containing *cheA1*, Cb	Alexandre lab, unpublished
pUT18cheW1	pUT18 containing *cheW1*, Cb	Alexandre lab, unpublished
pKNT25cheA4	pKNT25 containing *cheA4*, Km	Alexandre lab, unpublished
pKNT25cheW4	pKNT25 containing *cheW4*, Km	Alexandre lab, unpublished
pKNT25tlp1	pKNT25 containing *tlp1*, Km	Alexandre lab, unpublished
pKNT25tlp4a	pKNT25 containing *tlp4a*, Km	Alexandre lab, unpublished
pKNT25cheA1	pKNT25 containing *cheA1*, Km	Alexandre lab, unpublished
pKNT25cheW1	pKNT25 containing *cheW1*, Km	Alexandre lab, unpublished

Table 4. Primers used in chapter 1

Primer name	Sequence
CheA4 HindIII For BACTH	5’ - AAG CTT ATG GAC GGG GTG CGC AAC AC - 3’
CheA4 EcoRI Rev BACTH	5’ - GAA TTC GAC CGG TTC GAG TGC GGG GGC - 3’
Tlp4a HindIII For BACTH	5’ - AAG CTT ATG GCG AAA GGG GTC GGT TCG - 3’
Tlp4a EcoRI Rev BACTH	5’ - GAA TTC TGC CGC CCG TCC GCG GGC CAG - 3’
CheW4 HindIII For BACTH	5’ - AAG CTT ATG AGC AGT TCCACCGCGCTC - 3’
CheW4 EcoRI Rev BACTH	5’ - GAA TTC GGA TGC CCG CTC CAG CGC CGG - 3’
Tlp1 HindIII For BACTH	5’ - AAG CTT ATG AAT CCC CTC CGC ACG TTC - 3’
Tlp1 EcoRI Rev BACTH	5’ - GAA TTC GGC GAC CGC CGG AAG CGG GTG - 3’
CheW1 HindIII For BACTH	5’ - GC AAG CTTG ATG AGC AAC GCC AAG CTG - 3’
CheW1 EcoRI Rev BACTH	5’ - GC GAA TTCG GGC CGC TTC CAT CGT GGT - 3’
CheA1ΔTMX HindIII For BACTH	5’ - GC AAG CTTA GAC CGC CTG CCC TAC AAC - 3’
CheA1ΔTMX KpnI Rev BACTH	5’ - GC GGT ACC TGC GGC ACC TTT CTG CTC - 3’
Tlp4aRevEcoRIpkNT25	5’ - CACT GAATTC TGC CGC CCG TCC GCG GGA CAG - 3’

in 1X PBS buffer – NaCl 8g/L, KCl 0.2 g/L, KH_2PO4 0.24 g/L, Na_2HPO_4 0.144 g/L, pH 7.0) and covered with a cover slip. Cells were left undisturbed for 2 hr, or in some instances overnight, before being imaged. Images were captured using a Nikon ECLIPSE 80i fluorescence microscope equipped with a Nikon CoolSnap HQ2 cooled CCD camera. Fluorescence intensity was quantified using the Nikon NIS-Elements BR program (Nikon) by calculating the ratio of average fluorescence intensity in the polar foci compared to the cell body. The cell lengths and the distances from the pole to the fluorescent foci were measured using the straight line tool in ImageJ software. Measurements were taken from at least 80 cells from three independent cultures, and five fields of view were used for each sample. The results were graphed and analyzed statistically using GraphPad Prism software.

Western Blot

Cells were harvested and washed once with 1X PBS and resuspended in 0.2 mL of RIPA buffer (50 mM Tris-HCl, 150 mM NaCl, 1% Triton X-100, 0.1% SDS, 1mM PMSF, pH 8.0). Cells were lysed using sonication (5 cycles of 30 sec sonication followed by 1 min rest periods). Cell debris was removed by centrifugation at 20,800 × g for 10 min at 4°C. Protein concentrations were determined by the Bradford method (109). A cell lysate (10 µg of protein) was run in a 12% SDS- polyacrylamide gel and transferred to a 45 µm nitrocellulose membrane (Bio-Rad) using a semi-dry transfer apparatus. Transfers ran at 15V for 25 min. Immunoblots were carried out with an anti-GFP antibody (a gift from R. Goodchild) at a 1: 1,000 dilution in 1% nonfat dry milk in 1X TBST. The membrane was incubated overnight at room temperature before being washed three times in 1X TBST.

The membrane was then incubated with HRP-conjugated goat anti-rabbit antibody (ImmunoReagents, Inc.) at a 1: 5,000 dilution for 1 hr at room temperature. After washing three times in 1X TTBS, the membrane was incubated with Luminata Forte Western HRP Substrate (Millipore) for 2 min and exposed to X-ray film for 1 min.

Bacterial Two-Hybrid Assay

A bacterial two-hybrid assay specific for membrane proteins was used to investigate protein-protein interactions. Proteins of interest (CheA1, CheA4, CheW1, CheW4, Tlp1, and Tlp4a) were fused on the C-terminus of the T18 and T25 domains of *Bordetella pertussis* adenylate cyclase present in vectors pUT18 and pKNT25 (Fig. 8), respectively, as described by the manufacturer's protocol (Euromedex). The genes of interest were first PCR-amplified (Tables 3-4) and cloned into a TOPO 2.1 vector (Invitrogen). The resulting vectors were digested with the following enzyme pairs (HindIII and EcoRI for *cheA4*, *cheW1*, *cheW4*, *tlp1*, and *tlp4a*; HindIII and KpnI for *cheA1*) and ligated into their destination vectors (high copy pUT18 and low copy pKNT25) that were previously digested with the same enzymes using T4 ligation (New England Bio Labs). Resulting plasmids were propagated in XL-1 Blue cells (Agilent Technologies), and the presence of an insert was confirmed by colony PCR. To test for protein-protein interactions, two plasmids expressing genes of interest were co-transformed into BTH101 competent cells and plated on Luria Broth (LB) plates with kanamycin (50 μg/mL) and carbenicillin (50 μg/mL). The plates were incubated for 48 hr at 30°C. Several colonies were picked from a plate, inoculated into 5 mL of liquid LB with kanamycin and carbenicillin (50 μg/ mL of each), and shaken (200 rpm) at 30°C. Two microliters of the overnight cultures were

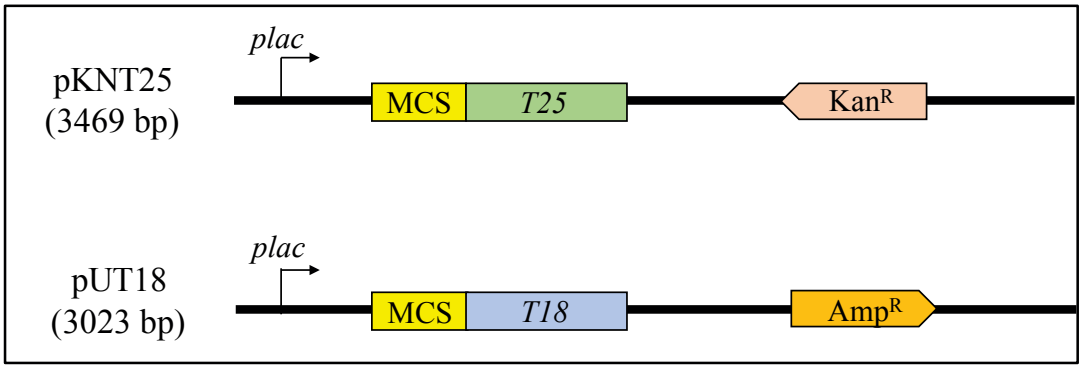

Figure 8. Schematic representation of BACTH fusions to genes of interest

Genes of interest were cloned into either pKNT25 (low copy) or pUT18 (high copy) vectors. These vectors use a *plac* promoter and encode one half of a catalytic domain (T18 or T25) of the *Bordetella pertussis* adenylate cyclase. The presence of the multiple cloning site (MCS) before the T18 or T25 catalytic domains ensures that the resulting protein is fused at its C-terminus to either the T18 or T25 domain. Also shown are the antibiotic resistances encoded for by each vector: pKNT25 having kanamycin resistance (50 µg/mL), pUT18 having ampicillin or carbenicillin resistance (100 µg/mL). *Adapted from Euromedex manual.*

spotted onto MacConkey plates with lactose as a carbon source and incubated at 30°C for up to 96 hr. The pUT18-zip and pKT25-zip vectors were used as positive controls and the empty vectors (pUT18 and pKNT25) were used as negative controls (100). For quantification of interactions, cells were grown in 5 mL liquid LB with kanamycin and carbenicillin (50 μg/mL of each) at 30°C while shaking at 200 rpm until they reached an OD_{600} of 0.5 - 0.6. A beta galactosidase assay was then performed as described in Ramsay, *et al* (110).

Results

Cryo-EM Reveals Two Distinct Receptor Arrays in A. brasilense

The *A. brasilense* genome encodes over 40 predicted chemoreceptors, from at least three different length classes (70) but the organization of the chemoreceptors contributing to chemotaxis within the cells has not been characterized. We used electron tomography (cryo-EM) to characterize the chemoreceptor arrays formed by interaction with Che1 or Che4 signaling proteins. Because chemoreceptor arrays do not assemble as organized clusters in cells lacking CheA or CheW in *E. coli* (111), we hypothesized that we could identify Che1- and Che-4 associated arrays using a combination of wild type strain, Δ*che1,* Δ*che4, and* Δ*che1*Δ*che4* mutant derivatives. In order to image *A. brasilense* cells by electron tomography, cells were grown under specific conditions to ensure cells were thin enough for imaging. In wild type cells, two structurally distinct types of chemoreceptor arrays were observed: out of 15 cell poles imaged, we found 7 short chemoreceptor clusters (28 nm) and 4 tall arrays (31 nm), as measured by the distance between the inner membrane and the base plate (Fig. 9). Top views of the chemoreceptor arrays (Fig. 9, power spectrum

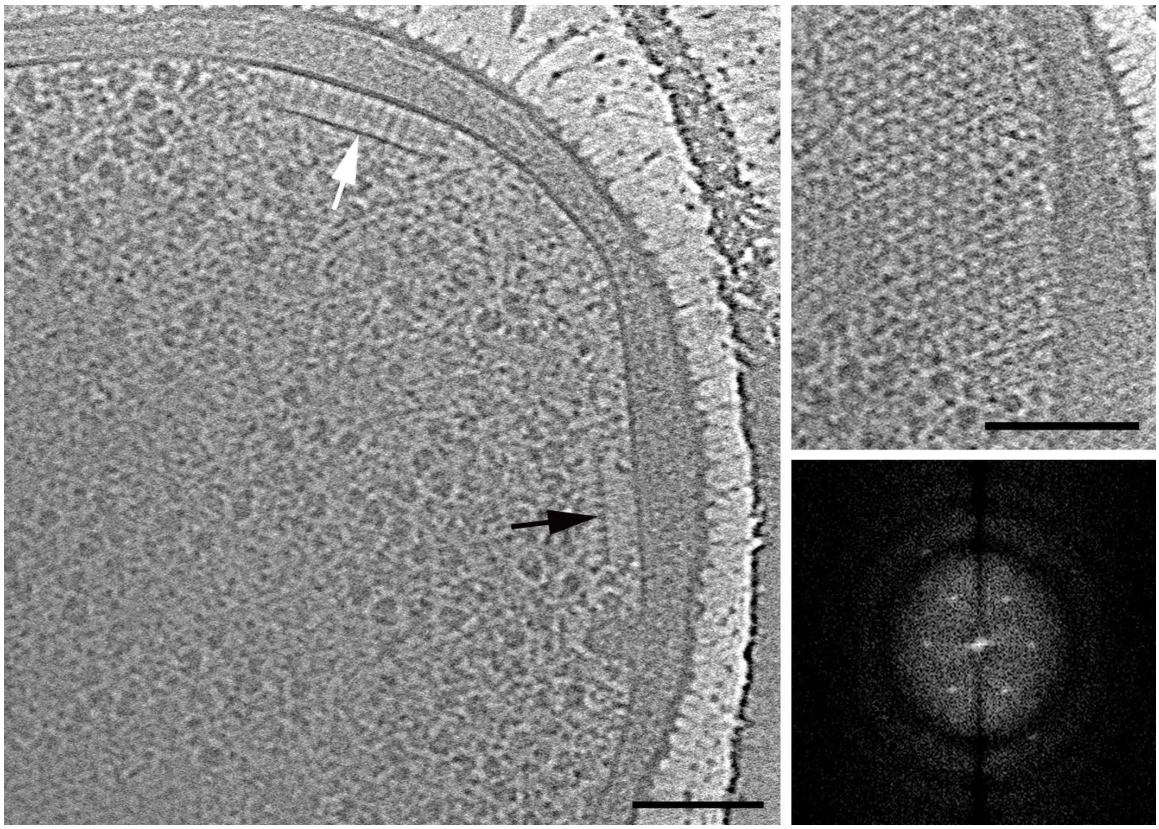

Figure 9. Electron cryotomography of wild type *A. brasilense*

Electron cryotomography of wild type *A. brasilense*. Left: Slice through a cell showing side views of both tall (white arrow) and short array (black arrow). Top right: top view. Scale bars: 100 nm Bottom right: power spectrum from top view of the array (not to scale).

(not to scale)) revealed the typical, highly ordered hexagonal packing with a 12 nm spacing between the neighboring hexagons. Tomography of cells lacking operon 1 (Δ*che1*) or operon 4 (Δ*che4*) revealed that both tall and short arrays could still be observed in both strains (Fig. 10, left). Eighteen cell poles of Δ*che4* cells still contained 14 short and 5 tall arrays. In Δ*che1* we observed 18 short and 6 tall arrays out of 24 cell poles. In contrast, neither short nor tall arrays could be observed in the Δ*che1*Δ*che4* mutant (20 cells imaged). At this point, we have not observed clusters that we can assign to the remaining Che operons, Che2 and Che3 suggesting they are either not expressed or simply not observed. Surprisingly, lack of Che1 or Che4 proteins alone still yielded cells capable of producing two membrane-anchored arrays. Only a strain lacking both Che1 and Che4 *(*Δ*che1*Δ*che4* mutant) lacked both arrays (Fig. 10, right). This result indicates that the two membrane-bound arrays detected by cryo-EM correspond to Che1- and Che4-dependent chemoreceptor arrays. Though not proven, the simplest interpretation is that chemoreceptors could utilize chemotaxis proteins belonging to either Che1 or Che4 to assemble extended arrays.

Localization of Chemotaxis Proteins Depends on Che1 and Che4

The results of the cryo-EM analyses suggested two possibilities for the arrays in wild type cells: first, each of the chemoreceptor arrays could be "pure" - comprised of either Che1 or Che4 proteins, with one chemotaxis system compensating for the absence of another in the deletion mutants or, second, each of the chemoreceptor arrays could contain a mixture of Che1 and Che4 proteins. To address these possibilities, we analyzed the ability of Che1 and Che4 proteins to localize to chemoreceptor clusters by using fusions of chemotaxis

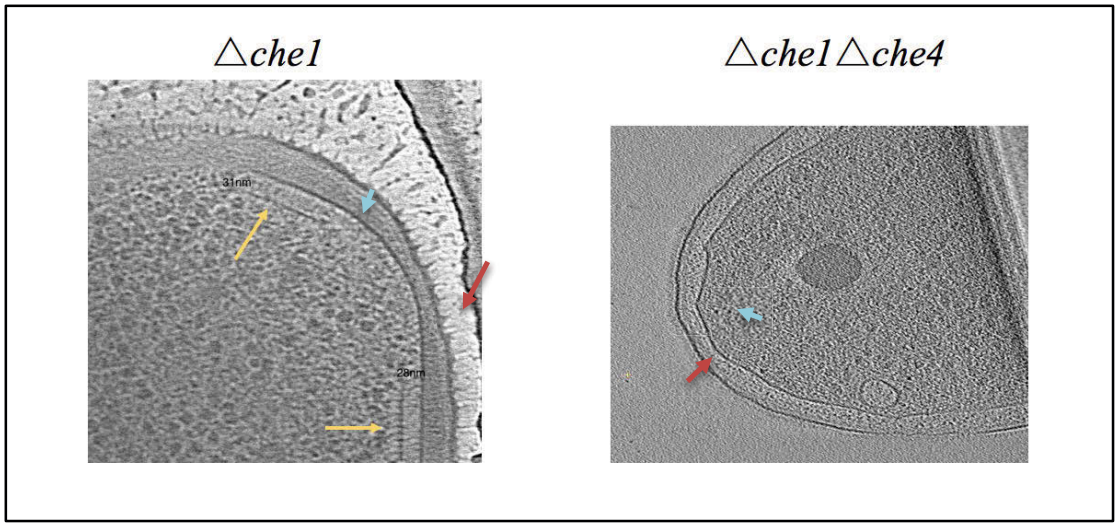

Figure 10. Electron cryotomography of *A. brasilense* mutants

Electron cryotomography of the Δ*che1* (left) and Δ*che1*Δ*che4* (right) mutant derivatives of *A. brasilense* Sp7. Red arrows denote the outer membrane of the cells while blue arrows denote the inner membrane. Left: Yellow arrows point to two membrane-bound chemoreceptor clusters measuring 28 nm and 31 nm. Right: No clusters were present in the double mutant.

proteins of the Che1 and Che4 signal pathways (CheA1ΔTMX, CheA4, CheW4, CheY4) to yellow fluorescent protein (YFP) tags and imaged each in wild type, Δ*che1*, Δ*che4*, and Δ*che1*Δ*che4* mutant backgrounds. The functionality of all tagged proteins was verified through chemotaxis soft agar assays before imaging (112). We used a fusion of the CheA1ΔTMX isoform to the YFP tag since the strain of *A. brasilense* (Sp7) we are using contains two CheA1 isoforms and only the CheA1ΔTMX isoform is indispensable for chemotaxis; it is also functional with a C-terminal YFP tag (112). In the wild type background, CheA1ΔTMX-YFP localized as bright foci to the cell poles as well as throughout the cell surface (Figs. 11-12). In the Δ*che1* and Δ*che4* backgrounds, CheA1ΔTMX-YFP localized to the cell poles. In the Δ*che1*Δ*che4* background, cells were diffuse and no distinct fluorescent foci were detected (Figs. 11-12). Fluorescence intensity of CheA1ΔTMX-YFP foci showed increased fluorescence in the Δ*che1* and in the Δ*che4* strain background but it decreased in the Δ*che1*Δ*che4* background, as compared to the intensity measured in the wild type (Fig. 13). We note that in the wild type strain, there are two isoforms of CheA1 that include polarly-localized CheA1ΔTMX and membrane-bound surface localized full length CheA1, with each isoform able to recruit CheA1ΔTMX-YFP by dimerization (112). Given the localization of CheA1ΔTMX-YFP at the poles and within the cell surface of wild type cells, we hypothesize that the increased fluorescence of polar foci in the Δ*che1* mutant and in the Δ*che4* mutant result from the absence of full length membrane-bound CheA1, permitting all available CheA1ΔTMX-YFP expressed in the cell to localize as polar clusters in the Δ*che1* mutant. In the Δ*che4* mutant as well as in the Δ*che1* mutant, we hypothesize that it is the reduced clustering caused by the lack of Che4

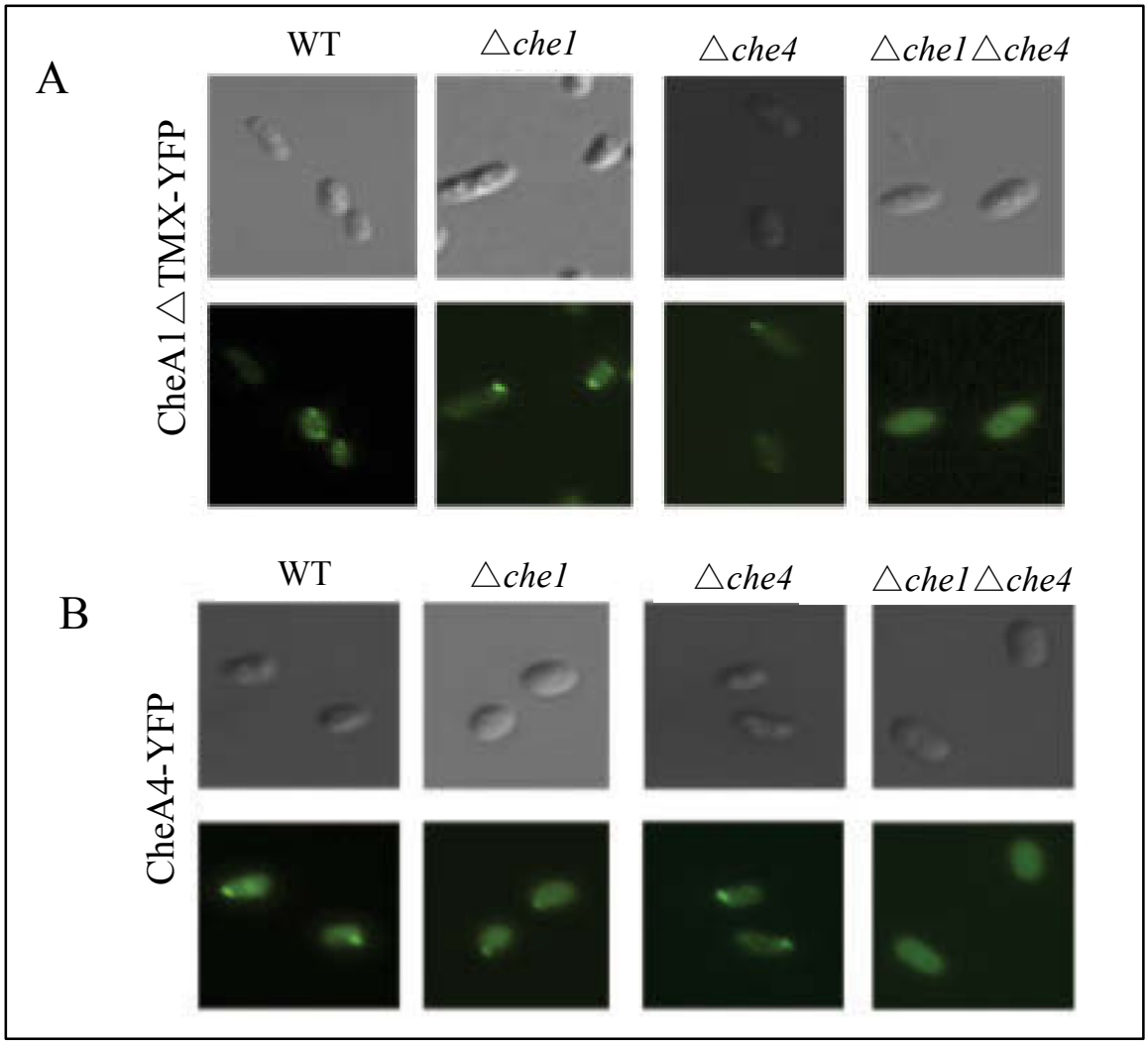

Figure 11. Localization of CheA1△TMX-YFP and CheA4-YFP in *A. brasilense*

Localization of YFP-tagged CheA1△TMX (Panel A) and CheA4 (Panel B) in wild type (Sp7) and mutant derivative backgrounds.

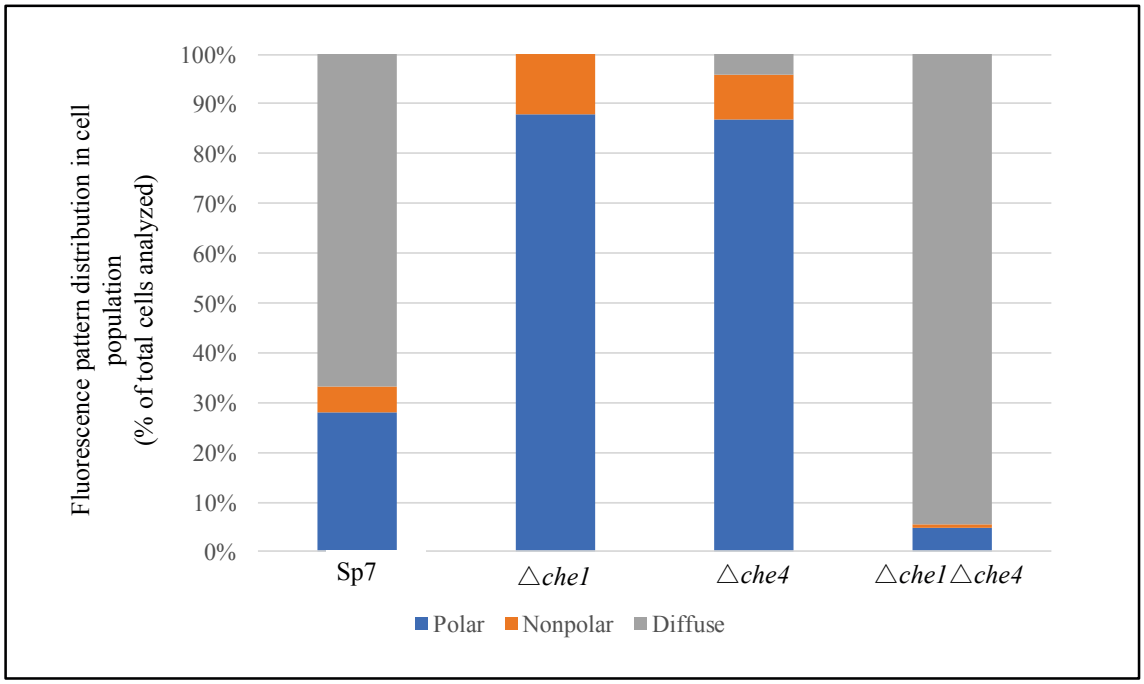

Figure 12. Quantification of the localization of cell population of CheA1△TMX-YFP

Quantitation of the distribution of fluorescence in the population of CheA1△TMX-YFP cells analyzed in wild type (Sp7) and mutant derivative backgrounds. N ≥ 50 cells for each.

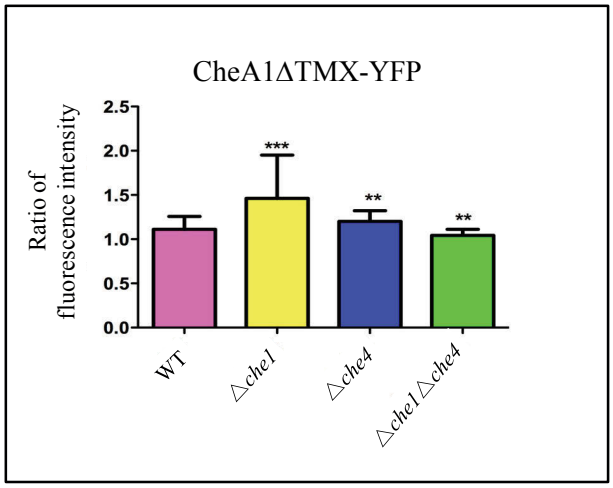

Figure 13. Quantification of fluorescence intensity of CheA1ΔTMX-YFP

Quantification of the fluorescence intensity of foci in CheA1ΔTMX-YFP in wild type and mutant backgrounds. Results were quantified by measuring the ratio of fluorescence intensity in the foci relative to the fluorescence of the rest of the cell body. Significant values are compared to the wild type background. *, **, *** indicate a p value < 0.05, 0.01, 0.001, respectively.

(Δ*che4*) or Che1 (Δ*che1*) proteins in these mutants that leads to a redistribution of the pool of soluble CheA1ΔTMX-YFP so that larger overall fluorescent foci are detected.

CheA4-YFP localized exclusively as polar foci in the wild type, Δ*che1*, and Δ*che4* mutant strains and was diffuse in the Δ*che1*Δ*che4* strain background (Figs. 11,14). Fluorescence intensity of CheA4-YFP foci showed similar values for the wild type and Δ*che4* while fluorescence intensity decreased in Δ*che1* and Δ*che1*Δ*che4* (Fig. 15). These data suggest that the ability of chemotaxis proteins to localize and form polar clusters seen as fluorescent foci when using tagged proteins may depend on the presence of proteins from either Che1 or Che4. We did not see an increase in polar fluorescence intensity with CheA4-YFP in either of the strain backgrounds, weakening the argument that Che1 or Che4 proteins are able to compensate for one another in the Δ*che1* and Δ*che4* backgrounds and rather supporting that both Che1 and Che4 proteins occupy both chemoreceptor arrays. Similar observations about fluorescent foci formation were made using a YFP fusion to CheY4 (CheY4-YFP), which functions downstream of CheA4 (83) and to the adaptor proteins, CheW1 or CheW4, which are encoded within the Che1 or Che4 pathways, respectively (CheW1-YFP and CheW4-YFP). These proteins localized to the cell poles in wild type, Δ*che1*, Δ*che4* backgrounds but were diffuse in the Δ*che1*Δ*che4* mutant background (Figs. 16-18). A CheY1-YFP fusion is diffuse since CheY1-YFP will interact with the two isoforms of CheA1—a polarly localized CheA1ΔTMX and a membrane-bound CheA1—therefore producing a different distribution pattern of foci as compared to other chemotaxis proteins (Fig. 19).

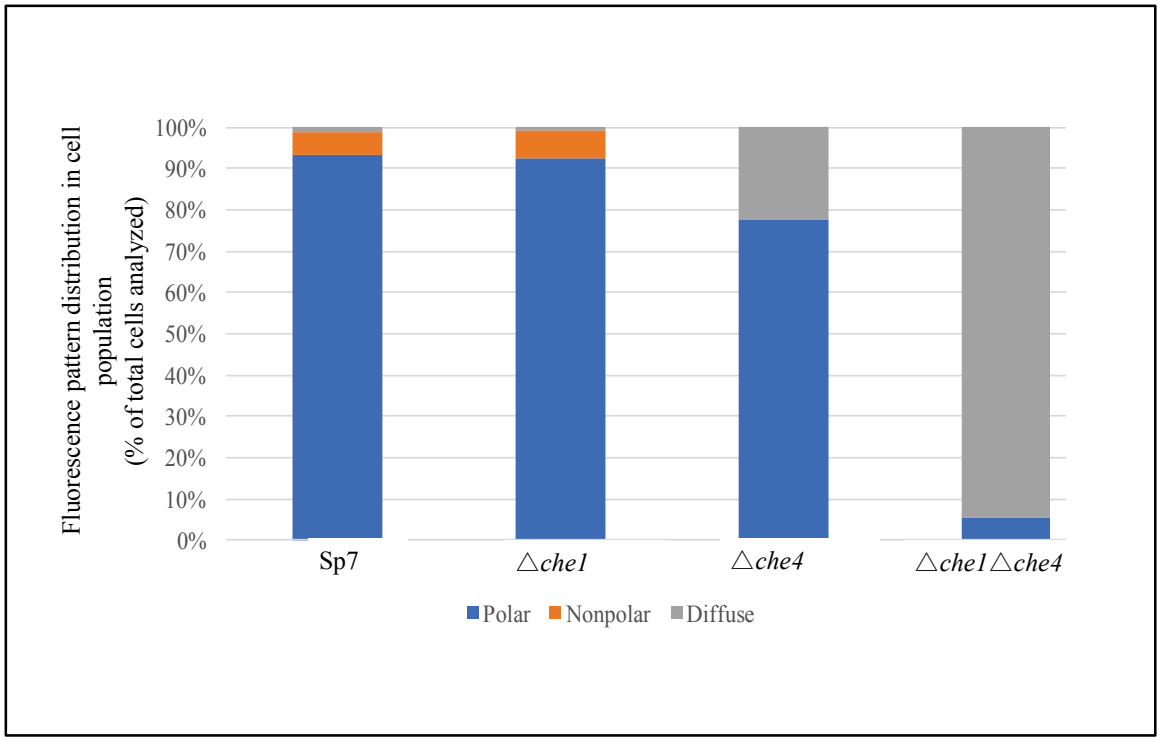

Figure 14. Quantification of the localization of cell population of CheA4-YFP

Quantification of the distribution of fluorescence in the population of CheA4-YFP cells analyzed in wild type (Sp7) and mutant derivative backgrounds. N ≥ 30 cells for each bar.

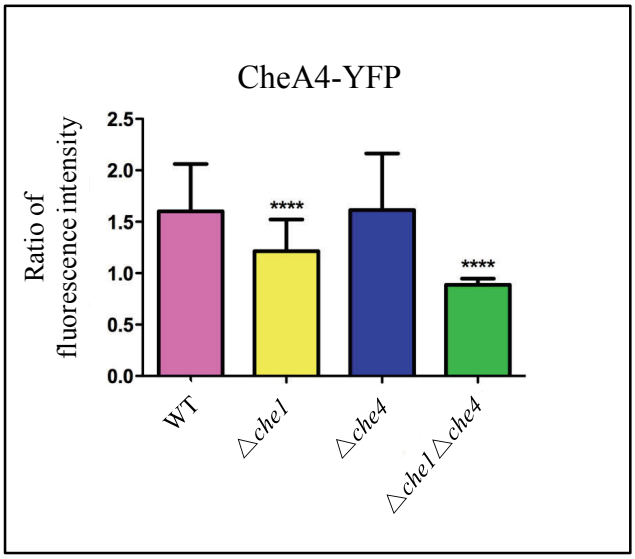

Figure 15. Quantification of fluorescence intensity of CheA4-YFP

Quantification of the fluorescence intensity of foci in CheA4-YFP in wild type and mutant backgrounds. Results were quantified by measuring the ratio of fluorescence intensity in the foci relative to the fluorescence of the rest of the cell body. Significant values are compared to the wild type background. *, **, *** indicate a p value < 0.05, 0.01, 0.001, respectively.

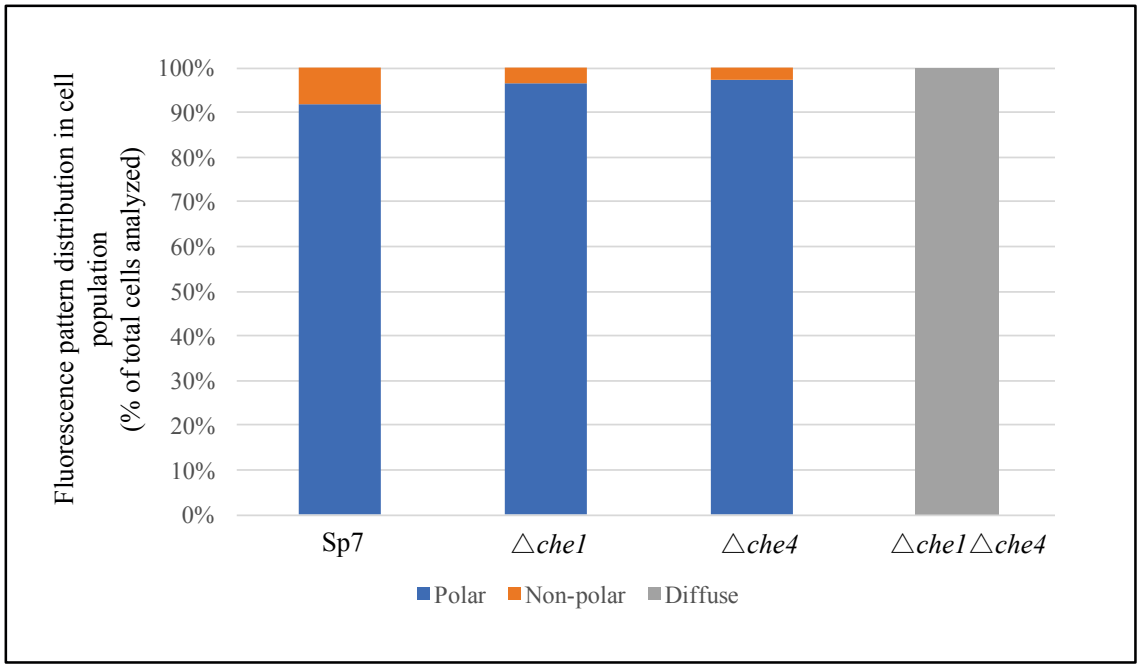

Figure 16. Quantification of the localization of cell population of CheY4-YFP

Quantification of the distribution of fluorescence in the population of CheY4-YFP cells analyzed in wild type (Sp7) and mutant derivative backgrounds. N ≥ 100 cells for each bar.

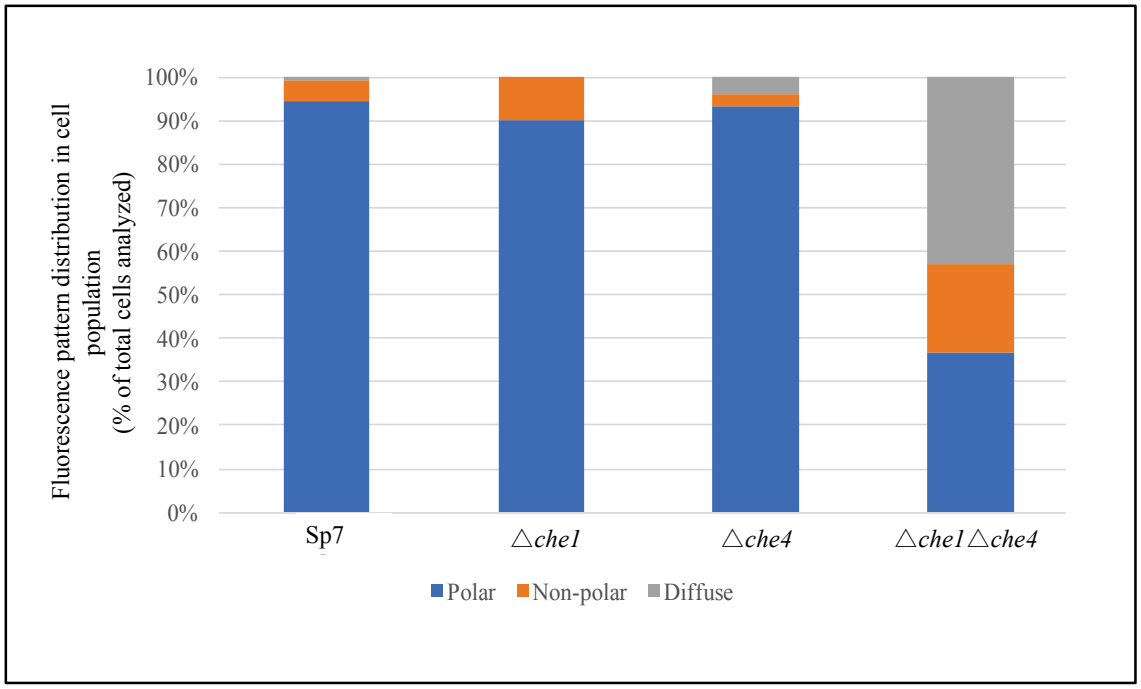

Figure 17. Quantification of the localization of cell population of CheW1-YFP

Quantification of the distribution of fluorescence in the population of CheW1-YFP cells analyzed in wild type (Sp7) and mutant derivative backgrounds. N ≥ 73 cells for each bar.

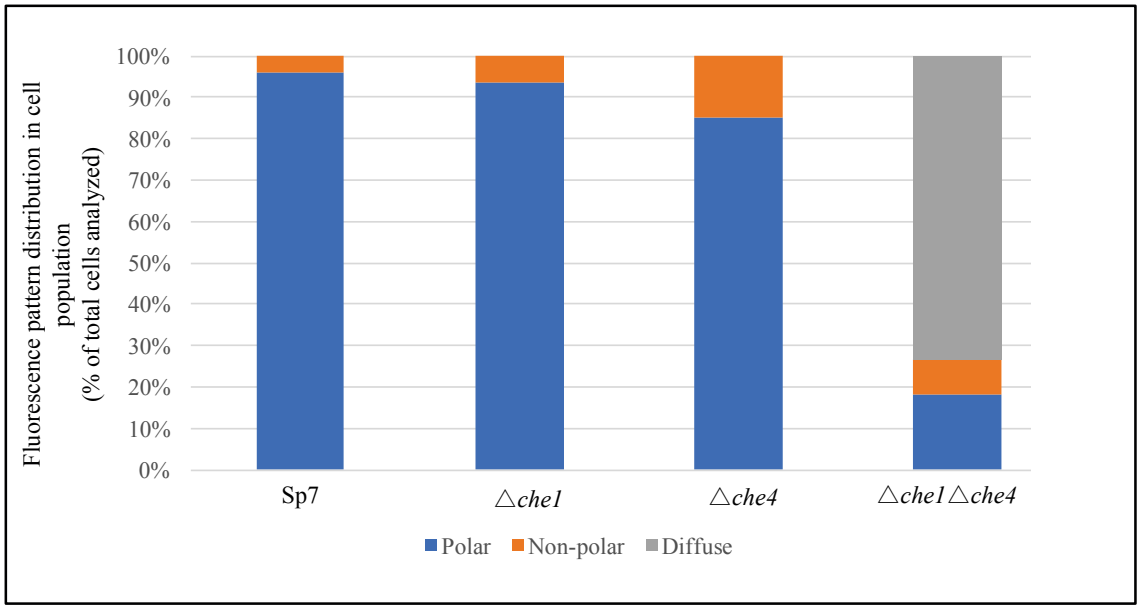

Figure 18. Quantification of the localization of cell population of CheW4-YFP

Quantification of the distribution of fluorescence in the population of CheW4-YFP cells analyzed in wild type (Sp7) and mutant derivative backgrounds. N ≥ 60 cells for each bar.

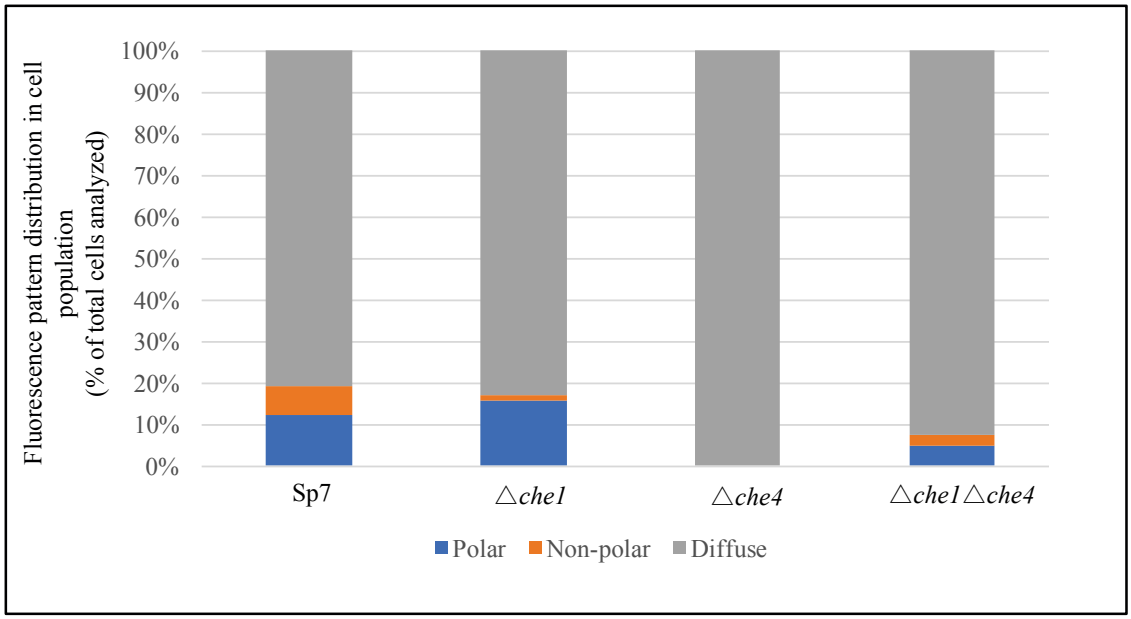

Figure 19. Quantification of the localization of cell population of CheY1-YFP

Quantification of the distribution of fluorescence in the population of CheY1-YFP cells analyzed in wild type (Sp7) and mutant derivative backgrounds. N ≥ 60 cells for each bar.

Che1 and Che4 Chemotaxis Proteins Interact with Each Other in the Bacterial Two-Hybrid Assay

Thus far we do not provide evidence that Che1 and Che4 proteins physically interact, which would be required in order to form stable chemoreceptor arrays. To test interactions between paralogs, we used a bacterial adenylate cyclase two-hybrid (BACTH) assay. In this assay, genes of interest were cloned into either pKNT25 (low copy) or pUT18 (high copy) vectors. These vectors each encode one half of a catalytic domain (T18 or T25) of the *Bordetella pertussis* adenylate cyclase. If protein-protein interaction occurs, functional complementation occurs between the two halves of the catalytic domain and cyclic AMP (cAMP) is produced. This activates the *lac* and *mal* operons in *E. coli*; positive interactions plated on MacConkey agarose utilize the carbon source in the agar and appear pink. From here, pink colonies can be grown in liquid media and subjected to a beta-galactosidase assay to quantify the strength of interactions. Given that YFP fusions to the C-terminus of CheA1, CheA4, CheY1, CheY4, and Tlp1 are functional (25, 26), we tested all interactions with the catalytic domains fused at the C-terminus of the proteins expressed from both BACTH vectors (Fig. 8). To ensure that the assay was suitable for assessing the interactions among *A. brasilense* chemotaxis proteins, we first determined whether we could detect an interaction between CheA4 and CheW4 in this system since both proteins are encoded by genes found together within the che4 operon and because we have genetic evidence they function in the same pathway (20). All interactions were first plated on MacConkey agar (data not shown) and interactions were quantified through the beta-galactosidase assay. Here, we only show the strength of interactions expressed in Miller units. Significance for

each interaction is relative to the negative control (interaction between empty pKNT25 and empty pUT18 vectors) ran alongside it on its individual 96-well plate. In our results, we compared the interactions of interest to the Miller units produced by the empty vectors, instead of a protein of interest and an empty vector (interaction between pKNT25-gene of interest and empty pUT18 vector or vice versa), because there are no reports in the literature of proteins showing positive interaction with empty vectors. To be thorough, we did test some proteins against empty vectors but found no interaction (data not shown).

As expected, CheA4 and CheW4 exhibited strong interaction with one another (Fig. 20). For Che1 proteins, we detected positive interactions between not only proteins encoded for in the Che1 operon, CheA1 and CheW1, but also between proteins encoded for in the che4 operon such as CheA4 and CheW4 (Figs. 20-21). Additionally, CheA4 and CheW4 interacted with each other and themselves (Figs. 20-21). These results concur with our microscopy observations and indicate that, in this assay, proteins from Che1 could physically interact with proteins from Che4.

Relative Contribution of CheA4 and CheA1 to Clustering of Chemotaxis Receptors into Polar Arrays

To further explore the possible interaction of Che1 and Che4 proteins within each of the two membrane-anchored arrays, we next characterized the interactions of these proteins with chemoreceptors using fluorescence microscopy and the BACTH assay. Che1 is the ancestral chemotaxis pathway controlling chemotaxis in *A. brasilense* (95) and most chemoreceptors predicted within the genome, which belong to the 38H length class are likely to interact with components of Che1. Furthermore, previous data indicated that Tlp1,

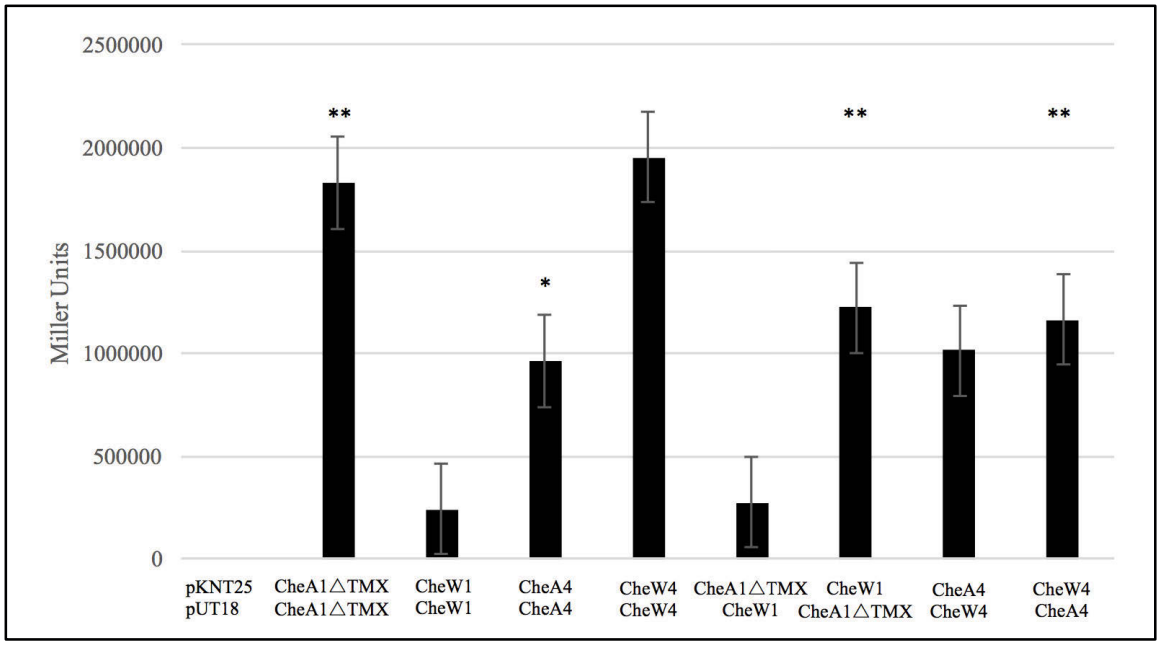

Figure 20. BACTH interactions of chemotaxis proteins encoded in the same pathway

Figure represents bacterial two-hybrid interactions between chemotaxis proteins encoded within the same signal transduction pathway. Each gene of interest was cloned into either pKNT25 (low copy plasmid) or pUT18 (high copy plasmid) and all interactions were quantified using a beta-galactosidase assay. Each gene was cloned into both pKNT25 and pUT18 to assess differences in interactions based off plasmid copy number. * denotes p value < 0.05; ** denotes p value < 0.005. Significance for each interaction is relative to the negative control (interaction between empty pKNT25 and empty pUT18 vectors) ran alongside it on its individual 96-well plate.

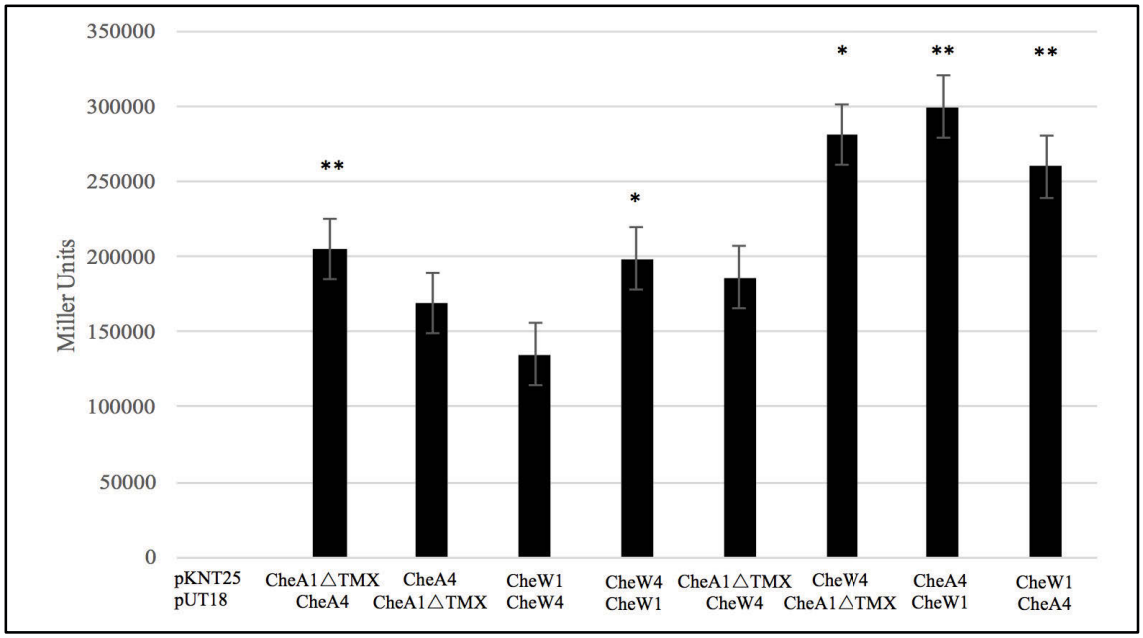

Figure 21. BACTH interactions of chemotaxis proteins encoded in different pathways

Figure represents bacterial two-hybrid interactions between chemotaxis proteins encoded within different signal transduction pathway. Each gene of interest was cloned into either pKNT25 (low copy plasmid) or pUT18 (high copy plasmid) and all interactions were quantified using a beta-galactosidase assay. Each gene was cloned into both pKNT25 and pUT18 to assess differences in interactions based off plasmid copy number. * denotes p value < 0.05; ** denotes p value < 0.005. Significance for each interaction is relative to the negative control (interaction between empty pKNT25 and empty pUT18 vectors) ran alongside it on its individual 96-well plate.

a predicted 38H length class chemoreceptor, interacted with Che1 and perhaps another chemotaxis pathway, which we later identified as Che4 (99). On the other hand, *tlp4a* encodes for a predicted membrane-anchored chemoreceptor of the 36H class and is found within the che4 operon and is thus likely to function with Che4 proteins (83). Therefore, we chose to test both Tlp1 and Tlp4a. Since we were assessing the contribution of CheA1 and CheA4 in clustering of chemoreceptor arrays, we tested receptors in wild type, Δ*cheA1,* Δ*cheA4,* and Δ*cheA1*Δ*cheA4* backgrounds. Both Tlp4a-YFP and Tlp1-YFP, which are functional fusions (Alexandre lab, unpublished) localized at the cell poles as punctate foci when expressed in the wild type strain (Fig. 22). In the Δ*cheA1* strain background, Tlp4a-YFP was "spotty", localizing as numerous lateral foci that also appeared smaller in size relative to the large polar foci. The average number of fluorescent foci per cell in the wild type background was 2.1 ± 0.7 while the number of fluorescent foci per cell in the Δ*cheA1* strain was 3.8 ± 1.3 (Student's t test, p-value < 0.0001, N = 90). This change in the distribution of the fluorescent foci, however, was not accompanied by a detectable change in the relative fluorescence intensity of the polar clusters as compared to the wild type (Fig. 23). In the Δ*cheA4* and Δ*cheA1*Δ*cheA4* strains, Tlp4a-YFP fluorescent foci were dimmer as compared to wild type cells (Figs. 22-23). In addition, the Tlp4a-YFP fluorescent foci were slightly off polar and were detected at greater distance from the cell poles (Figs. 24-25). Together, these observations suggest that polar localization of Tlp4-YFP in clusters seen as tight fluorescent foci require both CheA1 and CheA4. In the Δ*cheA1* strain, Tlp1-YFP was unable to localize as punctate foci and instead was diffuse throughout the cell (Fig. 23). While Tlp1-YFP localized to the cell poles in the Δ*cheA4* strain, it was diffuse

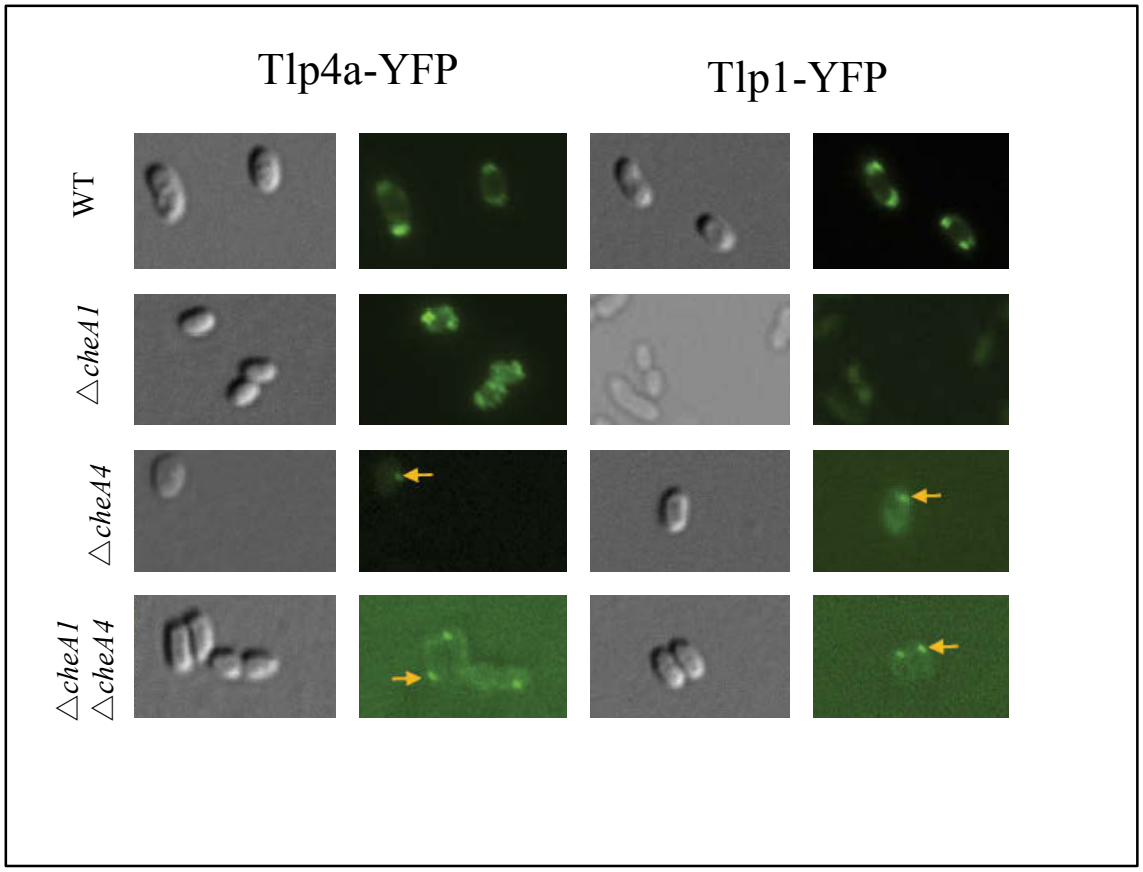

Figure 22. Localization of YFP-tagged chemoreceptors in *A. brasilense*

DIC and fluorescence microscopy images of Tlp4a-YFP and Tlp1-YFP in the wild type and mutant derivative backgrounds. Orange arrows point at non-polar (mislocalized) foci.

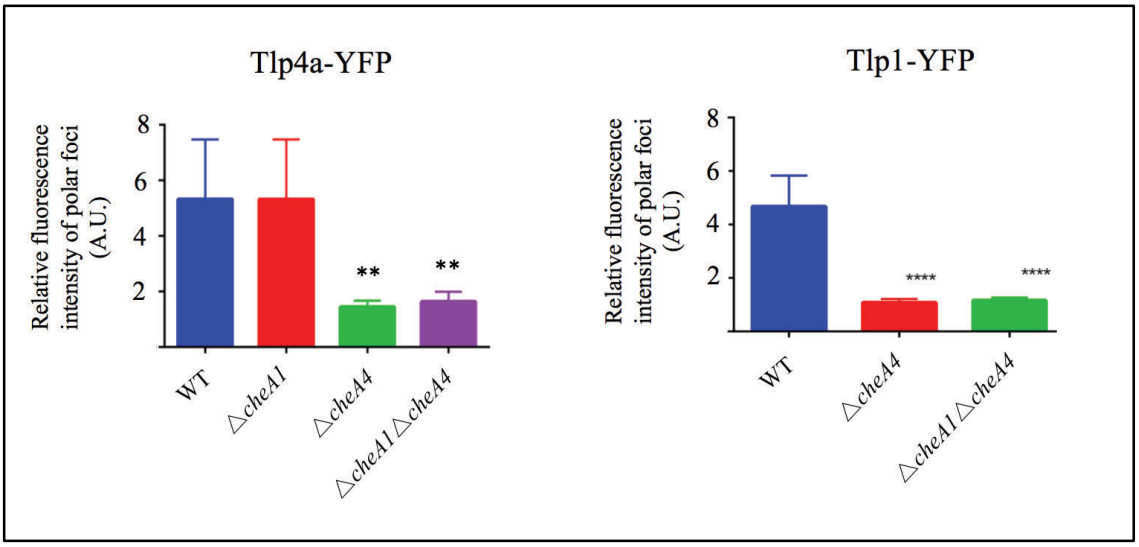

Figure 23. Fluorescence intensity of chemoreceptors in *A. brasilense*

Relative fluorescence intensity of Tlp4a-YFP and Tlp1-YFP. Bar graphs depict fluorescence intensity of the polar foci relative to the fluorescence intensity of the cell body. For Tlp1-YFP, no data could be collected for △*cheA1* as these cells did not form polar foci. All data are shown as mean +1 SD. N ≥ 80 cells. ** denotes a p value < 0.0001

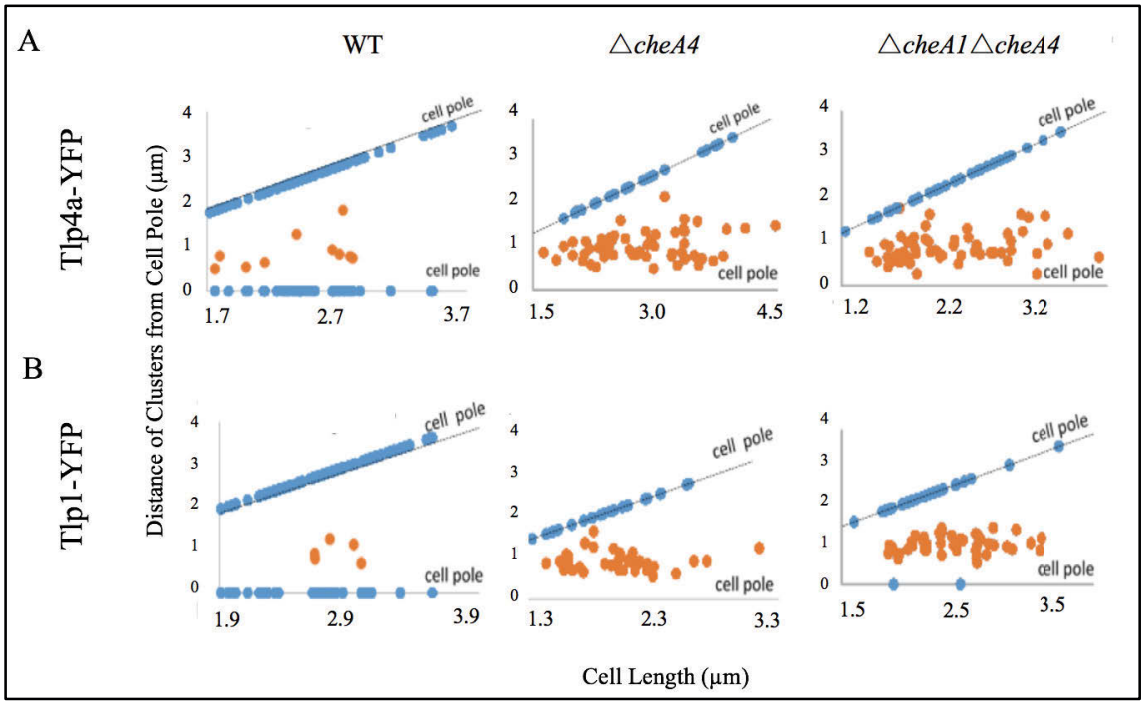

Figure 24. Distribution of YFP-tagged chemoreceptors in wild type and mutants

Distance of Tlp4a-YFP (A) and Tlp1-YFP (B) clusters from the cell poles as a function of cell length. Blue dots represent fluorescent foci at the pole; orange dots represent mislocalized foci localized away from the cell pole. Chemoreceptors localize at the cell pole in WT background as shown by the large number of blue dots (and the presence of few orange dots) along the cell poles for both Tlp1-YFP and Tlp4a-YFP. In Δ*cheA4* and Δ*cheA1*Δ*cheA4* backgrounds, the number of polar foci, represented by blue dots, decreases as the number of non-polar or mislocalized foci, represented by orange dots, increases. All data are shown as averages +1 SD, N ≥ 80 cells. *** denotes p value < 0.001.

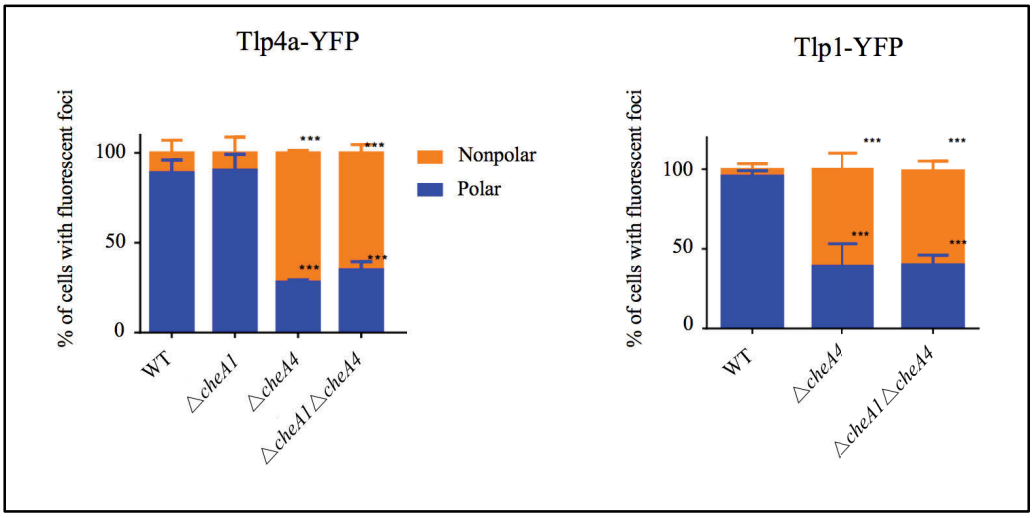

Figure 25. Analysis of the mislocalization of chemoreceptor clusters in wild type and mutants.

Stacked bar graphs depict polar (blue) and nonpolar (orange) localization of Tlp4a-YFP and Tlp1-YFP clusters. For Tlp1-YFP, no data could be collected for △*cheA1* as these cells did not form polar foci. All data are shown as averages +1 SD, N ≥ 80 cells. *** denotes p value < 0.001

in the Δ*cheA1*Δ*cheA4* strain (Figs. 22, 24-25). Further, overall fluorescence of Tlp1-YFP in both strain backgrounds was less intense as compared to its expression in the wild type (Fig. 23). These findings suggest that in the absence of CheA1, Tlp1-YFP does not form polarly localized foci, suggesting an absence of cluster formation and formation of smaller clusters when CheA4 is lacking. Together, these data indicate that both CheA1 and CheA4 are required for proper chemotaxis receptor localization and clustering of receptors from 36H and 36H classes at the cell poles. These findings also corroborate the *in vitro* BACTH results. The dim fluorescence of Tlp4a-YFP and Tlp1-YFP observed in the mutant backgrounds could be due to protein degradation, perhaps as a result of destabilization when not assembled in clusters. To test this, we performed western blots using an anti-GFP antibody and observed increased degradation of Tlp1-YFP and Tlp4a-YFP when expressed in the Δ*cheA1*, Δ*cheA4*, or Δ*cheA1*Δ*cheA4* backgrounds compared to expression in the wild type (Fig. 26). This is consistent with both CheA1 and CheA4 required for the formation of chemoreceptor arrays. The results also indicate that receptors that fail to assemble into arrays are degraded more rapidly.

Contribution of Che1 and Che4 Proteins, other than CheA Paralogs, in Clustering of Chemotaxis Receptors

We also tested the possible physical interaction between CheA1, CheW1, CheA4, CheW4 and Tlp1 and Tlp4a in the BACTH assay. Tlp1 positively interacted with CheW1 and itself (Figs. 27-28). This finding was expected given that chemoreceptors are known to dimerize and that Tlp1 was shown to signal in a Che1-dependent manner (99). Tlp1 also positively interacted with CheA1ΔTMX, CheA4, and CheW4 (Fig. 27). Tlp4a interacted with CheA4

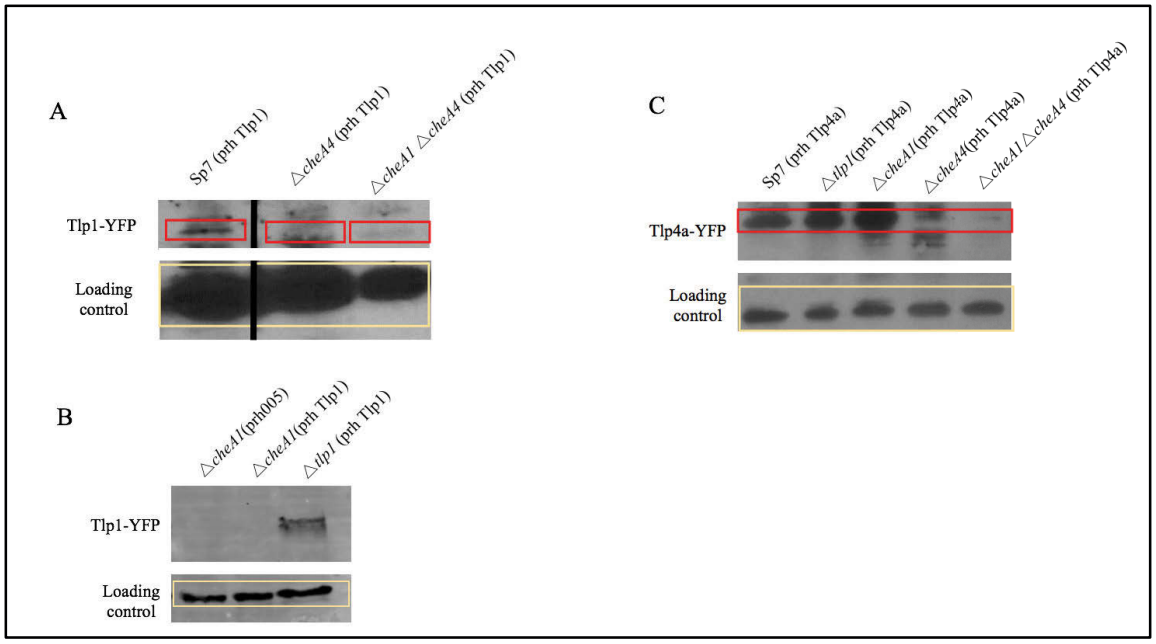

Figure 26. Expression levels of YFP-tagged chemoreceptors in mutant backgrounds

Cellular levels of Tlp1-YFP and Tlp4a-YFP expressed form the pRH005 plasmid. Equivalent total protein concentrations were analyzed in all samples. Expression of Tlp1-YFP (panels A and B) and Tlp4a-YFP (panel C) from the pRH005 plasmid were probed with anti-GFP primary antibodies. Bands in red boxes correspond to Tlp1-YFP (panel A, top) and Tlp4a-YFP (panel C). The bands in yellow boxes represent loading controls. The black lines in panel A indicate junctions separating lanes that were spliced from the original image in order to show samples run on the same gel in a single row.

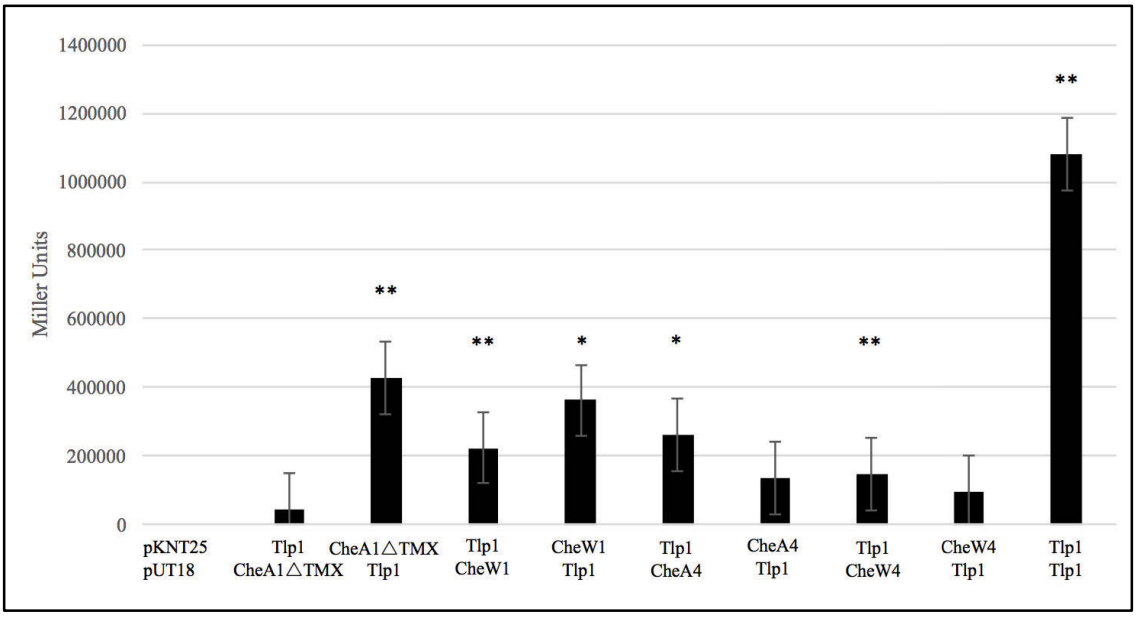

Figure 27. BACTH of chemotaxis proteins and Tlp1

Figure represents bacterial two-hybrid interactions between chemotaxis proteins and the chemoreceptor Tlp1. Each gene of interest was cloned into either pKNT25 (low copy plasmid) or pUT18 (high copy plasmid) and all interactions were quantified using a beta-galactosidase assay. Each gene was cloned into both pKNT25 and pUT18 to assess differences in interactions based off plasmid copy number. * denotes p value < 0.05; ** denotes p value < 0.005. Significance for each interaction is relative to the negative control (interaction between empty pKNT25 and empty pUT18 vectors) ran alongside it on its individual 96-well plate.

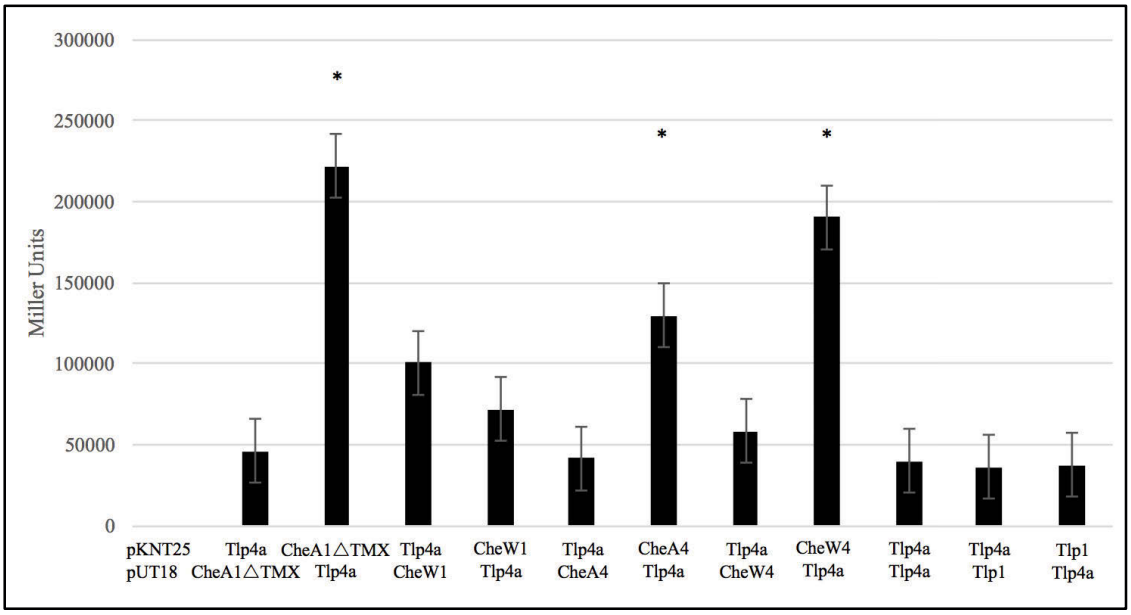

Figure 28. BACTH of chemotaxis proteins and Tlp4a

Figures represent bacterial two-hybrid interactions between chemotaxis proteins and the chemoreceptor Tlp4a. Each gene of interest was cloned into either pKNT25 (low copy plasmid) or pUT18 (high copy plasmid) and all interactions were quantified using a beta-galactosidase assay. Each gene was cloned into both pKNT25 and pUT18 to assess differences in interactions based off plasmid copy number. * denotes p value < 0.05; ** denotes p value < 0.005. Significance for each interaction is relative to the negative control (interaction between empty pKNT25 and empty pUT18 vectors) ran alongside it on its individual 96-well plate.

and CheW4, as expected, but it also interacted with CheA1ΔTMX in this assay (Fig. 28). Surprisingly, Tlp4A was not found to interact with itself at detectable levels in this assay. As expected from their difference length class, Tlp1 and Tlp4a did not interact. Together these data suggest that chemotaxis receptors from the 38H (Tlp1) and 36H (Tlp4a) classes can physically interact with some of the Che1 and some of the Che4 proteins, in particular both CheA paralogs, in *A. brasilense*. While only predicted as possible physical interactions in the BACTH assay, these results are fully consistent with the fluorescence imaging data described above and in particular, the increased receptor proteolytic degradation of chemoreceptors failing to assemble into signaling clusters in the absence of CheA1 or CheA4.

Discussion

Based on our results, we suggest that each of the two membrane-bound chemoreceptor arrays detected by cryo-EM utilize paralogs from both Che1 and Che4 chemotaxis signaling pathways to build extended stable arrays. Our experimental evidence strongly suggests that CheA1ΔTMX and CheA4, and likely, CheW1 and CheW4, are recruited to form the baseplates of each of the two *A. brasilense* chemotaxis receptor arrays, each of which likely comprise Tlp1 and other 38H receptors or Tlp4a and other 36H receptors. These results provide a straightforward mechanism by which two chemotaxis signaling pathways, Che1 and Che4, could function in a coordinated manner to regulate chemotaxis responses in *A. brasilense*, despite each of Che1 and Che4 regulating different signaling outputs. Che1 regulates transient changes in swimming speed while Che4 regulates transient changes in swimming reversals (83, 96). Stimuli detected by chemotaxis receptors

could be transduced and trigger coordinated responses from both Che1 and Che4 by having both Che1 and Che4 proteins at the baseplates of each of the two chemoreceptor arrays implicated in chemotaxis.

The bacterial adenylate cyclase two-hybrid data suggest that paralogs from Che1 and Che4 could physically interact, which would be necessary to form mixed baseplates. We detected positive interactions between the histidine kinases of both signaling pathways, CheA1ΔTMX and CheA4. CheA functions as a dimer with dimerization occurring via the P3 domain. CheA1ΔTMX and CheA4 share 37% sequence identity and more specifically, the P3 domains share a 35% sequence identity (113). These results implicate the existence of possible CheA heterodimers. We also detected positive interactions of CheA1ΔTMX and CheA4 with both CheW1 and CheW4 adaptor proteins. In the signaling complex, CheA and CheW bind to the signaling domains of receptors. These signaling domains are highly conserved among chemoreceptors and therefore the proteins that bind may share certain characteristics in order to be able to bind to such a conserved domain. Interestingly though, not much sequence conservation exists in CheW homologs (67).The CheA domain that binds to the receptors is the P5 domain, also referred to as the CheW-like domain. The sequence identity of the P5 domain of CheA4 with CheW4 is 27%, and the sequence identity of the P5 domain of CheA4 and CheW1 is 53% (113). There are two P5 domains, P5A and P5B, in CheA1ΔTMX and their sequence identities with CheW1 and CheW4 are as follows: P5A with CheW1, 0%; P5A with CheW4, 33%; P5B with CheW1, 29%; P5B with CheW4, 33% (113). Though this assay does not provide *in vivo* evidence of interactions between proteins, we do note that in the closely related alphaproteobacteria,

Rhodobacter sphaeroides, one membrane-bound histidine kinase, CheA2, forms signaling clusters with two CheWs (CheW2, CheW3) (114-117), each with drastically different sequence identities as compared to CheA2: The P5 domain of CheA2 with CheW2, 0%; the P5 domain of CheA2 with CheW3, 27% (113). This provides reasonable evidence to support the hypothesis that the paralogs found to interact through the bacterial two-hybrid assay may actually interact *in vivo.* We believe the positive interactions observed here to be true positives due to the fact that there is a low instance of false positives in this assay (118); the level of cAMP will rise only when there is sufficient interaction between proteins of interest; this "threshold" level is not likely to be reached with arbitrary interactions. Furthermore, there have been no reports of auto-activation of a protein of interest tested against an empty vector (118) suggesting that interactions are from the proteins of interest and not a result of a protein's interaction with the features of the vector itself.

Each protein-protein interaction was tested bi-directionally since the vectors had different copy numbers; for example, we first tested CheA1ΔTMX in the pKNT25 vector and CheW4 in the pUT18 vector, then tested CheA1ΔTMX in the pUT18 vector and CheW4 in the pKNT25 vector. For interactions with chemotaxis proteins (excluding chemoreceptors), we noted that our interactions were more robust when the histidine kinase was in the high copy pUT18 vector. This could possibly be due to the stoichiometry of the core signaling complex. The literature reports varying stoichiometric ratios of chemoreceptors, CheA, and CheW in organisms performing chemotaxis (119-122). These varying ratios may be due to the varying stoichiometric assemblies of chemotaxis proteins in these signaling clusters or the variation could be due to the sensitivities of the

experimental procedures used to obtain these ratios which did, in fact, vary in each of these studies. We are limited in what we can extrapolate about the stoichiometry of the signaling complex from our results, but it does seem to be beneficial for the CheA to be present in higher amounts in terms of strength of interaction. For chemoreceptors, no distinct pattern emerged with Tlp1, but positive interactions could only be detected when Tlp4a was in the high copy pUT18 vector. However, it should be noted that chemoreceptors are known to form dimers and though this assay, we could not detect interaction between Tlp4a and itself. Furthermore, this assay is optimized for membrane-bound proteins; the T18 and T25 catalytic domains interact in the membrane; perhaps some of the differences in the strength of interactions when we swap vectors could also be due to the fact that our chemotaxis proteins are soluble. However, these results should also be verified by *in vivo* experiments such as co-immunoprecipitation with primary antibodies raised against a specific chemotaxis protein since the fusion of these proteins to the catalytic domain could lead to structural changes which may alter the ability of some proteins to interact.

Signal procession via multiple chemotaxis signaling pathways has not yet been described but is unlikely to be unique to *A. brasilense* given the number of bacterial genomes with multiple chemotaxis pathways (123) and experimental evidence of cross-talk between chemotaxis signaling pathways in other species (124). In addition, evidence of cross-talk implicating chemotaxis receptors and multiple signaling pathways exists between the Che7, Dif and Frz chemotaxis-like signaling pathways of *Myxococcus xanthus* (125-127). However, the exact mechanism underlying the cross-talk is not known.

Despite recent examples of cross-talk at the level of phosphotransfer between histidine kinases and non-cognate response regulators, such as in *Bacillus subtilis* between the PhoR-PhoP and YycG-YycF two-component pathways where PhoR could phosphorylate a non-cognate response regulator, YycF (128), cross-talk is generally thought not to occur at the level of phosphotransfer between a histidine kinase and its non-cognate response regulator given the selectivity of the interaction between these signaling proteins (129-132) as well as the expected decrease in the specificity of response to a specific input (129, 133). Results obtained here do not invoke the possibility of phosphotransfer between non-cognate partners for cross-talk and, in fact, we present no evidence for cross-talk between paralogs. We do, however, present evidence of co-binding of chemotaxis paralogs at the level of the baseplate which allows for the integration and coordination of two otherwise independent signaling pathways without incurring the potential disadvantages of cross-talk. It rather seems that co-localizing chemotaxis signaling kinases to receptor arrays would ensure that sensory information processed from a common pool of receptors is sufficient to ensure response a coordinated response.

Coordinating signaling by multiple chemotaxis signaling pathways is not limited to *A. brasilense*. In the alphaproteobacteria, *Rhodobacter sphaeroides*, three chemotaxis operons produce two functional chemotaxis clusters that display distinct subcellular localization: one is a polar membrane-anchored cluster and the second one is localized in the cytosol (114-116). In the polar cluster, one CheA and two distinct CheW paralogs that are all encoded within operon 2, transfer the signal to all six CheY paralogs (114-117). In the cytosolic cluster, one CheW and two CheAs, all encoded within chemotaxis operon 3,

also transfer sensory signals but to only two of the CheY paralogs (114-117). These clusters are physically separated from each other in the cell and each of the chemotaxis proteins specifically assemble in a single chemotaxis signaling cluster, with experimental evidence suggesting this organization prevents detrimental signaling cross-talk (114-116, 134). The subcellular organization of chemotaxis signaling clusters in *R. sphaeroides* suggests stringent specificity in the interactions between chemoreceptors and baseplate proteins, CheA and CheW, to form signaling clusters which would be relaxed in the chemoreceptor-CheA-CheW clustering our results in *A. brasilense* suggest.

However, the ability for different baseplate proteins to mix within a single cluster is suggested in some model systems. Chemotaxis CheV proteins, which structurally and functionally are CheW-REC hybrids (135), are widespread in bacterial genomes and recent evidence indicates that in *Helicobacter pylori*, CheV-comprising chemoreceptor-kinase clusters can join a larger CheW-receptor-kinase membrane-anchored cluster. In *E. coli*, recent comparative genomics combined with analysis of experimental evidence also imply a role for CheV in bringing specific chemoreceptors to stable arrays (136). While we have not specifically addressed the role of CheW paralogs in the present study, CheA paralogs possess P5 domains that are structurally and functionally similar to CheW and the interfaces between the CheA-P5 domain and CheW are critical for stabilizing chemoreceptor arrays, maintain connectivity and signal cooperativity (137). Thus, results here suggesting that Che1 and Che4 proteins form mixed baseplates is not incompatible with maintaining signal cooperativity within the chemoreceptor arrays. Data obtained in *A. brasilense* imply that physical separation of chemoreceptors into two distinct membrane-

bound receptor arrays is dictated by segregation of chemoreceptors into length classes. This observation further raises questions on the relative contributions of the different chemoreceptor arrays to sensing, that our research will address in the future.

Comparison of the complete genome sequences of several species of the *Azospirillum* genus (95) suggests that the ancestor of *Azospirillum* spp. possessed three chemotaxis signaling pathways, with only one (corresponding to Che1), contributing to chemotaxis while the other two are predicted to have non-chemotaxis functions (95). The signaling pathway corresponding to Che4 was acquired next during evolution and Che4 is now the major signaling pathway controlling chemotaxis in *A. brasilense* (83). Relaxing specificity for the assembly of chemotaxis baseplates proteins to facilitate signaling from chemoreceptors of different length classes could provide a straightforward mechanism for ensuring beneficial signaling from this laterally transferred chemotaxis signaling pathway. Whether similar strategies have been used to accommodate laterally transferred chemotaxis signaling pathways in other bacteria remains to be seen.

CHAPTER II
DISTINCT DOMAINS CONFER CHEA WITH UNIQUE FUNCTIONS IN CHEMOTAXIS AND CELL LENGTH IN *AZOSPIRILLUM BRASILENSE* SP7

A version of this chapter was originally published by Jessica M. Gullett, Amber Bible, and Gladys Alexandre:

Gullett JM, Bible A, Alexandre G. 2017. Distinct domains of CheA confer unique functions in chemotaxis and cell length in *Azospirillum brasilense* Sp7. J Bacteriol 199:e00189-17. https://doi.org/10.1128/JB.00189-17

Author contributions to this work included: JMG, AB, GA designed research; JMG and AB performed research; JMG, GA, AB analyzed data; JMG and GA wrote the paper.

Abstract

Chemotaxis is the movement of cells in response to gradients of diverse chemical cues. Motile bacteria utilize a conserved chemotaxis signal transduction system to bias their motility and navigate through a gradient. A central regulator of chemotaxis is the histidine kinase CheA. This cytoplasmic protein interacts with membrane-bound receptors, which assemble into large polar arrays, to propagate the signal. In the alphaproteobacterium *Azospirillum brasilense*, Che1 controls transient increases in swimming speed during chemotaxis, but it also biases the cell length at division. However, the exact underlying molecular mechanisms for Che1-dependent control of multiple cellular behaviors are not known. Here, we identify specific domains of the CheA1 histidine kinase implicated in modulating each of these functions. We show that CheA1 is produced in two isoforms: a membrane-anchored isoform produced as a fusion with a conserved seven-transmembrane domain of unknown function (TMX) at the N terminus and a soluble isoform similar to prototypical CheA. Site-directed and deletion mutagenesis combined with behavioral assays confirm the role of CheA1 in chemotaxis and implicate the TMX domain in mediating changes in cell length. Fluorescence microscopy further reveals that the

membrane-anchored isoform is distributed around the cell surface while the soluble isoform localizes at the cell poles. Together, the data provide a mechanism for the role of Che1 in controlling multiple unrelated cellular behaviors via acquisition of a new domain in CheA1 and production of distinct functional isoforms.

Introduction

Chemotaxis, the directed movement of motile bacteria in gradients of diverse chemoeffectors, promotes colonization of various niches and the establishment of plant-microbe associations (138, 139). The histidine kinase CheA is a central regulator of chemotaxis. In the *Escherichia coli* model, when chemical signals bind to chemoreceptors, CheA is autophosphorylated. This phospho-CheA then promotes changes in swimming direction via phosphotransfer to CheY, yielding phospho-CheY with an increased affinity to flagellar motors. A chemotaxis-specific phosphatase, CheZ, acts on phospho-CheY to terminate the signal. Phospho-CheA also plays a role in receptor adaptation to background conditions. Methylation levels of the chemoreceptors are altered through either a phosphotransfer from phospho-CheA to the methylesterase CheB or by the addition of methyl groups via the methyltransferase CheR (60, 61). *E. coli* possesses a single chemotaxis system, and the functional CheA is a homodimer, with each monomer containing five domains denoted P1 to P5 (Fig. 29) (68). The ATP binding domain of CheA (P4) phosphorylates at the conserved histidine residue in the N-terminal phosphorylation domain (P1) (Fig. 29). P2 is a docking site for interactions with CheY and CheB, which are both activated through a phosphorylation event from phospho-CheA; P3 serves as a dimerization domain. The P5 domain closely resembles and also interacts with the adaptor

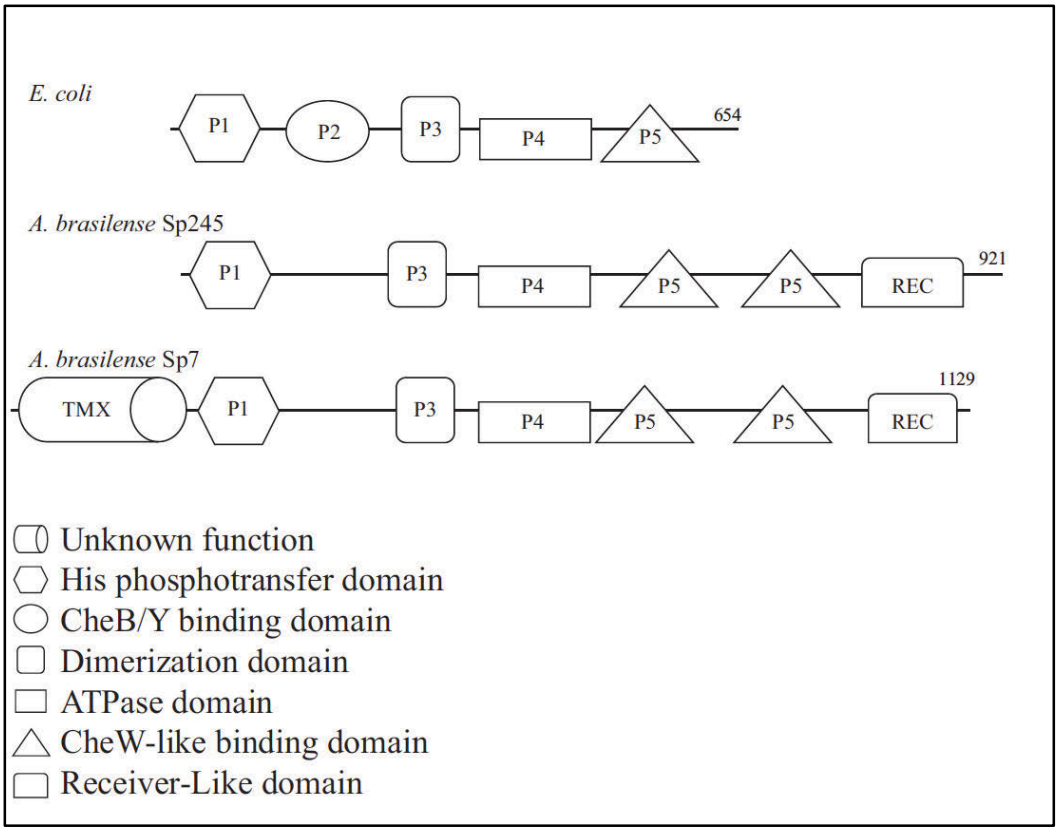

Figure 29. Domain analysis of CheA orthologs in *E. coli* and *A. brasilense*

Domain architecture of CheA orthologs in *E. coli* and *A. brasilense* strains Sp7 and Sp245. Top, the *E. coli* CheA contains a histidine phosphotransfer domain which harbors the conserved His residue (P1) followed by a CheB/Y binding domain (P2). The dimerization (dimer) domain (P3) precedes the ATPase domain (P4), which is necessary to phosphorylate the His residue. The binding domain (P5) resides in the C-terminal region. Middle, *A. brasilense* strain Sp245 CheA1 possesses the P1, P3, P4, and P5 domains and also a receiver-like (REC) domain. Bottom, *A. brasilense* strain Sp7 CheA1 possesses domains similar to those of strain Sp245, but it also possesses an N-terminal seven-transmembrane region of unknown function (TMX). Numbers at the C termini denote the total number of amino acids present.

protein CheW, which couples chemoreceptors to CheA (76). Together, CheA, through its P5 domains, and CheW interact with the cytoplasmic tips of the trimers of receptor dimers to form a ring-shaped baseplate (62, 64). Each baseplate interacts with neighboring baseplates, making chemotaxis signal transduction a cooperative process that both amplifies and propagates the chemotaxis signal (62, 64, 119). Compared to the case for *E. coli* chemotaxis, the complete genome sequences of most motile bacteria indicate the presence of more than one chemotaxis (Che) operon. In addition to chemotaxis, some chemotaxis systems are implicated in the regulation of cellular functions other than flagellar motility: some systems regulate the extension-retraction cycle of type IV pili to promote twitching (77), others regulate enzymatic activities implicated in the transition from a vegetative to a sessile lifestyle (78), and some exert control of developmental programs (79, 80, 82). Chemotaxis systems that regulate alternative cellular functions often lack a CheY homolog and instead possess enzymes or transcription factors that function to mediate the signaling output (123). Chemotaxis systems that control type IV pili activities are characterized by CheA homologs which possess multiple P1 domains at their N terminus (123). Therefore, comparative analysis of the architecture of chemotaxis systems can provide clues as to the putative function of some chemotaxis operons.

The alphaproteobacterium *Azospirillum brasilense*'s genome encodes four signal transduction pathways. The Che1 pathway controls transient changes in the swimming speed that accompany the simultaneous suppression of changes in the swimming direction during a response to a chemoattractant (96). These changes in swimming velocity modulate the propensity of cells to clump by cell-cell interactions (96, 97, 140). However, deletion

of *che1* or of the gene for the histidine kinase of the Che1 pathway, *cheA1*, has a minor effect on chemotaxis (97). An additional Che pathway, which has a more dominant role in controlling chemotaxis, has recently been identified (83). In addition to regulating transient increases in swimming speed, Che1 is implicated in regulating cell length: mutations that render *cheA1, che1, or cheY1* nonfunctional also result in cells of relatively shorter lengths than the wild type, while mutations that abolish the function of enzymes required for chemotaxis receptor adaptation, CheB1 and CheR1, result in cells significantly longer than the wild type, with these effects most evident in dividing cells (97). These data thus suggest that Che1 regulates two distinct functions, i.e., transient changes in swimming speed upon chemo-stimulation and cell length, but the underlying mechanisms are not known (96). The *A. brasilense* Che1 pathway comprises all homologs of the *E. coli* chemotaxis operon, including a CheY1 homolog that functions to regulate transient increases in swimming velocity but excluding CheZ (96). Che1 also includes a CheA1 homolog with an additional N-terminal domain of unknown function (108). In this study, we aimed to identify the domain(s) of CheA1 that contributes to these distinct functions, namely, chemotaxis and cell length regulation. We provide experimental evidence that the N-terminal domain of CheA1, which we name TMX, is dispensable for chemotaxis but is associated with the function of CheA1 in cell length regulation. We also show that CheA1 is produced in two isoforms: (i) a soluble isoform lacking the N-terminal TMX which localizes as small foci at the cell poles and (ii) a larger, membrane-anchored, full-length protein that is distributed throughout the cell surface. Together, our data suggest a molecular mechanism by which the *A. brasilense* pathway regulates unrelated cellular functions via the production of

functionally and spatially distinct populations of CheA1.

Materials and Methods

Strains, Media, and Chemicals

The bacterial strains used in this study are listed in Table 5. *A. brasilense* strain Sp7 (ATCC 29145) (141) and mutant derivatives were grown at 28°C on minimal medium for *A. brasilense* (MMAB) plates supplemented with malate (10 mM final concentration) or with both malate (5 mM) and fructose (5 mM) for cell size measurements (see below), since these were determined to be the best substrates to observe cell size differences (142). MMAB is either supplemented with a nitrogen source (ammonium chloride at 18.7 mM), with cells incubated with shaking (200 rpm), or without nitrogen supplementation for growth under nitrogen fixation conditions, without shaking to limit oxygen diffusion. The Δ*cheA1* and *cheA1*H252Q derivatives were described previously (96, 97).

Behavioral Assays

For comparison of chemotaxis responses in the soft agar assay, bacteria were inoculated into MMAB solidified with 0.3% (wt/vol) agar (soft agar plates) and supplemented with 18.7 mM ammonium chloride and 10 mM malate. Plates were inoculated with culture in the mid-log phase of growth (optical density at 600 nm [OD_{600}], 0.4 to 0.6) and grown at 28°C. Chemotactic rings were measured after 48 h of incubation. The temporal gradient assays for aerotaxis and computerized motion analysis were performed as previously described (99). Briefly, free-swimming cells were incubated on a slide placed inside a microchamber with an atmosphere of nitrogen gas (anaerobiosis) or air, which represents

Table 5. Strains and plasmids used in chapter 2

Strain or plasmid	Genotype or relevant characteristic	Reference or source
Escherichia coli		
Top10	Cloning strain	Invitrogen
OMNImax	Cloning strain	Invitrogen
S17-1	*thi endA recA hsdR* with RP4-2Tc::Mu-Km::Tn7	25
Azospirillum brasilense		
Sp7	Parental strain, wild type	ATCC29145
Sp245	Parental strain, wild type	20
Δ*cheA1*	Δ(*cheA1*)::*gusA*-Km (Km)	17
Δ*che1*	Δ(*cheA1-cheR1*)::Cm (Cm)	17
$\Delta cheA1_{Sp245}$	*ΔcheA1*:Gm insertion in Sp245	This work
Plasmids		
pDONR 221	Cloning vector	Invitrogen
Topo 2.1	Cloning vector	Thermo Fisher
pBBR1MCS3	Cloning vector	23
pBSKII(+)	Cloning vector	Stratagene
pRH005	Gateway destination vector for C-terminal YFP fusion with protein of interest	27
pDONRTMX	pDONR221 carrying TMX	This work
pDONRCheA1	pDONR221 carrying CheA1	This work
pDONRCheA1ΔTMX	pDONR221 carrying CheA1ΔTMX	This work
pDONRTlp1	pDONR221 carrying Tlp1	This work
pBBRCheA1	pBBR1MCS3 expressing CheA1	17
pBBRCheA1ΔTMX	pBBR1MCS3 expressing CheA1 with the TMX domain deleted	This work

Table 5. continued

Strain or plasmid	Genotype or relevant characteristic	Reference or source
pBBRCheA1ΔREC	pBBR1MCS3 expressing CheA1 with the REC domain deleted	This work
pBBRTMX	pBBR1MCS3 expressing the TMX domain of CheA1	This work
pRHCheA1	pRH005 expressing CheA1	This work
pRHTMX	pRH005 expressing TMX domain	This work
pRHCheA1ΔTMX	pRH005 expressing CheA1 with TMX domain deleted	This work
pRHTlp1	pRH005 expressing Tlp1	This work
pKGmob—Gm	Mobilizable suicide plasmid	Lab strain
pKGmob-cheA1	pKGmob-Gm expressing Sp245 CheA1	This work
pBBRCheA1^{H252Q}	pBBR1MCS3 expressing CheA1^{H252Q}	Lab strain
pBBRCheA1^{D1055N}	pBBR1MCS3 expressing CheA1^{D1055N}	This work
pBSKCheA1	pBSKII(+) carrying CheA1	This work
pBSKCheA1ΔTMX	pBSKII(+) carrying CheA1 with the TMX domain deleted	This work

an attractant signal for the cells. Videos (10 s in length) for each time point were recorded, and swimming speed was analyzed through these videos using CellTrack software. The swimming speed of free-swimming cells was determined from a minimum of 75 cells tracked in 3 independent experiments. The swimming speeds denote averages calculated from the tracks of free-swimming cells 1 min prior to and 1 min after a switch from an atmosphere of N_2 to air.

Mutant Construction

To generate a *cheA1* gene in which the sequence corresponding to the N-terminal TMX domain was deleted, CheA1ΔTMX, the full-length CheA1 with its putative promoter region, was amplified by PCR from genomic DNA using the CheOp-HindIII-F and CheOp-BamHI-Rev primers (Table 6). These primers include HindIII and BamHI restriction sites at their 5′ and 3′ termini, respectively, to facilitate cloning. The PCR fragment was digested with HindIII and BamHI and cloned into the pBSKII(+) vector digested with the same enzymes, yielding pBSKCheA1. An in-frame deletion of the TMX domain was obtained using pBSKCheA1 as a template in an inverse PCR strategy as described previously (143). The outward-facing primers used were CheA1ΔTMX-F2 and CheA1ΔTMX-Rev. These primers also included BglII restriction sites at their 5′ ends to facilitate recircularization after inverse PCR, generating pBSKCheA1ΔTMX. These primers allowed for an in-frame deletion of the *tmx* region from nucleotide 66 to 215 of the *cheA1* sequence (GenBank accession number AAL47021.1). The *cheA1*D1055N mutant was generated using the QuikChange II site-directed mutagenesis kit (Stratagene), verified by sequencing, and then cloned into pCR 2.1 TOPO vector (Invitrogen). The putative *cheA1* promoter was

Table 6. Primers used in chapter 2

Primer Name	Sequence
CheOp-HindIII-F	5’ CCC*AAGCTT*CAGCGCGATGAACTGGTTGGACC
CheOp-BamHI-Rev	5’ CGC*GGATCC*CGTAATCAGACGGTCCTGGTTAG
CheA1ΔTMX-F2	5’ GA*AGATCT*GCGGTCGCGCGGAATTC
CheA1ΔTMX-Rev	5’ GA*AGATCT*GACCGCGTCCGCCGCACG
CheA1promXhoI-F	5’ CCG*CTCGAG*CAGCGCGATGAACTGGTT
CheA1DNupHindIII-R	5’ *AAGCTT*CACGGCGGTGACGTC
Sp245cheA1-F	5’GAATCACGTGACGTCGGA
Sp245cheA1-R	5’ CGACGCCGCGGCCCGACA
CheA1prom KpnI-F	5’ CGG*GGTACC*CAGCGCGATGAACTGGTTG
CheA1ΔREC XhoI-R	5’ *CTCGAG*TCATGGAGCGCCCTCTCC
GWCheA1-F	5’ GGGGACAAGTTTGTACAAAAAAGCAGGCTCAGCGCGATGAACTGGTT
GWCheA1-R	5’ GGGGACCACTTTGTACAAGAAAGCTGGGTTGCGGCACCTTTCTGCTCG
GWCheA1TMX-R	5’ GGGGACCACTTTGTACAAGAAAGCTGGGTTTCCACGTCGAGCAACGAC
Tlp1GWFwd	5’ GGGGACAAGTTTGTACAAAAAGCAGGCTCCGGCATGCGGATCAGGGC
Tlp1GWRev	5’ GGGGACCACTTTGTACAAGAAAGCTGGGTCCGGCCAGCCCACCGGGCGCCT

isolated from a plasmid containing full-length *cheA1* using CheA1promXhoI-F and CheA1DNup HindIII-R, which amplify a region upstream of the *cheA1* start codon. The promoter was then cloned into the pCR2.1 TOPO vector and sequenced for verification. The *cheA1*D1055N mutant and the *cheA1* promoter were then isolated by using restriction enzymes (HindIII and XbaI for isolating the *cheA1*D1055N fragment and XhoI and HindIII for isolating the *cheA1* promoter) and ligated into the pBBR1MCS3 cloning vector (144). The pBBRCheA1D1055N plasmid was then transformed into chemically competent *E. coli* S17-1 cells, followed by biparental conjugation into the *A. brasilense* Δ*cheA1* mutant background, as described previously (98). An *A. brasilense* strain Sp245 mutant derivative in which *cheA1* is inactivated was constructed as following. First, a 509-bp internal segment within the *cheA1* from *A. brasilense* strain Sp245, $cheA1_{Sp245}$, was amplified using Sp245cheA1-F and Sp245cheA1-R and then cloned into pCR 2.1 TOPO, sequenced for verification, cloned into the suicide vector pKGmob-cheA1 (Table 5), and introduced into *E. coli* chemically competent S17-1 cells (101, 145). Biparental mating was used to introduce the suicide vector carrying the internal $cheA1_{Sp245}$ fragment into the wild-type Sp245 strain, as described above. Single recombination mutation events were selected and verified by PCR, and a representative was used as an *A. brasilense* Sp245 Δ$cheA1_{Sp245}$ mutant derivative. To generate Δ*cheA1*(pBBRCheA1ΔREC), pBBRCheA1 was used as a template with the primers CheA1prom KpnI-F and CheA1ΔREC XhoI-R (Tables 5-6). The insert generated by PCR was digested with KpnI and XhoI, cloned into pBBR1MCS3, and digested with the same restriction enzymes. This vector was then transformed into *E. coli*

S17-1 chemically competent cells and mated into the *A. brasilense* Δ*cheA1* derivative via biparental mating as described above.

Fluorescence Tagging of CheA1 and its Variants

Gateway cloning (Invitrogen) and the pRH005 vector were used to construct all yellow fluorescent protein (YFP) fusions (105). The pRH005 vector allows cloning of any gene to generate products fused in frame with YFP at their C termini. All genes to be fused in frame with the YFP gene in pRH005 (*cheA1, cheA1*Δ*TMX, tmx, and tlp1*) were amplified by PCR using pBBRCheA1 or pBBRCheA1ΔTMX (*cheA1, cheA1*Δ*TMX, and tmx*) or Sp7 genomic DNA (*tlp1*) as a template along with the following primers: for amplification of *cheA1*, GWCheA1-F and GWCheA1-R; for amplification of *cheA1*Δ*TMX*, GWCheA1-F and GWCheA1-R; for amplification of *tmx*, GWCheA1-F and GWCheA1TMX-R; and for amplification of *tlp1*, Tlp1GWFwd and Tlp1GWRev (Table 6). The PCR products, flanked by gateway sites on 5′ and 3′ ends, were then introduced into pDONR221 (Invitrogen), via a BP Clonase reaction (Invitrogen) and transformed into *E. coli* OmniMax chemically competent cells following the manufacturer's recommendations (Invitrogen). The constructs were verified by sequencing prior to transfer into the pRH005 vector via an LR Clonase reaction, performed per the manufacturer's instructions (Invitrogen). Final constructs were introduced into wild-type *A. brasilense* strain Sp7 and Δ*cheA1* mutant backgrounds via biparental conjugation, as described above.

Fluorescence Imaging

All cells expressing fluorescently tagged proteins were prepared by growing them to low density (OD_{600} of 0.2 to 0.4) in 5 ml of MMAB supplemented with 10 mM malate. Cells from these cultures were then pelleted via centrifugation. Thirty microliters of concentrated cells were pipetted onto a 1% low-melting-point (LMP) agarose pad in 1X phosphate-buffered saline (PBS) with a coverslip and left undisturbed for 2 to 3 min. Images were acquired using the YFP or fluorescein isothiocyanate (FITC) filter on a Nikon ECLIPSE 80i fluorescence microscope with a Nikon CoolSnap HQ2-cooled charge-coupled device (CCD) camera.

Cell Length Measurements

Cells to be analyzed were grown at 28°C to mid-log phase (OD_{600} of 0.4 to 0.6) in 5 ml of liquid MMAB supplemented with 18.5 mM ammonium chloride, 5 mM malate, and 5 mM fructose (97). Cells were concentrated by centrifugation, stained with 1 μM FM4-64 vital fluorescent dye (Invitrogen Molecular Probes), incubated for 5 min in the dark, centrifuged at maximum speed for 1 to 2 min, and pipetted on top of 1% LMP agarose prepared in 1X PBS. Images were acquired using the tetramethyl rhodamine isocyanate (TRITC) filter on a Nikon ECLIPSE 80i fluorescence microscope with a Nikon CoolSnap HQ2-cooled CCD camera. Cell length measurements in micrometers were obtained using the Nikon NIS-Elements BR program from at least 50 cells per sample in four different fields of view.

Doubling Time

Cells were grown at 28°C to mid-log phase (OD_{600} of 0.4 to 0.6) either in 5 mL of liquid MMAB supplemented with 18.5 mM ammonium chloride and 10 mM malate and with tetracycline (10 μg/ml) or in 5 ml of liquid TY with the same supplements. Forty microliters of the liquid culture were inoculated into 260 μl of fresh MMAB with tetracycline (10 μg/ml), and the resulting cultures underwent a growth curve on a microplate reader. The absorbance (OD_{600}) of each sample was taken every 20 min for a total of 16 h, and the doubling time was calculated from the growth curve. All curves were determined in triplicate.

Cell Fractionation

Cultures were collected at log phase (OD_{600} of 0.4 to 0.6) via centrifugation at 10,000 × g for 10 min at 4°C, and the pellets were resuspended in 50 mM potassium phosphate buffer containing 2 mM $MgCl_2$ and 1 mM proteinase inhibitor phenylmethylsulfonyl fluoride (PMSF) (pH 7.0). Cells were then disrupted by passage through a French press three times at a cell pressure of 25,000 lb/in2. The cell lysate was centrifuged (Fiberlite F13-14 × 50cy fixed angle rotor) at 10,000 × g for 20 min at 4°C, and the supernatant centrifuged at 110,000 × g for 120 min at 4°C (Ti 50.2 fixed-angle ultracentrifuge rotor). The pellet was suspended in the phosphate buffer once more and centrifuged again at 110,000 × g for 120 min at 4°C. The membrane pellet was solubilized in 1X PBS with 2% Triton X-100 and 1 mM PMSF. Protein concentrations were measured for each sample using the Bradford assay (109), and each sample was adjusted to the same protein concentration prior to loading into the SDS-polyacrylamide gel. Cell fractions were verified as membrane or

cytosolic by differential staining with the hydrophobic molecular dye FM1-43, which is a lipophilic dye that fluoresces exclusively upon insertion into the cell membrane (Invitrogen Molecular Probes). The cell fractionated samples were mixed in a 1:1 ratio with the membrane-specific FM1-43 molecular dye (Invitrogen), incubated at room temperature for 15 min in the dark, and imaged by fluorescence microscopy using an FITC filter. Fluorescence intensity was compared between samples and with buffer controls exposed under similar conditions.

Western Blotting

For constructs containing the pBBR1MCS3 cloning vector, 50 ml of each sample were grown to mid-log phase (OD_{600} of 0.7 to 0.8) in liquid MMAB supplemented with 18.5 mM ammonium chloride, 10 mM malate, and tetracycline (10 μg/ml). Cells were pelleted and resuspended in 200 μl fresh radioimmunoprecipitation assay (RIPA) buffer. The cells were sonicated (Fisher Sonic Dismembrator model 100) for 30 s at a 3% amplitude of pulse, followed by a 1 min rest period, for a total of five cycles. Equal volumes of protein (15 μg) and 2X Laemmli buffer with reducing agent were placed on the heat block at 70°C for 8 min and loaded into the wells of a 7.5% Mini-Protean precast gel (Bio-Rad). The gel ran at 120 V for 90 min or until the dye front reached the reference line. The gel was then transferred to a 0.45-μm hydrophobic polyvinylidene difluoride (PVDF) transfer membrane (Immobilon) using a semidry transfer apparatus (Bio-Rad). The transfer ran at 15 V for 35 min, and then the membrane was air dried for 45 min. The membrane was washed in 1X Tris-buffered saline–Tween 20 (TBST) for 5 min at room temperature before being blocked for 1.5 h at room temperature in a 5% milk solution in 1X TBST. Afterwards,

the membrane was rinsed for 5 min in 1X TBST. For detection of CheA1 and variants, an anti-CheA1ΔTMX polyclonal antibody was purified using a negative-affinity protocol. Briefly, 25 ml of Δ*cheA1* cells was grown to mid-log phase and spun down. The pellet was resuspended in 0.1 M $NaHCO_3$ buffer (pH 8.3) supplemented with 0.5 M NaCl. Cells were then disrupted by passage through a French press three times at a cell pressure of 25,000 lb/in^2 and were centrifuged before the supernatant was collected. The whole-cell proteins were then immobilized onto activated Sepharose 4B beads during an overnight incubation of proteins and beads at 4°C. Unreacted proteins were washed with coupling buffer (0.1 M carbonate buffer, 0.5 M NaCl, pH 8.3), and unreacted groups were blocked by incubating the beads overnight at 4°C in 0.2 M glycine (pH 8.0). The beads were washed with coupling buffer, resuspended in 1X PBS, and loaded into a column. The column was equilibrated with 1X PBS before antiserum was passed through the column and collected. The flow-through was reapplied to the column three times to remove any contaminants and to concentrate the antibody. We further purified this flow-through by preparing a column containing immobilized whole proteins extracted from the Δ*che1* mutant, which lacked the entire *A. brasilense* Che1 operon (97), and passed the antiserum through the column. The resulting antibody was used at a 1:100 dilution, and a secondary antibody (Li-Cor donkey anti-rabbit IRDye 800CW) was applied at a 1:5,000 dilution for 1 h. Membranes were imaged on an Odyssey CLx infrared imaging system, and band intensities were quantified using ImageStudioLite software (4.0; Li-Cor). A minimum of four images from independent samples was used. For cell fractionated samples, a total volume of 100 ml of cells was grown to mid-log phase (OD_{600} of 0.7 to 0.8) in liquid MMAB supplemented

with 18.5 mM ammonium chloride and 10 mM malate before being fractionated as described above. Equal volumes of the membrane pellet, which was resuspended in 1X PBS with 2% Triton X-100, 1 mM PMSF, and 2X Laemmli buffer with reducing agent, were boiled for 5 min prior to being loaded, at an amount of 31 μg, into an 8 to 16% Mini-Protean precast gradient gel (Bio-Rad). The gel was run at 200 V for 30 min before being transferred to a 0.2 μM nitrocellulose membrane using a semidry transfer apparatus (Bio-Rad). The transfer was performed at 15 V for 25 min, followed by membrane washes in 1X TBST for 5 min at room temperature. The membrane was blocked for 1 h at room temperature in a 5% milk solution in 1X TBST and rinsed for 5 min in 1X TBST. For the cytosolic fraction, the same protocol was followed except that the samples were loaded at a concentration of 20.5 μg and run on a 10% Mini-Protean precast gel (Bio-Rad). For detection of CheA1 in the cell fractionated samples, an anti-CheA1ΔTMX polyclonal antibody, raised against soluble CheA1ΔTMX from *A. brasilense* strain Sp7 but not further purified against whole proteins extracted from the Δ*che1* mutant, was used at a 1:4 dilution, and a secondary antibody (Li-Cor donkey anti-rabbit IRDye 800CW) was applied at a 1:10,000 dilution for 1 h. Membranes were imaged on an Odyssey CLx Infrared imaging system. For whole-cell extracts, the same protocol as for cells bearing the pBBR1MCS3 cloning vector was used. Cells were grown as described above, and then 15 μg was loaded into the wells of a 7.5% gel Mini-Protean precast gel (Bio-Rad) and run at 120 V for 90 min or until the dye front reached the reference line. The gel was then transferred to a 0.45-μm hydrophobic PVDF transfer membrane (Immobilon) using a semidry transfer apparatus (Bio-Rad). The transfer to the nitrocellulose membrane was performed at 15 V for 35 min,

and the membrane was air dried for 45 min and then washed in 1X TBST for 5 min at room temperature. The membrane was blocked for 1 h at room temperature in a 5% milk solution in 1X TBST and rinsed for 5 min in 1X TBST. The same anti-CheA1ΔTMX polyclonal antibody, which was further affinity purified with immobilized whole protein extracts from the Δ*che1* strain (97) as described above, was used at a 1:100 dilution, and the secondary antibody (Li-Cor donkey anti-rabbit IRDye 800CW) was applied for 1 h at room temperature at a 1:5,000 dilution. Samples were imaged using an Odyssey CLx infrared imaging system, and band intensities were quantified using ImageStudioLite software.

Results

Domain Architecture Reveals Unique N-Terminal Fusion to CheA1

To determine how CheA1 from *A. brasilense* may regulate multiple cellular functions, we first analyzed its domain architecture. Compared to the canonical *E. coli* CheA, the *A. brasilense* CheA1 lacks a P2 domain, contains a second P5 domain, and carries a receiver (REC) domain at the C terminus (SM00448) (Fig. 29) (113). Strikingly, the *A. brasilense* strain Sp7 CheA1 also possesses an additional N-terminal domain, which we refer to here as TMX, predicted to be closely related to a polytopic hemolysin III-related (HlyIII) protein of unknown function (Fig. 29). This particular CheA domain appears to be unique to strain Sp7; the CheA1 homolog from the closely related *A. brasilense* strain Sp245 lacks the N-terminal TMX domain but is otherwise similar to the CheA1 of strain Sp7. TMX found at the N terminus of CheA1 from *A. brasilense* Sp7 is thus a unique feature of this protein in this particular strain.

The Presence of the N-Terminal TMX Domain is Associated with the CheA1-Dependent Cell Length Phenotype but is Dispensable for Chemotaxis

The different architectures of CheA1 in two closely related strains of *A. brasilense* prompted us to repeat the behavioral studies performed in strain Sp7 on strain Sp245. We constructed a derivative of strain Sp245 lacking the CheA1 homolog (Δ*cheA1*$_{Sp245}$) and analyzed chemotaxis and cell length phenotypes. We found that the Δ*cheA1*$_{Sp245}$ mutant was defective in chemotaxis: the average swarm diameter on a soft agar plate was 4.1 ± 0.03 mm for the wild type and 1.8 ± 0.02 mm for the Δ*cheA1*$_{Sp245}$ mutant. We also observed that the doubling times of Sp245 and the Δ*cheA1*$_{Sp245}$ mutant were different (6.7 ± 0.9 h for the wild type and 8.1 ± 0.8 h for the Δ*cheA1*$_{Sp245}$ mutant), suggesting that the difference in the chemotaxis ring diameter is likely the result of differences in doubling times, since growth is required to observe chemotaxis in this assay. To further evaluate potential chemotaxis defects, we analyzed the swimming pattern of free-swimming cells and found that the Δ*cheA1*$_{Sp245}$ mutant strain was able to reverse swimming direction at a rate similar to that for its parent (data not shown). This suggests that the CheA1 of strain Sp245 is not the major CheA homolog regulating all chemotaxis responses, which is similar to the CheA1 in strain Sp7 (97). Interestingly, mutating *cheA1*$_{Sp245}$ had no effect on cell length: the average length of cells in a population of the wild-type strain Sp245 and its Δ*cheA1*$_{Sp245}$ mutant was 2.6 ± 0.3 μm. Therefore, the phenotype of the Δ*cheA1*$_{Sp245}$ strain is similar to that of its Sp7 counterpart in that it has no major role in chemotaxis. However, it is distinct from the Sp7 Δ*cheA1* phenotype in that mutating *cheA1* in strain Sp245 does not cause a defect in cell length. These observations suggest that the CheA1-dependent cell length

phenotype observed in strain Sp7 is linked to the presence of the TMX domain. To further characterize the roles of TMX and other CheA1 domains in the control of cell length and chemotaxis, we generated *cheA1* mutants carrying either site-specific mutations of conserved residues or in-frame domain deletions (Fig. 30). Specifically, we analyzed the CheA1H252Q, a variant with a mutation in the putative autophosphorylation histidine residue previously implicated in CheA1 function during chemotaxis (96), as well as CheA1D1055N, which is mutated in the conserved putative phosphorylatable Asp1055 residue in the C-terminal REC domain of the protein. We also constructed and analyzed a strain expressing only the TMX domain, as well as strains expressing CheA1ΔTMX or CheA1ΔREC, which carry in-frame deletions of the TMX domain or the REC domain, respectively (Fig. 30). As previously described (97), the Δ*cheA1* mutant strain carrying an empty vector produced significantly shorter cells than the Sp7 wild-type strain. However, this defect was complemented by introducing a medium-copy-number plasmid carrying the full-length *cheA1* gene (pBBRCheA1) (Fig. 31). Expressing CheA1H252Q or CheA1ΔREC from a broad-host-range plasmid fully restored cell length to the Δ*cheA1* mutant strain, indicating that CheA1 autophosphorylation and its REC domain play no role in cell length control. In contrast, expressing a CheA1 variant in which *tmx* was deleted in frame (CheA1ΔTMX) failed to restore the cell length phenotype to the Δ*cheA1* mutant strain (Fig. 31). Surprisingly, expressing CheA1D1055N or TMX alone in the Δ*cheA1* strain not only restored but further increased the cell length (Fig. 31). The effect of TMX on cell length could possibly result from altered growth rates of the strains carrying these vectors. To address this, doubling times of strains expressing these CheA1 constructs were

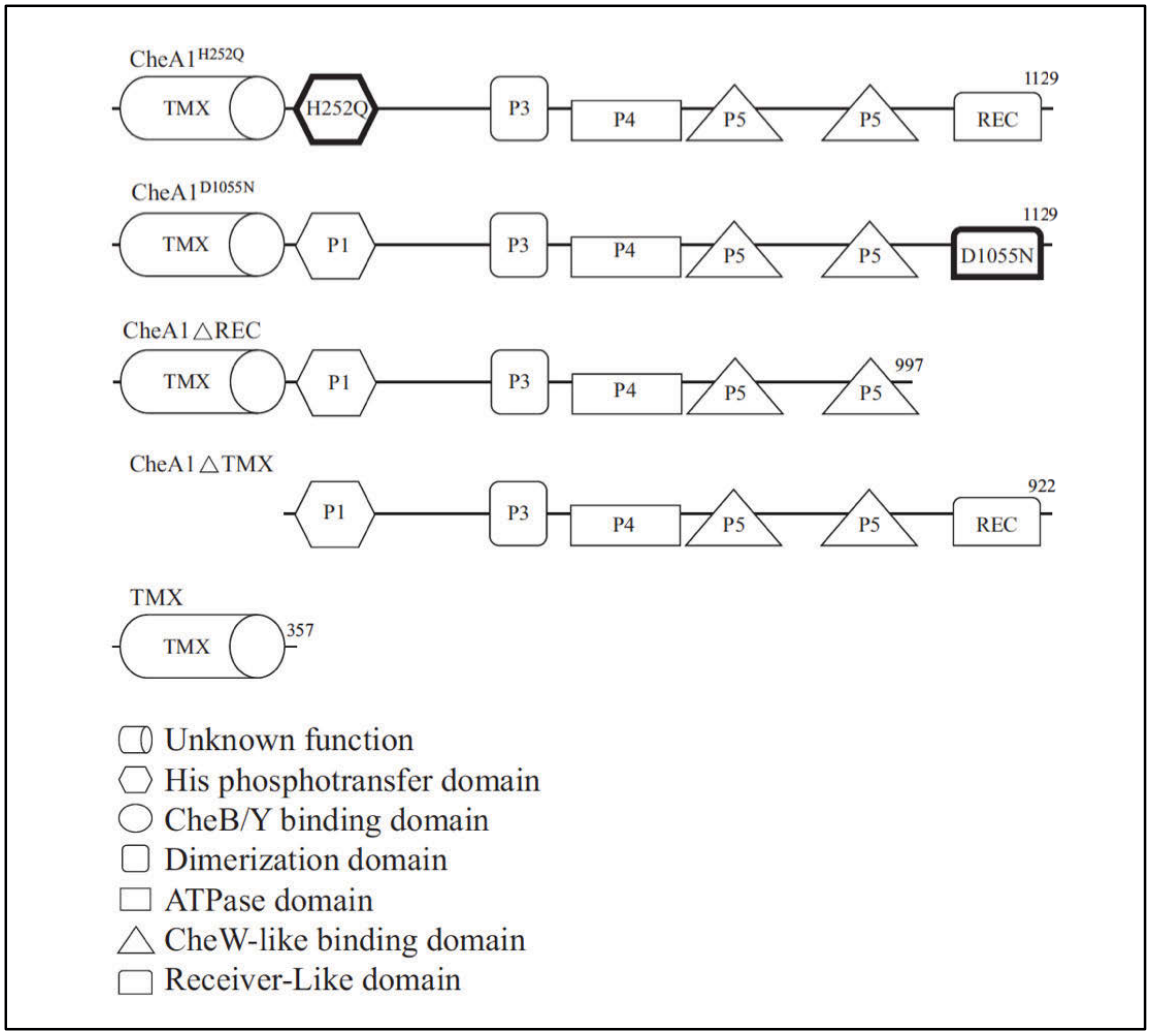

Figure 30. Representation of CheA1 variants constructed for this study

Schematic representation of *A. brasilense* strain Sp7 CheA1 variants used in this study. Variants with single-residue replacements (CheA1H252Q and CheA1D1055N) are in boldface. Each shape is indicative of a different putative domain of CheA1whose functions are described in the legend at the bottom left corner of the figure.

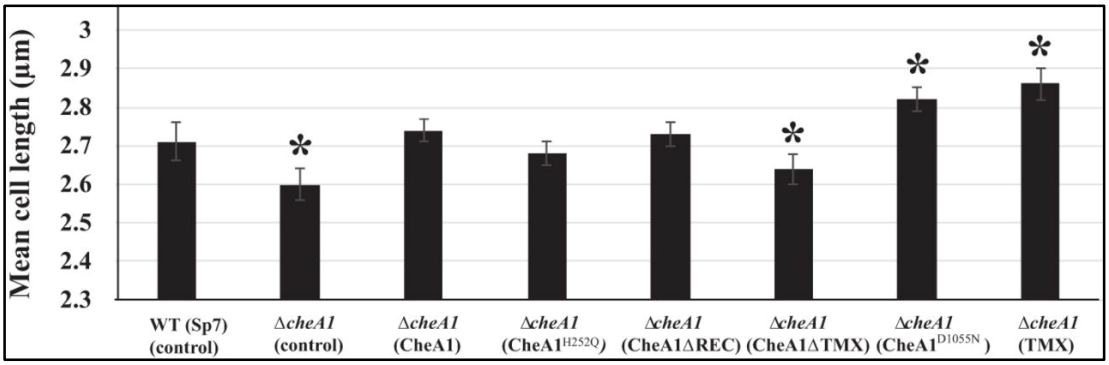

Figure 31. Role of CheA1 domains in cell length regulation

Roles of different domains of CheA1 in cell length regulation. *, statistically significant difference in average cell lengths relative to that of the wild-type strain, at a P value of < 0.05 (n = 50) by Student's t test. All values are an average of at least three biological replicates.

determined. The wild-type Sp7(pBBR) (control) strain doubled faster (2.6 ± 0.4 h) than any of the Δ*cheA1* mutant derivatives, but all Δ*cheA1* mutant derivatives had doubling times which were not significantly different from each other. The doubling times were 4.7 ± 0.3 h for the Δ*cheA1*(pBBR) mutant, 5.6 ± 0.5 h for the Δ*cheA1*(pBBRCheA1) mutant, 4.8 ± 0.5 h for the Δ*cheA1*(pBBRCheA1H252Q) mutant, 4.6 ± 0.2 h for the Δ*cheA1*(pBBRCheA1ΔREC) mutant, 4.8 ± 0.5 h for the Δ*cheA1*(pBBRCheA1ΔTMX) mutant, 5.3 ± 0.7 h for the Δ*cheA1*(pBBRCheA1D1055N) mutant, and 4.6 ± 0.2 h for the Δ*cheA1*(pBBRTMX) mutant. These data suggest that the cell length phenotype, which is different in the strains expressing these constructs (Fig. 31), is not directly the result of impaired growth. We also considered the possibility that membrane-bound CheA1 variants could have indirect effects on cell length due to altered protein expression levels from the medium-copy-number plasmid, including protein degradation. To test this, we used a polyclonal antibody raised against soluble CheA1 (CheA1ΔTMX) and Western blots to compare levels of protein expression in the wild type and the Δ*cheA1* mutant strains expressing membrane-bound CheA1 variants (Fig. 32). As expected, the anti-CheA1ΔTMX antibodies recognized a single large band, at the predicted molecular weight, in all strains except the Δ*cheA1* mutant control. Comparing the CheA1 band intensity across the samples revealed that, relative to the wild-type Sp7 strain carrying an empty vector control, the Δ*cheA1* mutant derivatives expressed CheA1 and its variants at levels that were comparable between them and represented about twice the levels of CheA1 detected in the wild type. Specifically, CheA1, CheA1H252Q, CheA1D1055N, and CheA1ΔREC expression levels were on average 1.8, 1.9, 2.0, and 2.2 times the wild-type

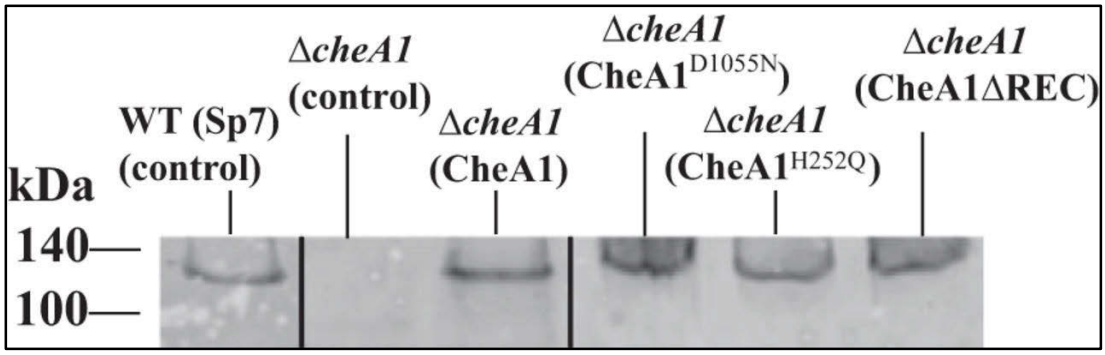

Figure 32. Expression of CheA1 in *A. brasilense* and mutant derivatives

Detection of CheA1 in whole-cell lysates of *A. brasilense* wild-type strain Sp7 and its Δ*cheA1* mutant derivatives expressing CheA1 and its variants from a plasmid by Western blotting. The mutant derivatives were expressing CheA1, variants with single-amino-acid residue replacements, or truncated variants of the protein from a medium-copy-number broad-host-range plasmid. A polyclonal antibody raised against CheA1ΔTMX was affinity purified as described in Materials and Methods prior to use. Each well is identified with the strain and with the parental or variant protein expressed from the broad-host-range vector in parentheses. The black lines indicate junctions separating lanes that were spliced from the original image in order to show samples run on the same gel in a single row.

levels, respectively. Based on these data, we hypothesize that TMX may also be produced at about twice the native levels under these conditions. Despite the observation that the expression of CheA1, or its variants, from the pBBR vector yielded about twice the amount of protein produced under native conditions, we did not see any evidence of degradation. Furthermore, all strains expressed similar CheA1 levels, but they each produced different cell length phenotypes, with expression of CheA1 or CheA1H252Q restoring the wild-type cell length phenotype while expression of CheA1D1055N or CheA1ΔREC caused an increase beyond the wild-type cell length. These data argue against altered protein expression levels causing the cell length phenotypes and rather suggest that it is the presence of TMX in CheA1 of *A. brasilense* strain Sp7 that is associated with the effect on cell length.

We then assessed TMX's role in chemotaxis through soft agar assays of the wild-type, Δ*cheA1* mutant, and mutant derivatives (Fig. 33A). Chemotaxis was fully restored when CheA1 or CheA1ΔTMX was expressed from the medium-copy-vector in the Δ*cheA1* mutant background (Fig. 33A). However, a plasmid expressing only the TMX domain was unable to restore chemotaxis and, in fact, appeared to inhibit chemotaxis. In *A. brasilense* strain Sp7, CheA1 controls transient increases in free-swimming cell speed in response to attractants, such as oxygen. Therefore, we also analyzed the same CheA1 alleles in a temporal gradient assay for aerotaxis (Fig. 33B). Similar to the response of the wild-type strain carrying an empty vector, expressing CheA1 or CheA1ΔTMX in the Δ*cheA1* mutant strain resulted in statistically significant increases in the swimming speed in response to a switch from anaerobiosis to air (Fig. 33B). As expected, a Δ*cheA1* mutant strain carrying

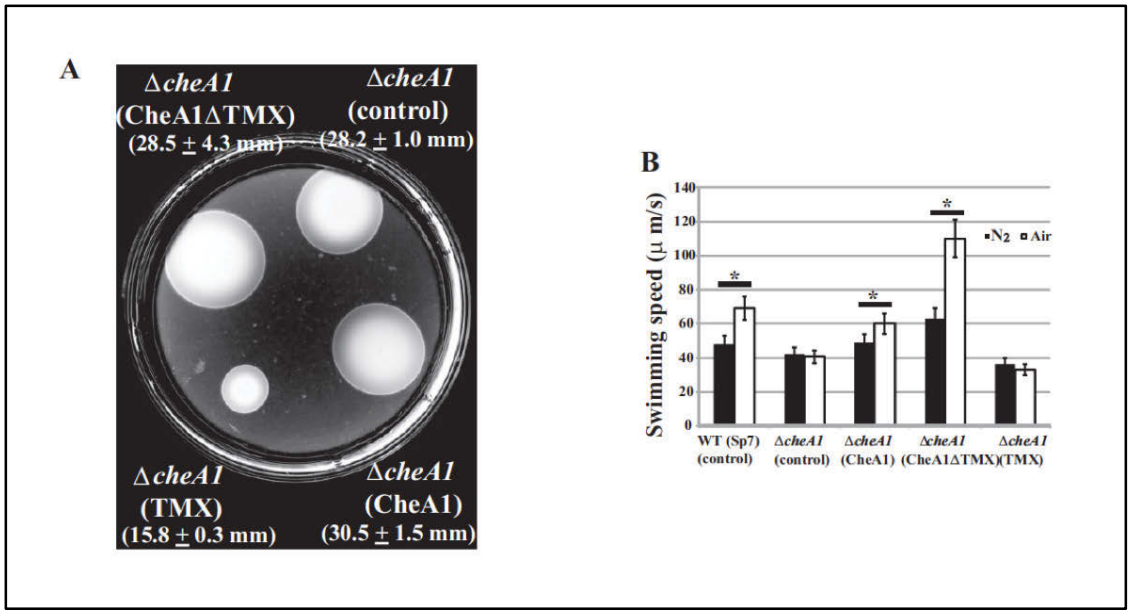

Figure 33. Soft agar assays of chemotaxis domains and swimming speed analysis

Roles of unique domains of *A. brasilense* strain Sp7 CheA1 in chemotaxis. (A) Chemotaxis of the Δ*cheA1* mutant strain expressing CheA1 or truncated versions of this protein from a broad-host-range plasmid was analyzed in the soft agar plate assay supplemented with appropriate antibiotics. The chemotaxis of the wild-type strain Sp7 carrying an empty vector control [Sp7(pBBR)]; not shown) was similar to that of the Δ*cheA1*(pBBRCheA1) strain, and the average ring diameter was 30.2 ± 2.9 mm. The picture was taken at 48 h post-inoculation. The average ring diameters obtained from three replicates are shown. (B) The temporal gradient assay for aerotaxis was used to measure transient increases in cell swimming speed upon switching free-swimming cells from an anaerobic atmosphere (nitrogen gas) to air. Each strain is identified, with the parental or variant protein it expresses from the broad-host-range vector in parentheses. *, statistically significant difference in the swimming speed between before and after switching to air ($P < 0.05$ by Student's t test).

an empty vector lacked this response. A similar defect was also observed when the TMX domain was expressed alone from a plasmid in this mutant. Together, the results suggest that TMX present within CheA1 in *A. brasilense* strain Sp7 is dispensable for chemotaxis.

CheA1 is Produced as Two Isoforms

The results above were puzzling regarding how distinct domains of CheA1 could function in chemotaxis or cell length regulation with no obvious functional overlap. Further, the presence of the predicted polytopic TMX domain at the N terminus of CheA1 suggested that CheA1 from *A. brasilense* may be anchored to the membrane, a proposition which, if confirmed, would challenge existing paradigms regarding the subcellular assembly of chemotaxis signaling complexes, namely, that CheA is a soluble protein which interacts with chemoreceptors at cell poles (60, 146). To address this issue, we analyzed whole-cell extracts of the wild-type strain and the Δ*cheA1* mutant derivative using a Western blot and affinity-purified anti-CheA1 antibodies raised against soluble CheA1 (CheA1ΔTMX). This analysis revealed the presence of two bands present exclusively in the wild-type lysates and absent from the Δ*cheA1* mutant lysates (Fig. 34). The molecular mass of the full-length CheA1 from strain Sp7 is predicted to be 120 kDa, which we detected as a thick band on whole-cell extracts. In addition, a very faint band that migrated at around 100 kDa was also detected in the whole-cell lysates of the wild-type strain. Similar Western blot analyses of whole-cell lysates of several *Azospirillum* strains, for which the genome is sequenced and not predicted to encode a membrane-anchored CheA1, revealed only one unique cross-reacting band at about 100 kDa (data not shown). Given the specific detection of this large band in Sp7 with antibodies raised against the soluble CheA1ΔTMX and the

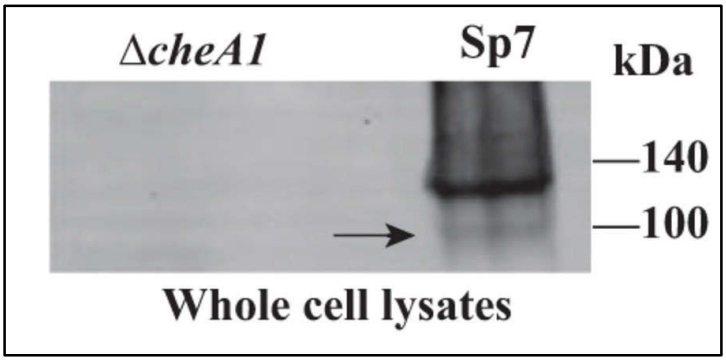

Figure 34. Western blot of CheA1 whole cell lysates

Detection of CheA1 in whole-cell lysates of the wild type and the Δ*cheA1* mutant were probed with affinity-purified polyclonal antibodies raised against a recombinantly produced soluble CheA1ΔTMX from *A. brasilense* Sp7.

fact that the N-terminal TMX domain is predicted to encode a protein with seven membrane-spanning segments, we hypothesize that the high-molecular-weight band detected in whole-cell lysates of the wild type corresponds to a full-length CheA1 containing the TMX domain and the smaller band corresponds to a soluble CheA1 without the TMX domain. We used cell fractionation to further investigate the subcellular localization of CheA1 (Fig. 35). A broad band at around 120 kDa, likely corresponding to full-length CheA1, was found exclusively in the membrane fraction of strain Sp7 and was absent in the soluble fraction of this strain or in the lysates of the Δ*cheA1* mutant treated under similar conditions. Analysis of the proteins produced in the soluble fractions of the wild-type strain indicated the presence of a single band corresponding to a product at about 98 kDa that was absent from both the membrane fraction and the Δ*cheA1* lysates (Fig. 35). The predicted molecular mass of a soluble CheA1 produced without the N-terminal TMX domain is 98 kDa, suggesting the presence of a soluble CheA1 in *A. brasilense* strain Sp7. We note that the samples corresponding to the soluble fraction analyzed here were also more concentrated than the whole-cell lysates or the membrane fraction (Fig. 35), underscoring the low concentration in cells. Based on this observation, we surmise that a soluble CheA1 isoform is present in the cytoplasm of *A. brasilense* at relatively low concentrations compared to the membrane-bound isoform. To determine the relative abundance of bands detected in the Western blots, we used densitometry analysis and found that the thicker band migrating at 120 kDa was about 11-fold more intense than the smaller band. Together, these data indicate that CheA1 from *A. brasilense* strain Sp7 is produced in two isoforms: a membrane-bound form corresponding to a full-length CheA1 anchored

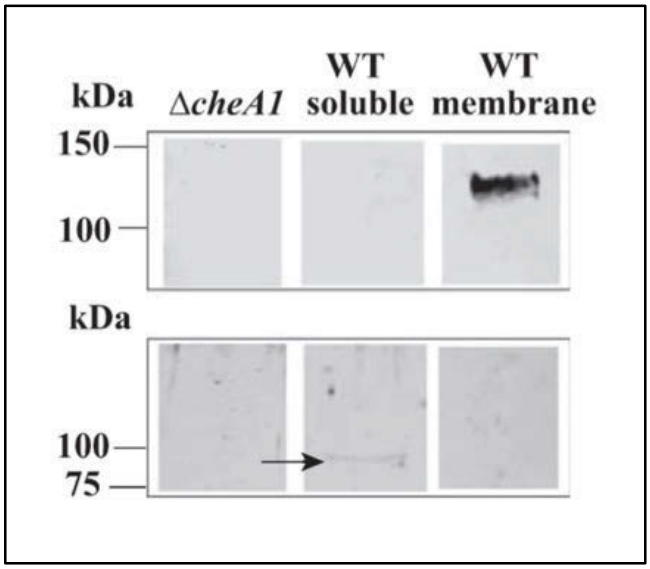

Figure 35. Cell fractionation and western blot analysis of *A. brasilense* Sp7

Detection of CheA1 in different subcellular fractions collected from the wild-type strain Sp7 were probed with affinity-purified polyclonal antibodies raised against a recombinantly produced soluble CheA1ΔTMX from *A. brasilense* Sp7. Note that different protocols were used for sample preparation and SDS-PAGE for the Western blots shown in panels A and B (see Materials and Methods). An anti-CheAΔTMX antibody which had not been further purified against whole proteins extracted from the Δ*che1* mutant was used. The membrane fraction was resuspended in a solubilizing buffer (1X PBS with 2% Triton X-100 and 1 mM PMSF) and run on an 8 to 16% gradient gel before being transferred to a nitrocellulose membrane. For the cytosolic fraction, these samples were concentrated via acetone precipitation before being loaded in a 10% gel and transferred to a nitrocellulose membrane. The numbers on the left indicate the positions of the molecular mass markers run on the same gels. The arrows point to the soluble, faint band corresponding to CheA1ΔTMX.

to the membrane via the polytopic TMX domain and a soluble form corresponding to CheA1 lacking the TMX domain and that most resembles the architecture of CheA homologs from other organisms.

The CheA1 Isoforms Localize to the Cell Surface and to the Cell Poles

To corroborate the cell fractionation data, we constructed and expressed, from broad-host-range plasmids, fluorescently tagged versions of the full-length CheA1 (CheA1-yellow fluorescent protein [YFP]), of CheA1ΔTMX (CheA1ΔTMX-YFP), and of isolated TMX (TMX-YFP). The fluorescent constructs were expressed in both the wild-type strain Sp7 and the Δ*cheA1* mutant backgrounds. The constructs were functional in that they restored the wild-type phenotype in cell length regulation and chemotaxis to a Δ*cheA1* mutant strain (Fig. 36). In both backgrounds, CheA1-YFP was diffuse throughout the cells with occasional foci, both polar and nonpolar, that were relatively dim and seen best when expressed in the Δ*cheA1* strain background (Fig. 37). In contrast, CheA1ΔTMX-YFP was present as punctate foci at the cell poles in both strain backgrounds (Fig. 37). The localization of TMX-YFP, expressed in either the Sp7 or Δ*cheA1* strain background, was diffuse throughout the cell, although occasional punctate foci were observed though they did not appear to localize in any particular region of the cell surface (Fig. 37). The localization of CheA1ΔTMX-YFP at the cell poles was similar to the localization of a chemotaxis receptor Tlp1-YFP, which was previously shown to function in chemotaxis (147). Quantitative evaluation of the distribution of fluorescence in the cell population expressing CheA1-YFP, CheA1ΔTMX-YFP, and TMX-YFP corroborated these observations (Fig. 38). In addition, cells expressing CheA1-YFP displayed localization

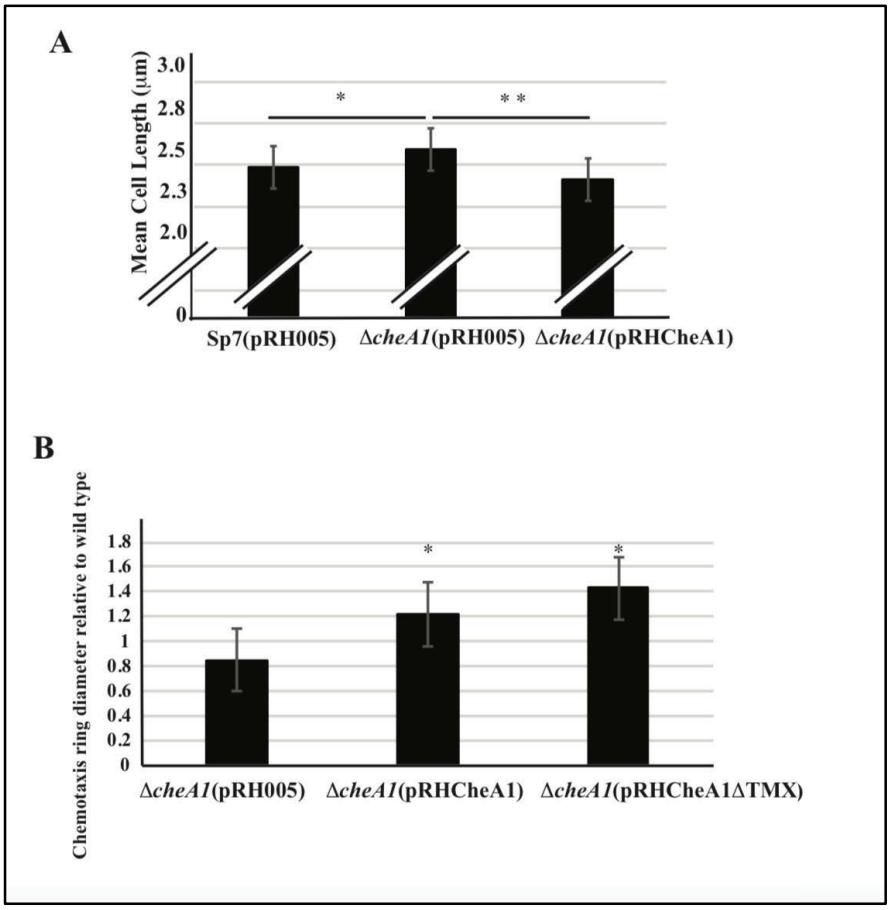

Figure 36. Analysis of fluorescent fusions of CheA1 and variants showing functionality

Fluorescent fusions between different alleles of CheA1 and YFP are functional. The fluorescent constructs were expressed from the native *cheA1* promoter on a broad host range plasmid, prH005. The constructs were analyzed for the ability to restore the wild type cell length (A) and chemotaxis in the soft agar plate assay (B). The data are means obtained from a minimum of 100 cells (cell length; panel A) and 9 replicates (chemotaxis, panel B). An (*) or (**) represent statistically significant differences at the $p < 0.05$ or $p < 0.005$ levels, respectively (Student's t test). In panel B, the chemotaxis phenotypes are compared to that of the Δ*cheA1*(prH005) strain.

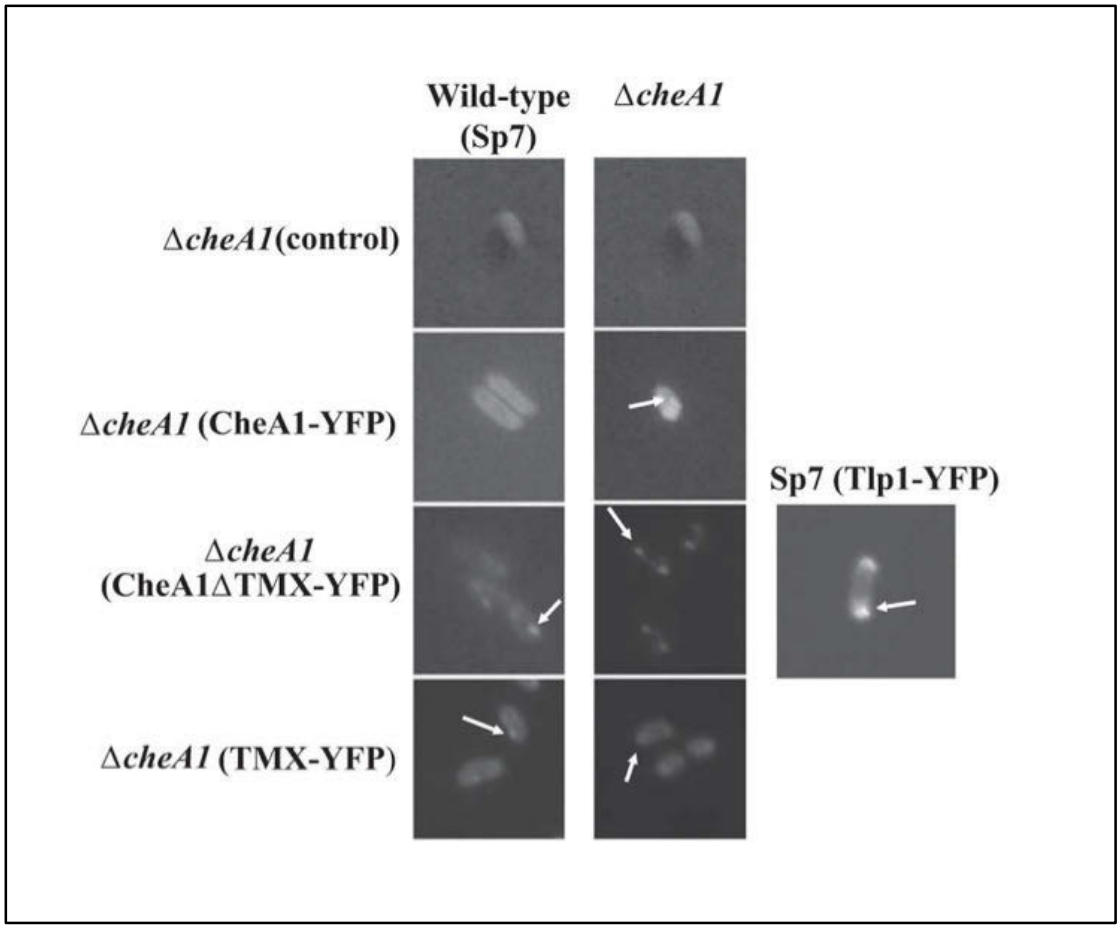

Figure 37. Fluorescence images of CheA1 and its variants in *A. brasilense*

Representative fluorescence microscopy images. The fluorescent constructs were expressed from the native *cheA1* promoter on a broad-host-range plasmid, pRH005. For expression of Tlp1-YFP, the fusion was expressed from the lac promoter present on the pRH005 vector backbone. Arrows indicate punctate foci in cells.

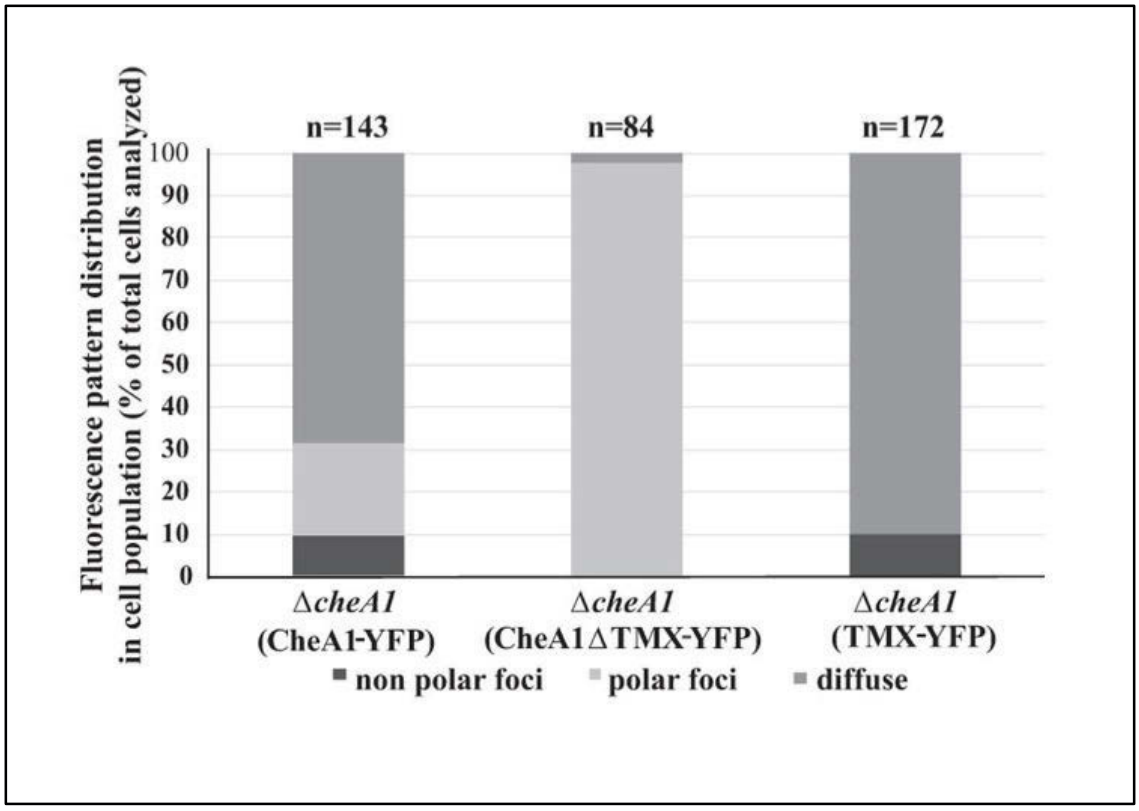

Figure 38. Quantification of the localization of the cell population of CheA1 variants

Quantitation of the distribution of fluorescence in the population of cells analyzed. Each strain is identified, with the variant protein fusion to YFP expressed from the broad-host-range vector in parentheses. The total numbers (n) of cells analyzed are shown on the graph. The cells included in the analysis were imaged from at least 3 independent cultures.

patterns more consistent with those seen in cells expressing TMX-YFP, presumably corresponding to the higher level of membrane-anchored CheA1-YFP relative to that of the soluble, polar-localized CheA1ΔTMX isoform. Together, these data are consistent with the hypothesis that the soluble isoform of CheA1 localizes as polar clusters while the full-length CheA1 localizes independently to the cell surface via the N-terminal TMX domain.

Discussion

Here we provide experimental evidence supporting a model for the multifunctional role of CheA1 from *A. brasilense* Sp7 in regulating chemotaxis and cell length at division (96, 97). In all Bacteria and Archaea analyzed to date, the chemotaxis receptors assemble together with cytoplasmic chemotaxis proteins, including CheA homologs, at the cell poles, where they form complex signaling arrays which function to amplify and propagate signals (60, 64, 65, 146). The soluble CheA1 isoform from the Sp7 strain studied here localized at the cell poles, consistent with its function in chemotaxis. The full-length, membrane-anchored CheA1 was distributed throughout the cells, with no apparent distinct localization. Given its localization on the cell surface, the function of the membrane-anchored CheA1, while unknown, is expected to be independent of the chemotaxis signaling function of the protein, consistent with results obtained here. This hypothesis is further supported by the observation that chemotaxis receptor mutants that were shown to signal (e.g., Tlp1 [(99)] and AerC [(107)] and localize at the cell poles (AerC [(107)]) in a Che1-dependent manner do not display any cell length phenotype, similar to those produced as a result of mutations in *cheA1* (97).

Our results suggest that the N-terminal TMX domain of CheA1 from strain Sp7 plays a role in modulating cell length. Deletion of the sequence corresponding to TMX from CheA1 yielded alleles unable to restore the wild-type cell length phenotype to the Δ*cheA1* mutant, but expression of TMX alone rescued this phenotype. TMX is a conserved, single-domain protein of unknown function that is homologous to a hemolysin III-related (HlyIII) protein in *Bacillus cereus* (148, 149). Some evidence, obtained using recombinantly expressed HlyIII proteins in the heterologous *E. coli* background, suggested that HlyIII-related proteins function as hemolysins (150), but their presence in all bacteria makes this hypothesis unlikely. The function of HlyIII proteins has not been conclusively determined (151), but they were shown to be distant homologs of AdipoR receptors found in yeasts and humans (151), the function of which also remains to be established. The data obtained here suggest that TMX, as shown here fused to the *A. brasilense* CheA1 protein, may have a function that ultimately alters how cells control cell length, but a direct role for TMX as a cell length regulator has yet to be established. Whether this is a conserved function of HlyIII-related homologs also remains to be determined.

Interestingly, expression of TMX alone or a mutation replacing the conserved aspartate residue within the CheA1 REC domain (D1055) yielded strains that were even longer than the wild-type strain. This is unexpected, and it also suggests possible features for TMX function. First, the deletion of the REC domain in CheA1ΔREC did not have this effect on the cell length phenotype, suggesting that it is not a direct function of the REC domain. The cell length phenotype of the CheA1D1055N mutant supports our findings that CheA1 is produced as a full-length, membrane-anchored isoform, and it further suggests that

phosphorylation of the conserved aspartate residue within the REC domain has a regulatory role in the TMX output. This is consistent with the previously described functions of REC domains as regulatory modules in other hybrid histidine CheA homologs (152, 153). For example, mutating the REC domain of CheA3, which is involved in controlling cyst development in the closely related *Rhodospirillum centenum*, causes a loss of regulation of cyst formation, as those mutant derivatives produce more cysts than wild-type cells do (77, 153). One interpretation of our data in light of these previous findings is that phosphorylation of D1055 causes a conformational change within the full-length, membrane-anchored CheA1, which ultimately alters the ability of TMX to interact with the target protein(s), thereby affecting the cell length phenotype. The effect of expressing TMX alone, from a plasmid, on cell length is also consistent with interfering with protein-protein interactions that TMX may be engaged in for its function. This hypothesis is also consistent with previous data showing that other mutations within Che1 proteins (e.g., CheY1) that interact with CheA1 also affect cell length bias (97). Interactions of Che1 proteins with CheA1 are expected to depend on canonical CheA1 domains, which are present in both the soluble and the membrane-anchored CheA1 isoforms. Together, the data thus suggest that the function of TMX in regulating cell length in *A. brasilense* Sp7 may depend on interactions with other proteins.

The existence of CheA isoforms in chemotactic bacteria is not a new concept; *E. coli* produces CheA in two isoforms by utilizing a second translational start site (154, 155). What is unique about the CheA1 isoforms in *A. brasilense* strain Sp7 is that each isoform contributes to the regulation of two unrelated cellular functions. How the two CheA1

isoforms in *A. brasilense* are produced remains to be determined. Unlike in *E. coli*, there is no evidence for the presence of a ribosome binding site that would permit initiation of translation of the soluble CheA1 isoform (108, 154). Other possible mechanisms include transcriptional regulation from an alternative promoter as well as posttranscriptional and/or posttranslational processing. Further experimental investigation is required to establish the exact molecular mechanism involved in the production of these two isoforms. Our data indicate that the insertion of the polytopic TMX domain at the N terminus of CheA1 of *A. brasilense* strain Sp7 is a recent event. None of the other *Azospirillum* species strains sequenced to date shows evidence of a similar domain insertion (95, 156-160). In fact, the draft genome of an Sp7 strain generated by a team of South Korean scientists also lacks the TMX fusion to CheA1 (NCBI BioProject PRJNA293508). *A. brasilense* genomes are organized as 7 replicons: one chromosome and 6 large plasmids named p1 through p6 (34–39). The DNA regions coding for CheA1 and for TMX are both located on the largest plasmid, p1, in all *A. brasilense* strains with available genome sequences, but they are not adjacent and are separated by several kilobases, precluding a simple frameshifting or slippage mutation between adjacent genes. Genome plasticity and extensive genomic rearrangements are evidenced in the *Azospirillum* genomes sequenced to date, including those of several strains of *A. brasilense* (95, 156-159). These include the lack of synteny between replicons of strains from the same species, the abundance and density of insertion sequence IS elements in all genomes, and evidence of plasmid loss or rearrangements and of repeated phage infections. The recent TMX acquisition by CheA1 of strain Sp7 is also supported by the lack of functional divergence between CheA1 proteins of different *A.*

brasilense strains. Our results show that the minor role of the soluble CheA1 in *A. brasilense* Sp7 chemotaxis (96) is conserved in strain Sp245, in which the fusion event between TMX and CheA1 has not occurred. Comparative genome analysis of diverse bacteria shows that most domain acquisition events that generate novel multidomain protein architectures occur at the N or C termini of proteins (161). The insertion of TMX at the N terminus of CheA1 from strain Sp7 is consistent with these observations, but the mechanism involved is unknown. Analyses of protein domain fusion or insertion events in completely sequenced genomes of closely related organisms have been previously used to predict protein-protein interactions (162). However, we have no evidence that TMX and CheA1 functionally interact. Our results here show that the domain acquisition event that fused TMX to CheA1 resulted in both protein functions being maintained through the production of two CheA1 isoforms. While we do not know how TMX exerts its effect on cell length, this function is not obviously related to the control of the motility pattern mediated by CheA1. Mechanistic insight into how TMX functions to regulate cell length in *A. brasilense* should provide conclusive experimental evidence regarding a possible functional relationship.

CHAPTER III
TMX: A UNIVERSAL REGULATOR OF MEMBRANE FLUIDITY

Text and figures were taken from the following:

Gullett JM, A, Hubler, F. Barrera, and Alexandre G. 2017. TMX: A universal regulator of membrane fluidity. *Nature Communications*. Manuscript in preparation.

Author contributions to this work included: JMG, FB, GA designed research; JMG, AH, performed research; JMG, FB, GA analyzed data; JMG, GA wrote the paper.

Abstract

Bacterial membranes are composed of phospholipids, which have two hydrophobic fatty acid chains linked to a hydrophilic polar head group. The nature of these phospholipids, specifically the fatty acid chains, determines the membrane fluidity. In response to abiotic stressors such as temperature change, bacteria modify the characteristics of their membrane to maintain appropriate fluidity. A membrane must be able to alter its fluidity during environmental changes or essential cell functions may suffer. Though it is known that the regulation of fatty acid biosynthesis is coupled with temperature, little is known about how this actually occurs or how these bacteria even sense the shift in temperature. Here, we identify an *E. coli* homolog of the PAQR family, TMX, which controls membrane fluidity as a response to temperature shifts. We also demonstrate that this effect is not limited to *E. coli* but also present in *Bacillus subtilis* as well, pointing to TMX as a universal fluidity sensor.

Introduction

Cellular membranes are essential to cell viability. The major molecules found in membranes are phospholipids, which consist of hydrophobic fatty acid chains linked to polar head groups. The nature of fatty acids and polar head groups vary, conferring the

membrane with various biophysical properties including changes in fluidity. Maintaining optimum membrane fluidity is crucial: a membrane too stiff or too fluid will not support the insertion and folding of proteins into the membrane or the activity of transmembrane and membrane-associated proteins (163). Environmental conditions, such as temperature change, affect membrane fluidity and alter essential functions. When the external temperature increases or decreases, bacteria adjust the composition of fatty acids in their membrane to adjust membrane fluidity (1, 3, 164). Similarly, antibiotic resistances can, and frequently do, emerge due to modifications of the bacterial membrane (165-168). The structures of fatty acids largely determine membrane fluidity. Bacteria have evolved the ability to regulate the fatty acid composition of the membrane in response to environmental challenges. Synthesis of fatty acids is well established in bacteria, especially in the model organism *Escherichia coli* which performs fatty acid biosynthesis using eight cytoplasmic enzymes via the Fatty Acid Synthase II system (169).

We have identified a protein, TMX, which regulates membrane fluidity in *E. coli*. TMX is predicted to have seven-transmembrane domains with an intracellular N-terminus, opposite of the orientation of GPCRs. These transmembrane regions are highly conserved, hydrophobic domains but vary in their amino acids (151). In *E. coli*, TMX is a protein of unknown function, spanning 219 amino acids in length with a predicted molecular weight of 24 kD. It is a homolog of the Progestin and AdipoQ (PAQR) receptor family which includes three classes: PAQR receptors related to hemolysin-III proteins, adiponectin (AdipoQ) receptors, and membrane progesterone receptors. Here, we demonstrate that the

E. coli homolog of the PAQR family functions to control membrane fluidity as a response to temperature shifts.

Materials and Methods

Membrane Staining

E. coli cells were grown in Luria broth (LB) to an $OD_{600} \leq 0.3$ before pelleted using a tabletop centrifuge at 5,000 rpm for 3 min. Cells were washed with minimal medium (M9) and centrifuged as described above. The pellet was resuspended in 500 mL M9 and stained with FM4-64 and/or FM1-43 per manufacturer's protocol (ThermoFisher). Ten microliters of the stained cells were placed on a microscope slide with a coverslip coated in poly-L lysine. Cells were imaged after 15 min using either the TRITC (Texas Red Isothiocyanate) filter, staining with FM1-43 was visualized with the FITC (Fluorescein Isothiocyanate) filter set. Photographs were taken using a Nikon ECLIPSE 80i fluorescence microscope equipped with a Nikon CoolSnap HQ2 cooled CCD camera.

Fatty Acid and Phospholipid Analysis

Fatty acid analysis of *E. coli* and *B. subtilis* were performed by Microbial ID (Newark, DE). For *E. coli* cells, various growth conditions were analyzed including growing the cells at different temperatures (28°C or 37°C), growing the cells to different growth stages ($OD_{600} \leq 0.2$ or $OD_{600} \leq 1.0$), and growing the cells with different carbon sources (minimal media with10 mM succinate or 10 mM glucose). *B. subtilis* was grown in NB media to a low optical density ($OD_{600} \leq 0.2$) at either 28°C or 35°C. Cells were collected and sent for analysis. Polar head group analysis was performed by the Biological and Small Molecule

Mass Spectrometry Core (UTK). Samples were prepared as described for the fatty acid analysis.

DPH Anisotropy

Bacterial cultures were grown overnight at 37ºC in 5 mL minimal media while shaking at 200 rpm. The OD_{600} was determined for each culture and diluted to 0.05. Aliquots of 3 mL samples were prepared; the samples prepared consisted of bacteria at the desired absorbance of 0.05 and diphenylhexatriene (DPH) dissolved in DMSO at a final concentration of 7 μM. Cultures with DPH incubated for 1 hr at 30ºC while shaking at 130 rpm. Samples were transferred to a 3 mL transparent cuvette. Fluorescence anisotropy measurements were performed in a Quanta Master fluorometer (Photon Technology International). The excitation for DPH was 350 nm, and the emission was at 440 nm. The excitation and emission polarizer positions were HV, HH, VH, and VH, where vertical (V) was 90 degrees, and horizontal (H) was 0 degrees. The slits were set to 6 nm (emission) and 6 nm (excitation). Steady-state fluorescence anisotropy, r, was calculated using PTI FelixGX software and the following equation: $r = I_{VV} I_{HH} - I_{HV} I_{VH} / I_{VV} I_{HH} + 2 (I_{HV} I_{VH})$.

Immunolocalization

E. coli cells were grown in M9 minimal media supplemented with 0.4% glucose, and *B. subtilis* cells were grown in NB, each to a low cell density ($OD_{600} \leq 0.3$). Collected cells were first washed and resuspended in 100 μl 1X PBS, then fixed in 1 ml of ice cold

methanol for 1 hr at -20ºC. Afterwards, cells were placed on poly-L-lysine coated coverslips and allowed to dry (about 10 min). Cells were then gently lysed using a 2 mg/ml lysozyme solution in GTE buffer (50 mM glucose, 20 mM Tris-HCl pH 8.0, 10 mM EDTA) for 10 min, prior to incubation overnight at 4ºC in a blocking solution consisting of 1% non-fat dry milk in 1X PBS, pH 7.0. Next, coverslips were washed twice with 1X PBS, prior to adding the antibody solution consisting of 1% non-fat dry milk in 1X PBS with a 1:300 antibody concentration. Coverslips were incubated in the antibody for 2 hr at room temperature in the dark, then washed 10 times with 1X PBS. Next, the coverslips were incubated with an Alexa Fluor 488 goat anti-rabbit IgG at a 1:500 dilution in 1% non-fat dry milk in 1X PBS for 2 hr at room temperature. Afterwards, the coverslips were washed and placed on to a slide and sealed with clear nail polish. Immunofluorescence microscopy was performed using rabbit polyclonal antibodies against the following: *Salmonella typhymurium* CheB and *Salmonella typhymurium* CheR (a gift from Ann Stock, Princeton), *E. coli* Tsr (a gift from J. S. Parkinson, Univ. of Utah), and *B. subtilis* McpB (a gift from G. Ordal, Univ. of Illinois).

Minimum Inhibitory Concentrations

E. coli cultures were grown from Luria broth (LB) plates with no antibiotics. A colony was inoculated into 5 mL liquid LB and shaken at 200 rpm at 37ºC overnight. Next, 100 µL of the overgrown cultures were placed in 5 mL of fresh LB and returned to the 37ºC incubator to shake until an optical density (OD_{600}) of 0.1 was reached. Cultures were then aliquoted into a 96-well plate along with the antibiotic to be tested. Concentrations were calculated using a total volume of 200 µL for each well. Plates were read using a BioTek

Cytation3 plate reader and Gen5 software. Experiments were conducted for 17 hr with optical density (OD_{600}) read every 10 min. The temperature was held at 37ºC and plates were continuously shaken. MIC values were determined by the lowest antibiotic concentration at which the growth rate was observably inhibited.

Biofilm Assay

Biofilm formation in polystyrene microtiter plates was tested using a crystal violet staining assay. Overnight cultures of *E. coli* and *B. subtilis* were diluted in Terrific broth (TB) to OD_{600} of 0.05 and 300 µl of each sample was added into the wells of a 96-well plate. Plates were incubated for 24 hr at 37ºC, the OD_{600} was measured again, and the wells were rinsed thoroughly with water. Then, a crystal violet solution (1%) was added to each well, incubated for 15 min at room temperature, and wells were rinsed three times with water. The remaining crystal violet was solubilized by adding 300 µl of 96% ethanol. The OD_{595} of the solutions were then measured.

Bacterial Two-Hybrid Assay

A bacterial two-hybrid assay specific for membrane proteins was used to investigate protein-protein interactions. Proteins of interest (TMX, FabA, B, D, F, G, H, I, Z) were fused on the C-terminus of the T18 and T25 domains of *Bordetella pertussis* adenylate cyclase present in vectors pUT18 and pKNT25 (Table 7), respectively, as described by the manufacturer's protocol (Euromedex). The genes of interest were first PCR-amplified (Table 8) and cloned into a TOPO 2.1 vector (Invitrogen) using the manufacturer's protocol. The resulting vectors were digested with the following enzyme pairs (PstI and

Table 7. Strains and plasmids used in chapter 3

Strains/plasmids	Genotype, relevant characteristics	Reference/source
MG1655	F- lambda- *ilvG*- *rfb*-50 *rph*-1	Blattner *et al*., 1997 (170)
tmx°	MG1655 strain with a *tmx* markerless deletion	Alexandre lab, unpublished
BTH101	F$^-$ *cya-99 araD139 galE15 galK16 rpsL1 hsdR2 mcrA1 mcrB1*	Karimova *et al.*, 1998 (100)
XL1-Blue	*recA1 endA1 gyrA96 thi-1 hsdR17 supE44 relA1 lac* [F′ *proAB lacIq ZΔM15* Tn*10* (Tet^r)]	Agilent Technologies
pkNT25	Derivative of pSU40 plasmid encoding T25 of CyA, Km	Karimova *et al.*, 1998 (100)
pKNT25-zip	a derivative of pKT25 in which the leucine zipper of GCN4 is genetically fused in frame to the T25 fragment, Km	Karimova *et al.*, 1998 (100)
pUT18	Derivative of pUC19 plasmid encoding T18 of CyA, Cb	Karimova *et al.*, 1998 (100)
pUT18-zip	a derivative of pUT18 in which the leucine zipper of GCN4 is genetically fused in frame to the T18 fragment, Cb	Karimova *et al.*, 1998 (100)
pKNT25*tmx*	pKNT25 containing *tmx*, Km	This work
pKNT25*fabA*	pKNT25 containing *fabA*, Km	This work
pKNT25*fabB*	pKNT25 containing *fabB*, Km	This work
pKNT25*fabD*	pKNT25 containing *fabD*, Km	This work
pKNT25*fabF*	pKNT25 containing *fabF*, Km	This work
pKNT25*fabG*	pKNT25 containing *fabG*, Km	This work
pKNT25*fabH*	pKNT25 containing *fabH*, Km	This work
pKNT25*fabI*	pKNT25 containing *fabI*, Km	This work
pKNT25*fabZ*	pKNT25 containing *fabZ*, Km	This work
pUT18*tmx*	pUT18 containing *tmx*, Cb	This work
pUT18*fabA*	pUT18 containing *fabA*, Cb	This work
pUT18*fabB*	pUT18 containing *fabB*, Cb	This work
pUT18*fabD*	pUT18 containing *fabD*, Cb	This work
pUT18*fabF*	pUT18 containing *fabF*, Cb	This work
pUT18*fabG*	pUT18 containing *fabG*, Cb	This work
pUT18*fabH*	pUT18 containing *fabH*, Cb	This work
pUT18*fabI*	pUT18 containing *fabI*, Cb	This work
pUT18*fabZ*	pUT18 containing *fabZ*, Cb	This work

Table 8. Primers used in chapter 3

Primer Names	Sequence
GWTMXH72FFwd	5’ GGGGACAAGTTTGTACAAAAAAGCAGGCTATGGTTCAGAAGCCCCTCATT 3’
GWTMXH72FRev	5’ GGGGACCACTTTGTACAAGAAAGCTGGGTTCGCCTGCCCAATATACAAATA 3’
TMXT25F	5’ CACTCTGCAGATGGTTCAGAAGCCCCTCATT 3’
TMXNT25R	5’ CACTGAATTCCGCCTGCCCAATATACAAATA 3’
fabAT25F	5’ CACTCTGCAGATGGTAGATAAACGCGAATCC 3’
fabANT25R	5’ CACTGAATTCGAAGGCAGACGTATCCTGGAA 3’
fabBT25F	5’ CACTCTGCAGATGAAACGTGCAGTGATTACT 3’
fabBNT25	5’ CACTGGTACCTACATCTTTCAGCTTGCGCAT 3’
fabDT25F	5’ CACTTCTAGAATGACGCAATTTGCATTTGTG 3’
fabDNT25R	5’ CACTGAATTCAAGCTCGAGCGCCGCTGC 3’
fabFT25F	5’ CACTCTGCAGGTGTCTAAGCGTCGTGTAGTT 3’
fabFNT25R	5’ CACTGAATTCGATCTTTTTAAAGATCAAAGA 3’
fabGT25F	5’ CACTCTGCAGATGAATTTTGAAGGAAAAATC 3’
fabGNT25R	5’ CACTGAATTCGACCATGTACATCCCGCCGTT 3’
fabHT25F-JG	5’ CACTCTGCAGATGTATACGAAGATTATTGGT 3’
fabHNT25R-JG	5’ CACTGGTACCGAAACGAACCAGCGCGGA 3’
fabIT25F	5’ CACTTCTAGAATGGGTTTTCTTTCCGGTAAG 3’
FabINT25R	5’ CACTGAATTCTTTCAGTTCGAGTTCGTTCAT 3’
fabZT25F	5’ CACTCTGCAGTTGACTACTAACACTCATACT 3’
fabZNT25R	5’ CACTGAATTCGGCCTCCCGGCTACGAGCACA 3’

EcoRI for TMX, FabA, F, G; PstI and KpnI for FabB, H; XbaI and EcoRI for FabD, I; PstI and EcoRI for FabZ) and ligated into their destination vectors, (high copy pUT18 and low copy pKNT25) that were previously digested with the same enzymes, using T4 ligation (New England Bio Labs). Resulting plasmids were propagated in XL-1 Blue cells (Agilent Technologies), and the presence of an insert was confirmed by colony PCR. To test for protein-protein interactions, two plasmids expressing genes of interest were co-transformed into BTH101 competent cells and plated on Luria Broth (LB) plates with kanamycin (50 μg/mL) and carbenicillin (50 μg/mL). The plates were incubated for up to 48 hr at 30 °C. Several colonies were picked from a plate, and inoculated into 5 mL of liquid LB with kanamycin and carbenicillin (50 μg/ mL of each), and shaken (200 rpm) at 30°C. Two microliters of the overnight cultures were spotted onto MacConkey plates with lactose as a carbon source and incubated at 30°C for up to 72 hr. Positive interactions produced pink colonies which were restreaked on to fresh MacConkey plates under the same growth conditions. Empty vectors (pUT18 and pKNT25) were used as negative controls while pUT18-zip and pKT25-zip (51) were used as positive controls. For quantification of interactions, cells were grown in 5 mL liquid LB with kanamycin and carbenicillin (50 μg/mL of each) at 30°C while shaking at 200 rpm until they reached an OD*600* of 0.5- 0.6. A beta galactosidase assay was then performed as described in Ramsay, *et al*. (110).

Site-Directed Mutants

The H72F and H23F site-directed mutants were synthesized by GENEWIZ and cloned into the pRH005 vector (105) using Gateway cloning (Invitrogen) following the manufacturer's

protocol. Cells were then transformed into *E. coli* MG1655 or Δ*tmx*^{o} chemically competent cells and plated on LB with kanamycin (50 mg/mL). Resulting colonies were verified with PCR. For analysis, cells were grown as previously stated in Membrane Staining.

Results

TMX Affects Membrane Permeability

Since TMX is predicted to span the membrane seven times, we hypothesized that its deletion would affect the way it responded to lipophilic membrane dyes. These fluorescent dyes bind to the outer leaflet of the membrane and, if they cannot insert into the membrane, they will not fluoresce. We stained live wild type and Δ*tmx*^{o} mutant cells with FM1-43 and FM4-64 dyes. The wild type stained much brighter than the mutant cells, suggesting the dye was not able to bind to the membrane in the mutant efficiently (Fig. 39). We also reasoned that deleting TMX may affect permeability of the cell. If this were true, we may see a difference in amount of antibiotics needed to kill or inhibit the growth of the bacteria. Therefore, we calculated the minimum inhibitory concentrations (MIC) of wild type and Δ*tmx*^{o} mutants for several pore-forming antibiotics. We tested a variety of antibiotics, all with different modes of action, including gentamycin, tetracycline, aminoglycosides, beta lactam antibiotics, ionophores, polymyxin B, and chloramphenicol. Except for polymyxin B which showed similar MIC values for wild type and Δ*tmx*^{o}, the wild type cells had dramatically lower MIC values than the Δ*tmx*^{o} mutant (Table 9). Together, these results Suggest the permeability of the bacterial membrane in the Δ*tmx*^{o} mutant is less than that of the wild type.

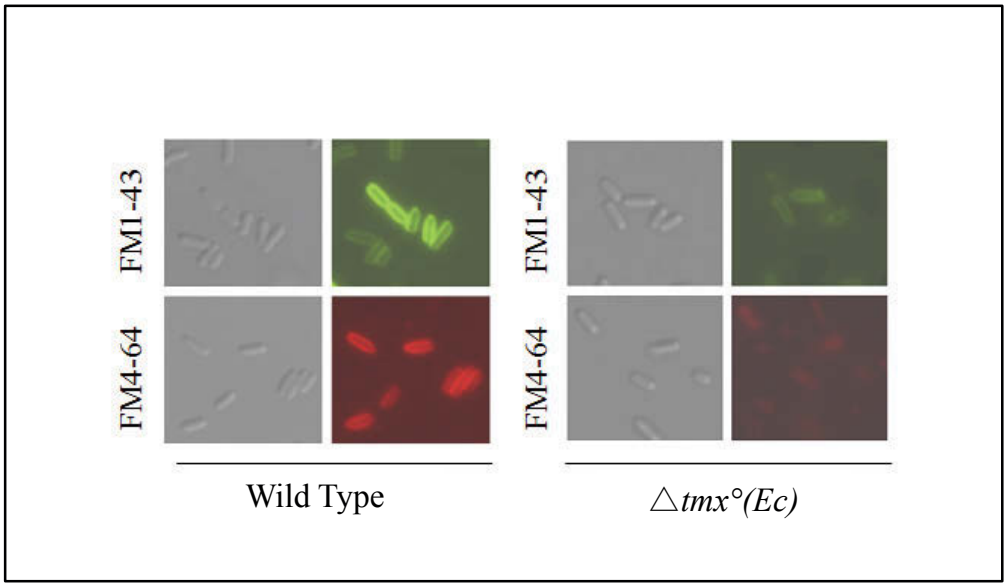

Figure 39. Membrane staining of *E. coli* wild type and Δ*tmx°* mutant cells

Membrane staining of wild type and Δ*tmx°* mutants using lipophilic membrane dyes. Quantification of fluorescence intensity was measured with background subtracted from each individual measurement. N > 30 for each panel.

Table 9. Minimum inhibitory concentrations of antibiotics grown with wild type *E. coli* or the △*tmx*° mutant

	Wild Type	**△*tmx*°**
Gramicidin[a]	5.6	16.5
Filipin III[a]	5.5	9.7
Polymyxin B[a]	2.1	2.2
Valinomycin[a]	8.2	23.3
Nigericin[a]	1.6	9.8
Chloramphenicol[b]	2.0	3.0
Tetracycline[b]	0.5	1.4
Ampicillin[b]	3.5	4.7
Gentamycin[b]	3.3	+++

[a] concentrations listed in uM; [b] concentrations listed as ug/mL.; +++ indicates that a MIC value exceeded the concentrations tested.

TMX Affects Localization of Membrane Proteins

Analysis of the distribution of membrane-bound or membrane-associated proteins provided additional support to the hypothesis that membrane permeability is altered in the mutant compared to the wild type. Immunolocalization of Tsr, a membrane-bound chemotaxis receptor which typically localizes at the cell poles, and of CheB and CheR which are chemotaxis proteins that associate with membrane-bound chemotaxis receptors, using antibodies specific for these proteins showed that Tsr localized as punctate foci at the cell poles in the wild type background (Fig. 40). In the Δ*tmx°* background, Tsr localization dramatically changed with numerous foci dispersed along the cell membrane, including many more foci localized on the lateral sides of the cells. When Δ*tmx°* cells were provided a plasmid expressing the *tmx* gene, near wild-type localization patterns emerged (Fig. 40). Approximately 50% of CheB and CheR cells displayed polar localization under our imaging conditions. These proteins were both mislocalized in the Δ*tmx°* background as indicated by a significant drop in the number of polar foci (CheB, 11%; CheR, 15%) but an increase in polar localization was observed when providing Δ*tmx°* cells with a plasmid expressing the *tmx* gene (CheB, 22%, CheR, 57%). Together these results suggest that the mislocalization of membrane proteins in the Δ*tmx°* background is linked to the lack of a functional TMX, which could result from similar effects on membrane permeability.

TMX Affects Biofilm Production

Affecting the phase order, or lipid packing order, of the bacterial membrane has been shown to alter biofilm production in *E. coli.* Therefore, we hypothesized that the deletion of membrane-bound TMX, if it in fact alters the membrane fluidity, would affect the

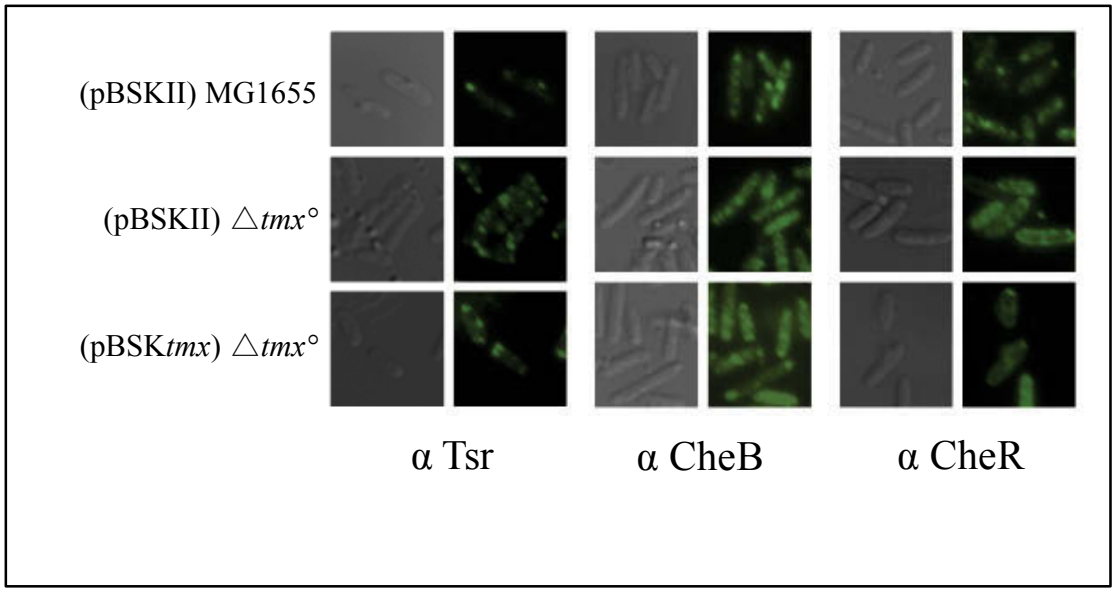

Figure 40. Immunolocalization of *E. coli* Tsr, CheB, and CheR

Immunolocalization experiments showing the localization of membrane-bound chemoreceptor, Tsr, and membrane-associated proteins, CheB and CheR, in wild type MG1655 (pBSKII), △*tmx*° (pbSKII), and complemented △*tmx*° (pBSK *tmx*) backgrounds using anti-Tsr, anti-CheB, and anti-CheR antibodies, respectively.

amount of biofilm produced. We measured biofilm formation via crystal violet staining assay and found that the Δ*tmx°* mutant produced significantly more biofilm than wild type as measured by quantifying the absorbance at 595 nm (Fig. 41, left two bars). This suggests that the absence of TMX may cause changes in the membrane such as affecting the lipid packing order, which ultimately affects biofilm production.

TMX Involved in Regulating Membrane Fluidity

The effect of TMX on the aforementioned experiments led us to believe that there was a difference in overall membrane fluidity between the wild type and Δ*tmx°* mutant cells. Therefore, we directly compared wild type and Δ*tmx°* membrane permeability as a function of temperature using DPH (1,6-diphenyl 1,3,5-hexatriene) anisotropy. As temperature increased, anisotropy readings decreased for the wild type cells, which is indicative of an increase in membrane fluidity while the anisotropy readings for Δ*tmx°* cells remained largely unchanged as temperature increased (Fig. 42). In addition, DPH anisotropy values of the Δ*tmx°* cells were higher compared to the wild type, regardless of the temperature. These results suggest that not only do the Δ*tmx°* cells have a more rigid membrane, they do not respond to temperature change as wild type cells.

Fluidizing the Membrane Rescues Phenotypes of Δtmx° Mutants

The results above implicate TMX in regulating membrane fluidity, with absence of TMX causing cells to have more rigid membranes. It follows that fluidizing the membrane should reverse any physiological effect seen in Δ*tmx°* mutants. To fluidize the membrane, we added benzyl alcohol to the growth media of the cultures. Benzyl alcohol is a well-

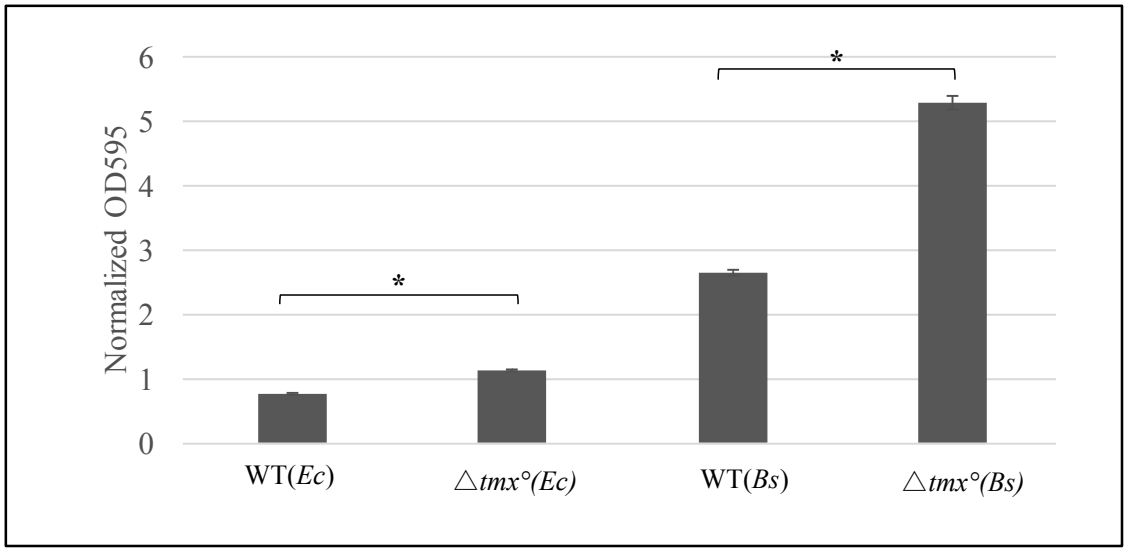

Figure 41. Biofilm assays of *E. coli* and *B. subtilis*

Biofilm formation assays in wild type *E. coli* (Ec), its △*tmx*° mutant, wild type *Bacillus subtilis* (Bs) and its △*tmx*° mutant. Each value is the quantification of crystal violet dye attached to the cells forming biofilm which has been normalized for optical density of each culture. Values are averages of at least three independent cultures. * denotes P value > 0.05.

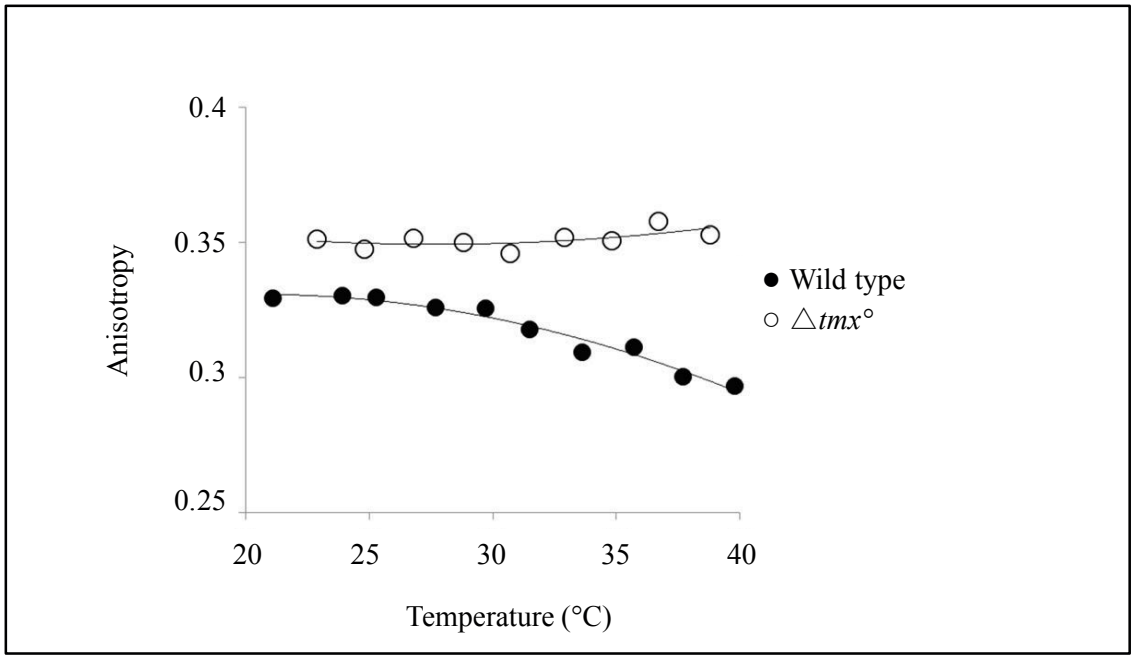

Figure 42. DPH anisotropy of *E. coli* and Δ*tmx°* mutant bacteria

DPH anisotropy measurements of whole cell wild type and Δ*tmx°* mutant cells as a function of temperature.

established fluidizer which is thought to fluidize by disrupting the lipid packing order and disturbing the interactions between membrane proteins and lipids. A concentration of 20 mM was used as it did not affect the growth rate of the wild type (data not shown). The addition of the fluidizer resulted in the Δ*tmx*^{o} mutant cells staining significantly brighter than the wild type treated under the same conditions (Fig. 43, bottom), reversing the phenotype of the mutant. In addition, we repeated the crystal violet staining assay to quantify biofilm production in the wild type and Δ*tmx*^{o} mutant only we added 20 mM benzyl alcohol to the growth media. The addition of this fluidizing agent caused the wild type and Δ*tmx*^{o} mutant to exhibit similar OD_{595} measurements which is indicative of similar biofilm production (Fig. 44).

Mutating Conserved Residues Affects Membrane Permeability

TMX is predicted to be a member of the PAQR family. Proteins in this family have several highly conserved residues which may be critical for structure and/or function. TMX shares these strictly conserved residues, and we hypothesized that mutating them may alter TMX's ability to affect membrane permeability. Therefore, we generated two site-directed mutants of highly conserved residues in the PAQR family, H72F and H23F, each harboring a histidine-to-phenylalanine mutation, and cloned them into a pRH005 vector. This vector fuses a C-terminal YFP tag in frame with the gene of interest (105). Our goal for using this approach is to use the YFP fluorescence as a marker of protein folding to rule out any structural deleterious effects of the mutations. However, for reasons that are yet unclear, we could not detect fluorescence. We then tested the ability of actively growing cells to incorporate the lipophilic dyes into their membrane. In the MG1655 wild type background,

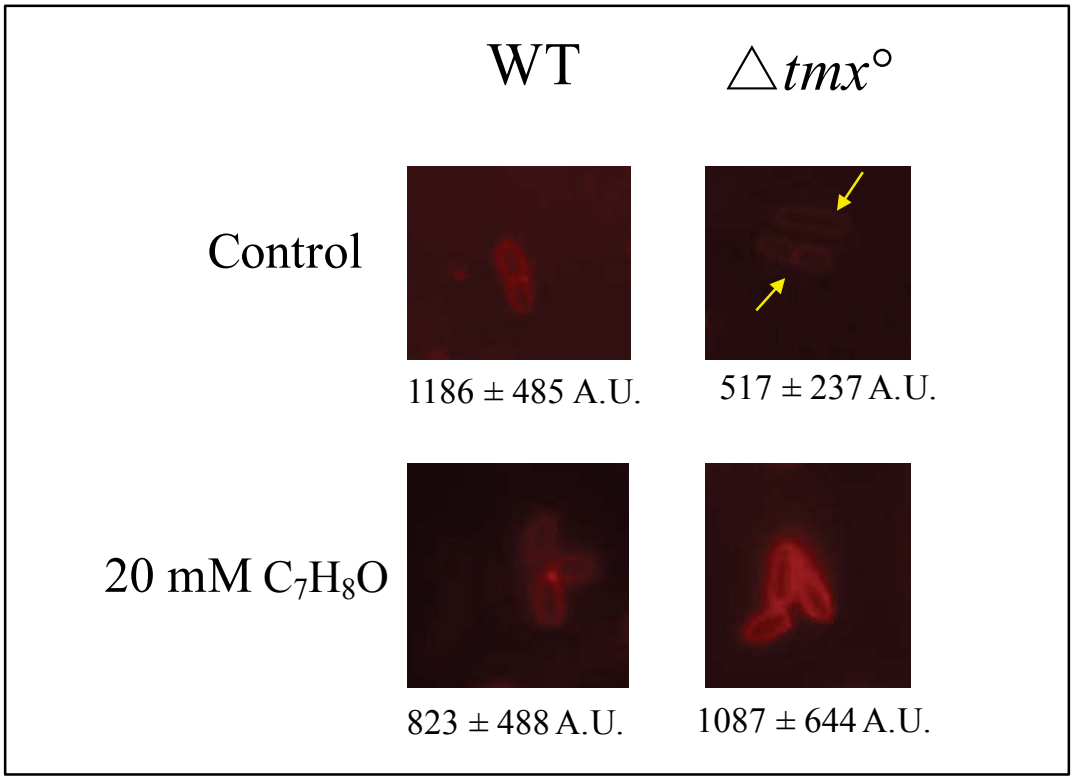

Figure 43. Membrane staining of wild type and Δ*tmx°* with and without fluidizer

Membrane staining of wild type and Δ*tmx°* mutants using lipophilic membrane dyes. Cells were grown with (bottom) or without (control, top) benzyl alcohol. Cells were grown for 40 min before being stained and imaged. Quantification of fluorescence intensity was measured with background subtracted from each individual measurement. Values are listed in A.U. below each corresponding picture. N > 30 for each panel.

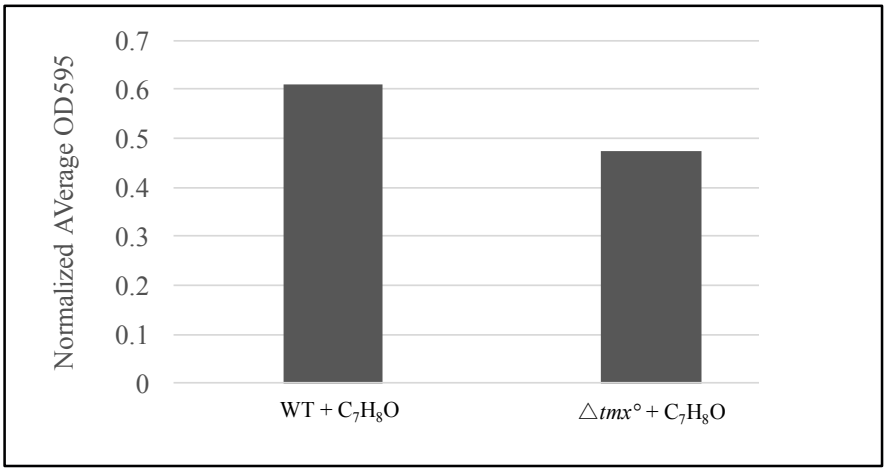

Figure 44. Biofilm assay of *E. coli* WT and Δ*tmx°* with benzyl alcohol

Quantification of biofilm production as shown through OD_{595} readings of a crystal violet staining assay. Wild type and Δ*tmx* mutant cells were grown in the presence of 20 mM benzyl alcohol to assess the effect of fluidizing the membrane on biofilm production. Each value is an average of three biological samples. P value > 0.2.

all cells whether they had a plasmid containing the *tmx* gene (prh*tmx*), or a plasmid containing a *tmx* site-directed mutant (prh*tmx* H72F or prh*tmx* H23F), stained more intensely than their Δ*tmx*^{o} mutant counterpart containing the same plasmid (Fig. 45). In comparing Δ*tmx*^{o} (prh*tmx*), Δ*tmx*^{o} (prh*tmx* H72F), and Δ*tmx*^{o} (prh*tmx* H23F), the plasmid containing the H23F mutant produced fluorescence intensity levels similar to Δ*tmx*^{o} (prh*tmx*) while the H72F mutant could not restore the staining phenotype (Fig. 45). These results suggest that the H72F mutation may be more important in TMX exerting its effects on membrane fluidity while H23F has no detectable effect on this phenotype.

Temperature Provokes Subtle Differences in the Fatty Acid Profiles of Wild Type and the tmx Mutant

In an attempt to understand how TMX could have these effects on membrane properties, specifically membrane fluidity, we performed a fatty acid analysis and a polar head group analysis on wild type and Δ*tmx*^{o} cells. The *tmx* gene is encoded in the fatty acid biosynthesis (FAB) regulon and regulated like two of the FAB genes, *fabA* and *fabB* (data not shown). Therefore, we reasoned that its deletion may affect the fatty acids it produces, which has been shown to alter the viscosity of the membrane. We analyzed the fatty acid profiles—fatty acid chain lengths, amount of unsaturated fatty acids (UFA) versus saturated fatty acids (SFA), amount of cyclopropane fatty acids, and phospholipid profiles—of the wild type *E. coli* strain MG1655 and a Δ*tmx*^{o} mutant, which was a deletion of the *tmx* gene in the MG1655 background. We analyzed the samples grown with varied carbon sources, growth temperatures, and analyzed them at different stages of growth (logarithmic versus stationary). The nature of the carbon source or growth stage did not result in any difference

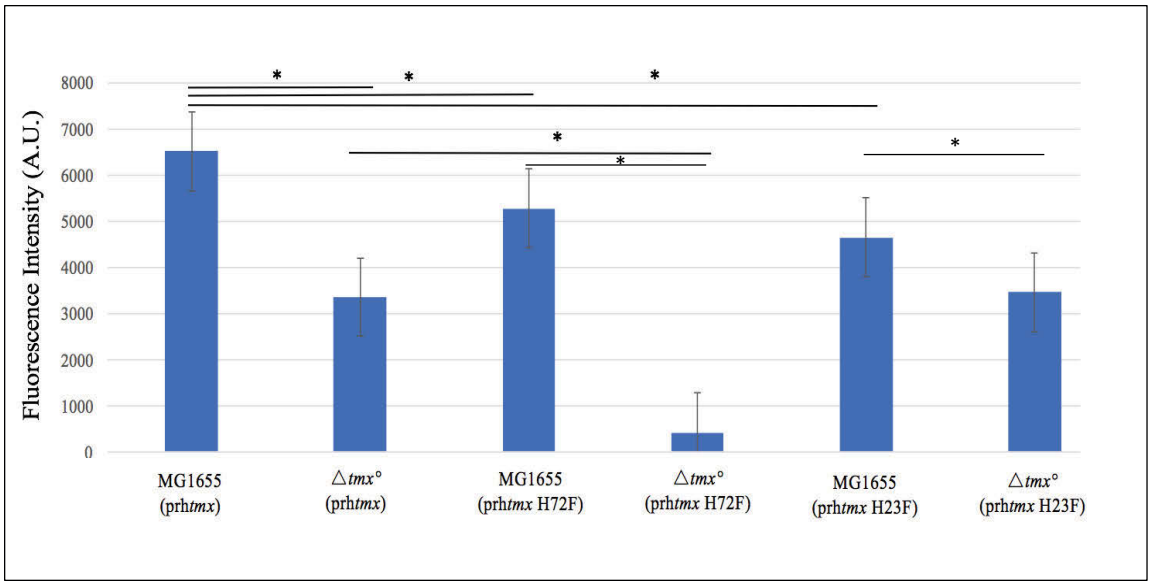

Figure 45. Fluorescence intensity of membrane staining of *E. coli* and Δ*tmx*^{o} site-directed mutants

Quantification of the FM1-43 membrane staining of wild type (MG1655) or mutant (Δ*tmx*^{o}) *E. coli* cells containing either a plasmid harboring the full length *tmx* gene (prh*tmx*), or a plasmid harboring one of the two site-directed mutants of the *tmx* gene: (prh*tmx* H72F) or (prh*tmx* H23F). Each value is an average of three biological samples.

in the fatty acid profiles of the wild type and mutant bacteria (data not shown). However, growing the bacteria at different temperatures provoked subtle differences in the fatty acid profiles for the mutant as compared to the wild type. The wild type produced similar percentages of C12-C14 fatty acids at both temperatures and slightly more C15 fatty acids at 37ºC (Fig. 46, Table 10). The majority were C16 fatty acids, and this value increased at 37ºC. There were less C17-C19 fatty acids produced at 37ºC as compared to 28ºC (Fig. 46, Table 10). The fatty acid chain lengths of Δ*tmx°* at 28ºC and 37ºC revealed similar trends as seen in the wild type for C12 and C13 fatty acids but similar levels of C15 fatty acids at 37ºC. The mutant also produced mainly C16 fatty acids, with more produced when grown at 37ºC compared to 28ºC (Fig. 46, Table 10). There were also less C17-C19 fatty acids produced at the higher temperature. We did note that though both wild type and Δ*tmx°* produced less C18 fatty acids at 37ºC than at 28ºC, Δ*tmx°* contained a higher percentage of the long-chained fatty acid (Fig. 46-47, Table 10). These differences were evident when comparing the ratio of C18:0 to C16:0 and C18:1 to C16:1 in the wild type and Δ*tmx°* at the different temperatures (Table 11). Further comparisons between the wild type and mutant fatty acid profiles determined that the mutant produced less odd-chained fatty acids than the wild type (Fig. 47). The amounts of saturated and unsaturated fatty acids were also analyzed. The ratios of UFA to SFA were identical for both wild type and Δ*tmx°* at both temperatures (UFA/SFA at 28ºC = 0.5 ± 0.04 for WT and 0.5 ± 0.08 for Δ*tmx°*; UFA/SFA at 37ºC = 0.6 ± 0.10 for WT and 0.6 ± 0.07 for Δ*tmx°*). The ratio of polyunsaturated to monounsaturated fatty acids was identical in the wild type and mutant at either temperature (PUFA/MUFA = 0.01 for wild type and Δ*tmx°* at 28ºC and 37ºC). Both wild type and Δ*tmx°*

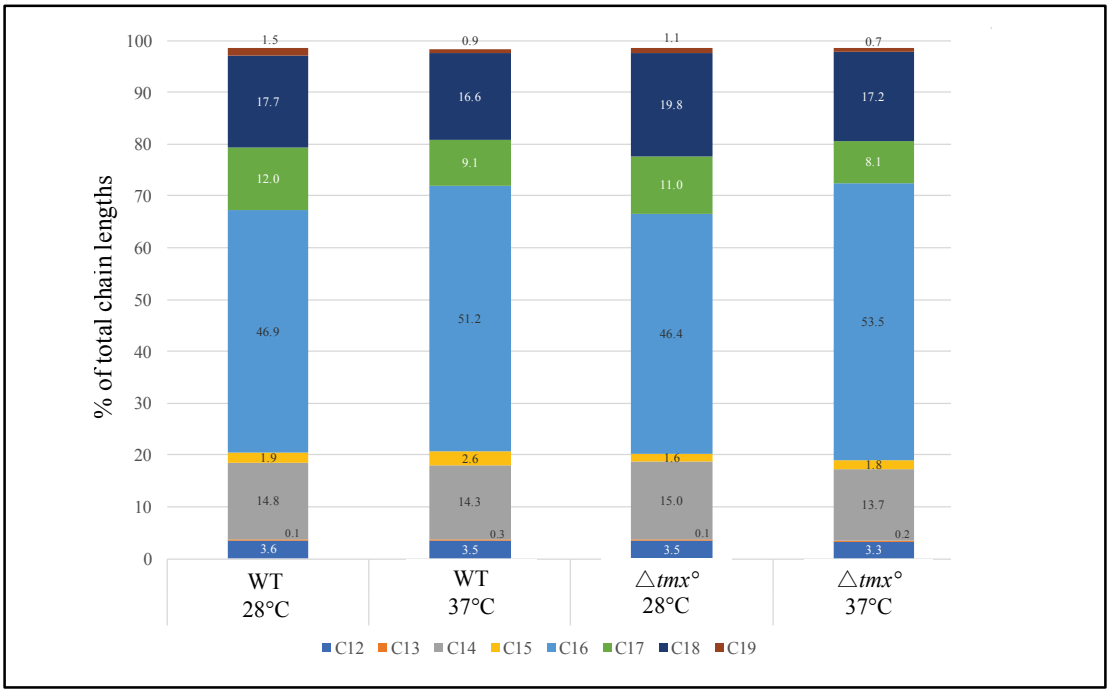

Figure 46. Fatty acid profiles of *E. coli* and the Δ*tmx°* mutant

Fatty acid profiles showing percentage of total chain lengths of wild type *E. coli* and the Δ*tmx°* mutant at 28ºC and 37ºC. Different chain lengths are represented by different colors with individual values listed for all chain lengths. Each value is an average of three biological samples.

Table 10. Percentages of fatty acid chains produced by WT *E. coli* and the Δ*tmx°* mutant

		C11	**C12**	**C13**	**C14**	**C15**	**C16**	**C17**	**C18**	**C19**	**C20**
28°C	WT	0	3.6 ± 0.8	0.1 ± 0.1	14.8 ± 2.4	1.9 ± 0.3	46.9 ± 3.7	12.0 ± 1.6	17.7 ± 1.1	1.5 ± 0.7	0
37°C	WT	0	3.5 ± 0.4	0.3 ± 0.2	14.3 ± 1.8	2.6 ± 1.1	51.2 ± 3.5	9.1 ± 3.2	16.6 ± 0.9	0.9 ± 0.5	0
28°C	△*tmx°*	0	3.5 ± 1.3	0.1 ± 0.1	15.0 ± 3.8	1.6 ± 0.2	46.4 ± 3.7	11.0 ± 1.7	19.8 ± 2.0	1.1 ± 1.0	0
37°C	△tmx°	0	3.3 ± 0.2	0.2 ± 0.1	13.7 ± 1.4	1.8 ± 0.5	53.5 ± 2.0	8.1 ± 1.1	17.2 ± 1.0	0.7 ± 0.1	0

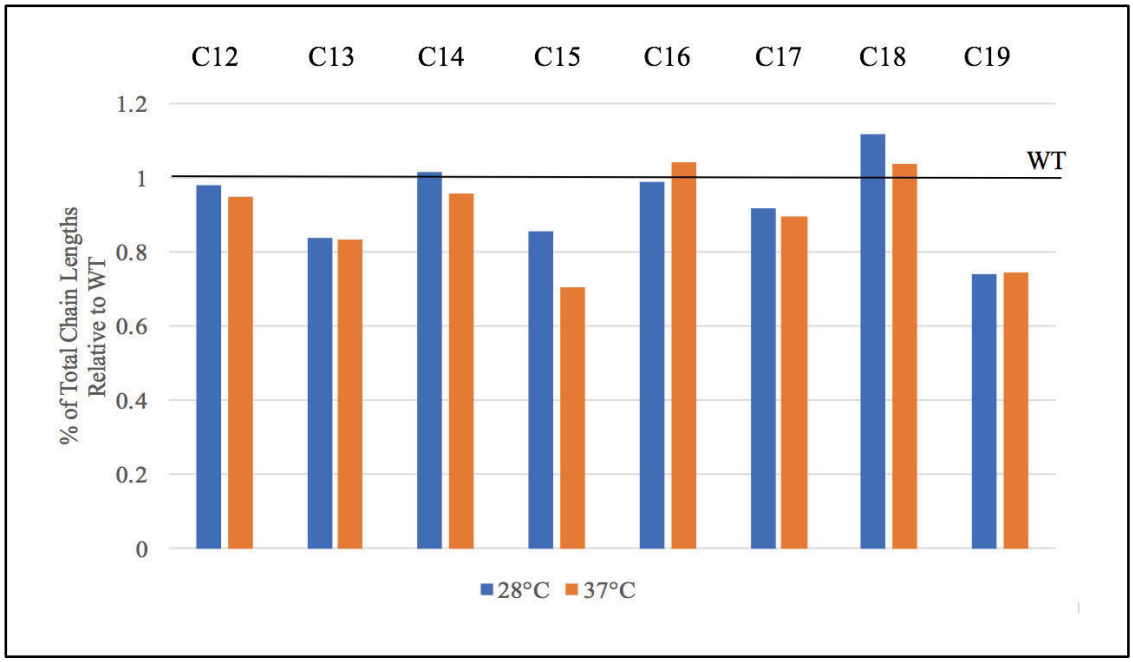

Figure 47. Percent of total chain lengths of the Δ*tmx*^{o} mutant relative to wild type

Percentage of total chain lengths of the Δ*tmx*^{o} mutant relative to wild type (value = 1). Chain lengths were analyzed at 28ºC (blue) and 37ºC (orange). Each value is an average of three biological samples.

Table 11. Percentages of long chained fatty acids produced at 28ºC and 37ºC in wild type and Δ*tmx°* in terms of SFAs (top) and UFAs (bottom)

Temperature		**C16:0**	**C18:0**	**C18:0/C16:0**
28ºC	WT	30.7	0.7	0.02
	Δ*tmx°*	31.1	0.9	0.03
37ºC	WT	30.5	0.6	0.02
	Δ*tmx°*	31.9	0.5	0.01

Temperature		**C16:1**	**C18:1**	**C18:1/C16:1**
28ºC	WT	16.1	16.7	1.0
	Δ*tmx°*	15.3	18.6	1.2
37ºC	WT	20.8	15.6	0.8
	Δ*tmx°*	21.8	16.3	0.8

had less cyclopropane at 37ºC than at 28ºC, but the only difference not within the standard deviation is the production of less cyclopropane fatty acids by the mutant at 37ºC (Table 12). Furthermore, a comparison of the ratio of cyclopropane at 37ºC to 28ºC was identical for the wild type and mutant (ratio = 0.7). Analysis of polar head groups revealed no differences between the wild type and the Δ*tmx°* mutant in the type or amount of each head group (data not shown). Though we cannot presume that these differences in fatty acids profiles are the reason the Δ*tmx°* membrane is more rigid, these results do suggest that the wild type and Δ*tmx°* mutant respond differently in reference to the fatty acids produced in response to temperature.

TMX Interacts with FAB Enzymes

Considering the results of the previous fatty acid analysis and that *tmx* is encoded in the FAB regulon and regulated like *fabA* and *fabB*, we hypothesized it may interact with the enzymes with which it is transcribed. We tested this by performing a bacterial two-hybrid assay, which has been successful at testing membrane-associated interactions, to determine whether membrane-bound TMX could interact with any of the cytosolic FAB proteins from *E. coli*. We tested all interactions with the catalytic domains fused at the C-terminus of the proteins expressed from both two-hybrid vectors, pkNT25 and pUT18, and found positive interaction of TMX with FAB enzymes (Fig. 48). TMX positively interacted with FabF, G, I, and FabA but showed no interaction with FabD, H, B, or FabZ (Fig. 48). TMX also did not interaction with itself (Fig. 48). This assay uses two vectors which have unequal copy numbers, therefore we did perform all two-hybrid assays by first cloning *tmx* into the low copy pKNT25 vector and testing FAB enzymes in the high copy pUT18 vector and

Table 12. Percentage of cyclopropane fatty acid produced by wild type and Δ*tmx°* at 28ºC and 37ºC

Cyclopropane fatty acids		
28ºC	WT	12.4 ± 2.2
	Δ*tmx°*	11.4 ± 2.0
37ºC	WT	8.3 ± 3.2
	Δ*tmx°*	7.7 ± 1.3

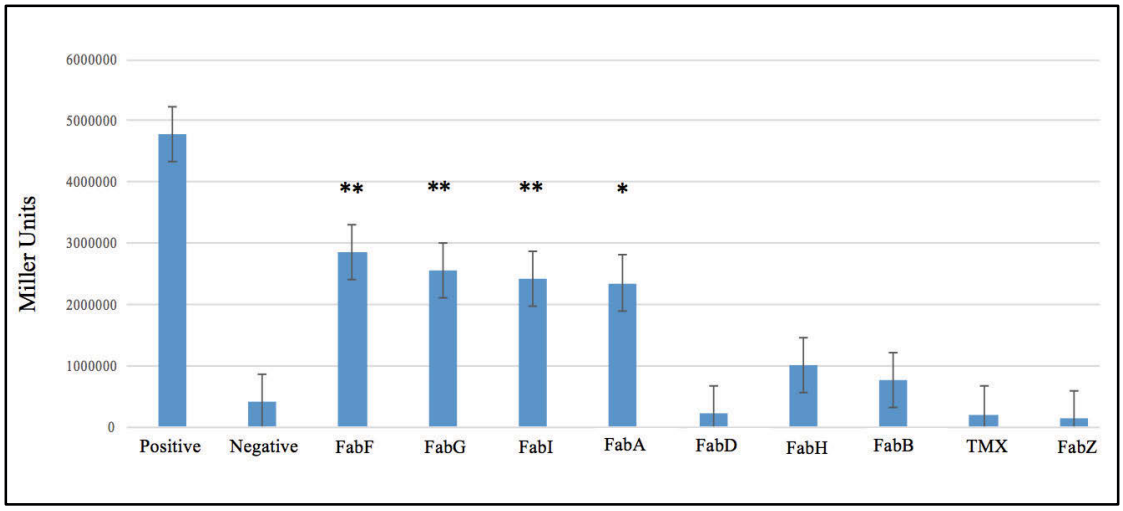

Figure 48. BACTH interactions of TMX with FAB enzymes

Interactions of TMX with fatty acid biosynthesis (FAB) enzymes as determined by the bacterial two-hybrid assay. Data shown are with *tmx* gene cloned into the pKNT25 vector and FAB enzymes cloned into the pUT18 vector. Interactions were quantified via beta-galactosidase assay and given in Miller units. All values are averages of at least three biological replicates. * denotes a p value of < 0.05, ** denotes a p value of < 0.005.

vice versa. Our analysis showed that the positive interactions were identical whether *tmx* was in the high copy or low copy vector (data not shown). However, the interactions produced higher Miller units if the FAB enzymes were in the high copy vector. Under these conditions in this assay, we show that TMX can physically interact with FAB enzymes.

TMX Site-Directed Mutants Lose Interaction with FAB Enzymes

To gain insight into how TMX could be interacting with FAB enzymes, we generated two site-directed mutants to be tested against the FAB enzymes via the bacterial two-hybrid assay. These were the same mutants previously used which both contain the aforementioned phenylalanine substitutions for conserved histidine residues. We tested the ability of the mutants, H72F and H23F, to interact with FabF, which previously showed the most significant interaction with TMX, and FabZ, which showed no interaction with TMX. The site-directed mutants both showed no interaction with FabF or FabZ in the two-hybrid assay (Figs. 49-50). However, further experiments should be performed to test the functionality of these site-directed mutants.

TMX Present in Bacteria and Eukaryotes

The presence of *tmx* is not limited to the *E. coli* genome. Homologs exist in other bacteria such as the gram-positive *Bacillus subtilis* (*yplQ*); where we designated it as tmx_{bs}. If TMX function regulating membrane permeability is conserved in Bacteria, then deleting tmx_{bs} would be expected to cause similar defects as those seen in *E. coli*. To test this, we used a *B. subtilis* mutant, void of the *tmx* gene (Δtmx_{bs}), and first, analyzed the fatty acid profiles at different temperatures, 28ºC and 35ºC. There were no detectable amounts of C12 or C13

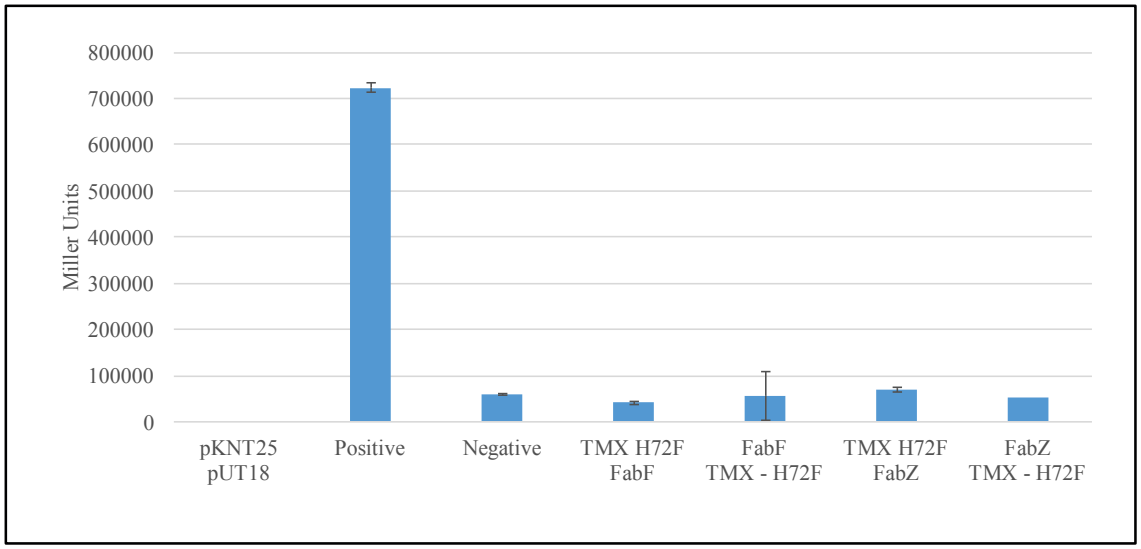

Figure 49. BACTH interactions of TMX mutant (H72F) with FAB enzymes

Interactions of the TMX site-directed mutant (TMX – H72F) with fatty acid biosynthesis (FAB) enzymes FabF and FabZ, as determined by the bacterial two-hybrid assay. Interactions were quantified via beta-galactosidase assay and given in Miller units. All values are averages of at least three biological replicates.

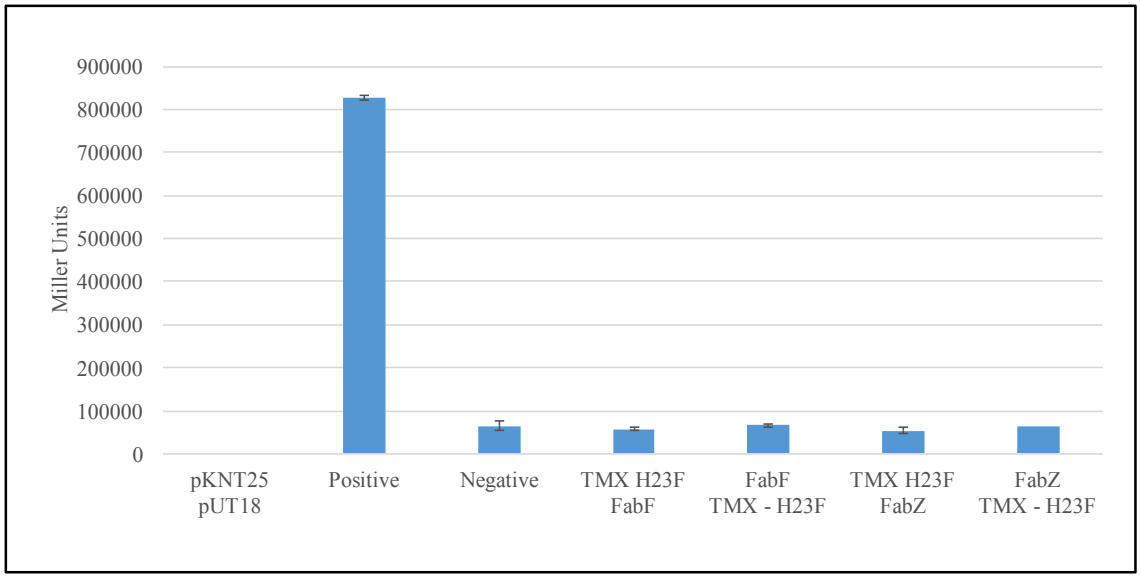

Figure 50. BACTH interactions of TMX mutant (H23F) with FAB enzymes

Interactions of the TMX site-directed mutant (TMX – H23F) with fatty acid biosynthesis (FAB) enzymes FabF and FabZ, as determined by the bacterial two-hybrid assay. Interactions were quantified via beta-galactosidase assay and given in Miller units. All values are averages of at least three biological replicates.

fatty acids produced, and both wild type and Δ*tmx*$_{bs}$ strains produced similar amounts of C14 fatty acids; these values were higher at 28ºC than at 35ºC (Fig. 51, Table 13). The majority of fatty acids were C15 fatty acids, comprising roughly 40% of the overall total. Since the C15 fatty acids are elongated to become C17 fatty acids, we calculated the ratio of C17-to-C15 fatty acids for each strain at different temperatures and found them to be similar (Table 14). The mutant did produce slightly more C15 and C17 fatty acids at both temperatures as compared to the wild type (Fig. 51-52, Table 14). C16 fatty acids also comprised a large percentage of the total fatty acids, roughly 20% (Fig. 51). For C16 fatty acids, the wild type produced less at 28ºC than at 35ºC while the mutant produced more at 28ºC than at 35ºC (Fig. 51, Table 14). For C18 fatty acids, the wild type produced more at 28ºC than at 35ºC while the mutant's level of C18 fatty acids remained relatively unchanged (Fig. 51, Table 14). These results show that similar to the effect in *E.coli*, a lack of TMX_{Bs} impairs the fatty acid chain length distribution very subtly, with the Δ*tmx*$_{bs}$ mutant adjusting to temperature change differently than the wild type. Since the fatty acid profile of *B. subtilis* is known to be different from that of *E. coli* in that much of the fatty acids produced are saturated and branched (iso and anteiso), we analyzed the total amounts of these fatty acids as well. As a trend, the amounts of iso- and anteiso- branched chained fatty acids were higher at the higher temperatures in both the wild type and mutant strains (Fig. 53). At both temperatures, the wild type produced more anteiso- than iso- branched chains. At 28ºC the mutant produced more anteio- than iso- branched chains but at 35ºC it produced more iso- than anteiso- branched chains. Comparing the total amount of branched chains between wild type and the mutant revealed that at 28ºC the wild type produced

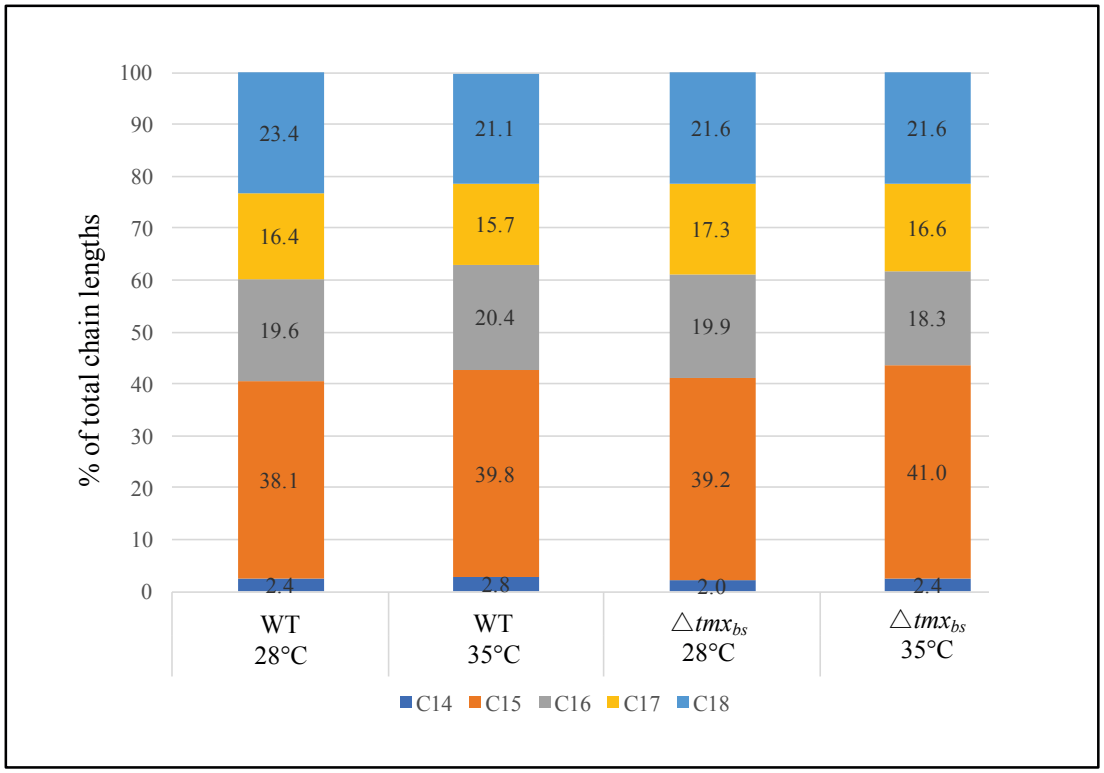

Figure 51. Fatty acid profile of *B. subtilis* and Δ*tmx*$_{bs}$

Fatty acid profiles showing percentage of total chain lengths of wild type *B. subtilis* and the Δ*tmx*$_{bs}$ mutant at 28ºC and 37ºC. Different chain lengths are represented by different colors with individual values listed for all chain lengths. Each value is an average of three biological samples.

Table 13. Percentages of fatty acids produced by wild type *B. subtilis* and Δtmx_{bs} at 28ºC and 35ºC

		C14	**C15**	**C16**	**C17**	**C18**
28ºC	WT	2.4 ± 0.1	38.1 ± 0.4	19.6 ± 1.0	16.4 ± 0.6	23.4 ± 1.3
35ºC	WT	2.8 ± 0.2	39.8 ± 8.7	20.4 ± 0.7	15.7 ± 2.6	21.1 ± 10.6
28ºC	Δtmx_{bs}	2.0 ± 0.3	39.2 ± 1.7	19.9 ± 0.6	17.3 ± 0.3	21.6 ± 1.8
35ºC	Δtmx_{bs}	2.5 ± 0	41.0 ± 4.5	18.3 ± 0.7	16.6 ± 1.4	21.6 ± 5.2

Table 14. Percentages of C15:0 and C17:0 fatty acids produced by wild type *B. subtilis* (WT) and the mutant, Δ*tmx*$_{bs}$

Temperature		**C15:0**	**C17:0**	**C17:0/C15:0**
28ºC	WT	38.2 ± 0.4	16.4 ± 0.6	0.43
	Δ*tmx*$_{bs}$	39.2 ± 1.7	17.3 ± 0.3	0.44
35ºC	WT	39.8 ± 8.7	15.7 ± 2.6	0.39
	Δ*tmx*$_{bs}$	41.1 ± 4.5	16.6 ± 1.4	0.40

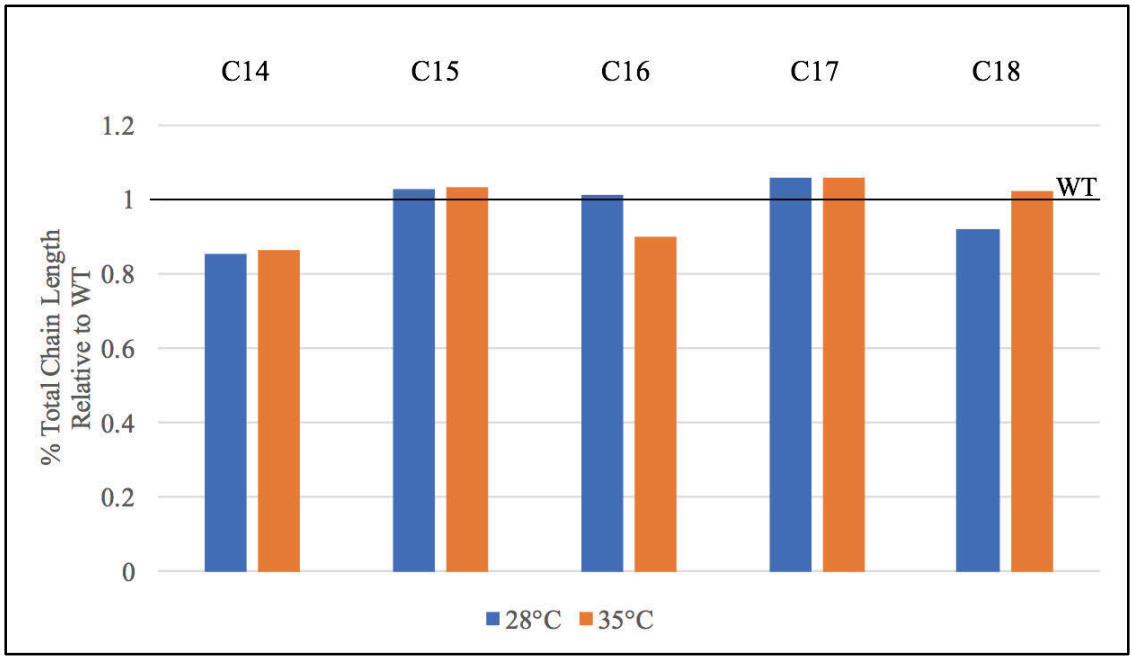

Figure 52. Percent of total chain lengths of the Δ*tmx*$_{bs}$ mutant relative to wild type

Percentage of total chain lengths of the Δ*tmx*$_{bs}$ mutant relative to wild type (value = 1). Chain lengths were analyzed at 28ºC (blue) and 35ºC (orange). Each value is an average of three biological samples.

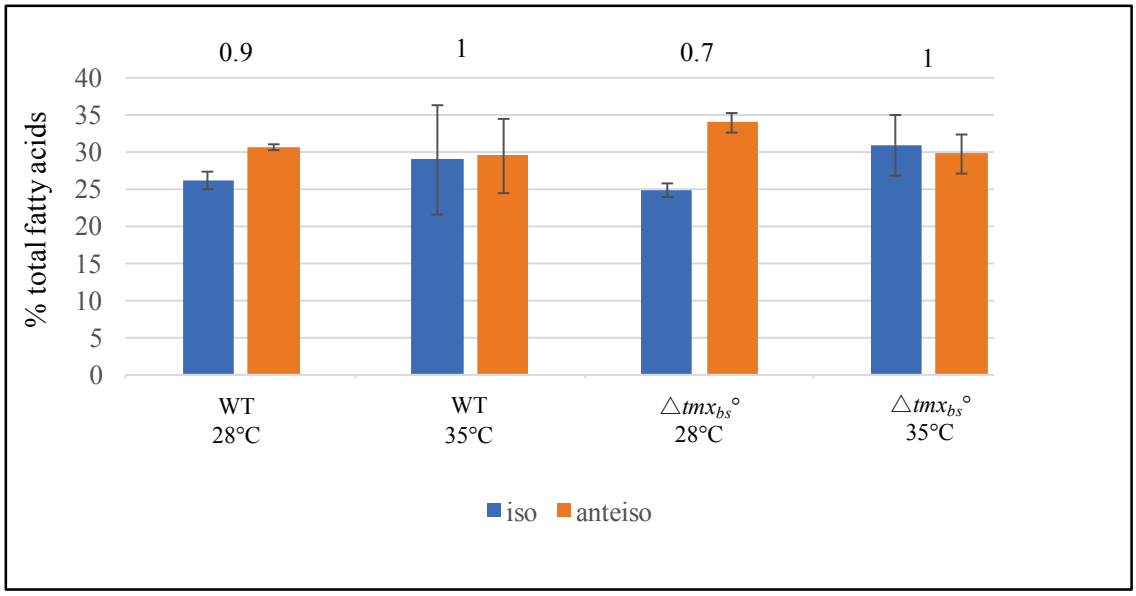

Figure 53. Percentage of branched chained fatty acids in *B. subtilis* and Δ*tmx*$_{bs}$

Percentage of total iso- (blue) and anteiso- (orange) branched chain fatty acids in wild type *B. subtilis* and the Δ*tmx*$_{bs}$ mutant at 28ºC and 35ºC. Each value is an average of three biological samples.

more iso- branched chains and less anteiso- branched chains than the mutant. At 35ºC, the wild type produced less amounts of both (Fig. 53). Similar to *E. coli*, the ratios of UFA to SFA were calculated and showed no differences between wild type and the Δ*tmx*$_{bs}$ mutant (wild type, 3.9 ± 0.4 at 28ºC and 5.5 ± 4.5 at 37ºC; Δ*tmx*$_{bs}$, 4.1 ± 0.4 at 28ºC and 4.8 ± 1.3 at 37ºC).

The Δ*tmx*$_{bs}$ mutant also displayed a mislocalization of the chemoreceptor, McpB, as compared to the wild type strain (Fig. 54). This membrane-bound protein was distributed as more foci along the lateral sides of the cell membrane, with this distribution reminiscent of that seen for CheB, CheR, and Tsr in *E. coli*. We also performed a bacterial two-hybrid assay assessing whether TMX$_{bs}$ could interact with fatty acid biosynthesis enzymes encoded in *B. subtilis*, however we were unable to detect positive interactions using this assay (data not shown). Lastly, there is a difference in biofilm production between the wild type and Δ*tmx*$_{bs}$ mutant. The mutant began producing biofilm sooner than the wild type and its overall production of biofilm was higher than the wild type (Fig. 41, right two panels).

Discussion

Here we have identified a conserved membrane-bound protein which regulates membrane fluidity in *E. coli* and *B. subtilis*. Given the phylogenetic distance between *E. coli* and *B. subtilis* (171, 172), these findings suggest that this is a conserved function of HlyIII-like proteins homologous to TMX. This protein seemingly exerts its effects after provocation via temperature change suggesting TMX acts as a temperature and/or fluidity sensor. The

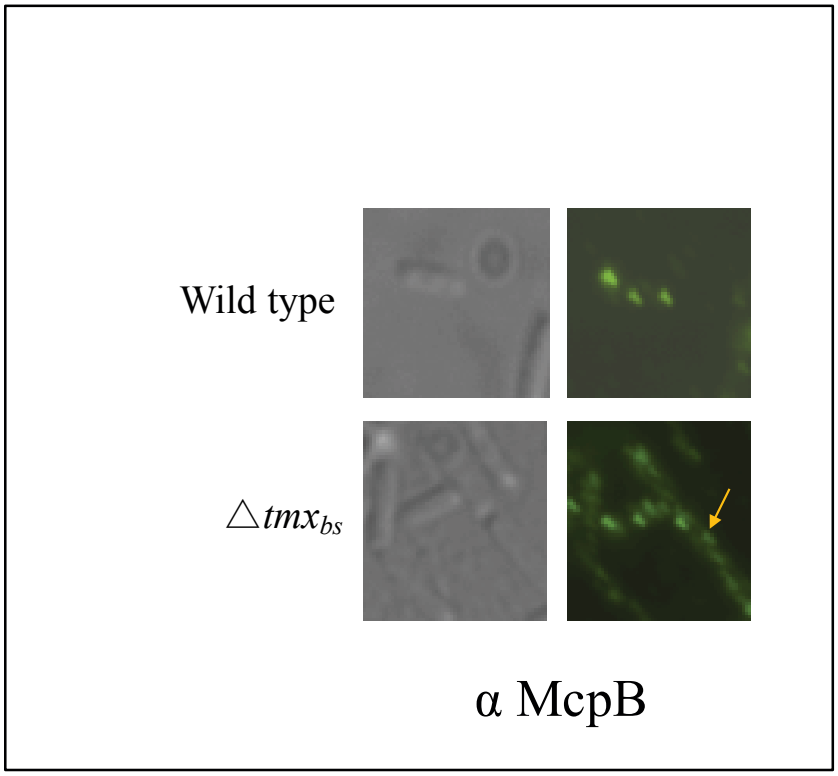

Figure 54. Immunolocalization of *B. subtilis* chemoreceptor McpB

Immunolocalization experiments showing the localization of membrane-bound chemoreceptor, McpB in wild type *B. subtilis* and the △tmx_{bs}° backgrounds using anti-McpB antibodies.

effect of TMX on membrane fluidity appears to be a direct result of the loss of TMX function because the phenotypic differences observed in the membrane staining assay and the biofilm assay could be rescued simply with the addition of a membrane fluidizer. Additional evidence for our hypothesis is the observation that a mutant lacking TMX maintains a membrane more rigid than the wild type regardless of the temperature and which fluidity does not change with temperature, in contrast to the wild type.

One of the most well-known examples of cellular membrane modification in response to temperature shifts comes from the DesK system of *B. subtilis*. These gram-positive bacteria respond to decreases in temperature through a dedicated two-component signal transduction system involving the membrane-bound histidine kinase, DesK, and its response regulator, DesR (38). Upon cooling, DesK is phosphorylated; this phosphoryl group is transferred to the aspartate residue of DesR and transcription of the *des* gene, which encodes for a desaturase, is increased. The DesK protein, acting as a thermosensor, increases the amount of unsaturated fatty acids in the membrane (38) allowing the bacteria to adjust the lipid order of the membrane. The increase in UFAs upon cooling is a trend all bacteria express (37) and has been noted in yeast (*Saccharomyces cerevisiae*), ciliates (*Tetrahymena*), amoeba (*Acanthamoeba*), and cyanobacteria (*Synechocystis*) (39-42, 164). Though it is known that membrane fluidity changes to compensate for temperature change and that gene transcription is altered due to that compensation, little is understood about how exactly the bacteria are sensing the temperature change to even be able to respond. However, one insight into this phenomenon comes from one of the cytoplasmic enzymes involved in fatty acid biosynthesis in *E. coli*, the 3-ketoacyl-ACP synthase FabF. This

enzyme is responsible for the production of long-chained fatty acids, specifically the elongation of C16-to-C18 fatty acids (45). The enzymatic activity of FabF is temperature-dependent (45); it is much more active at lower temperatures than higher temperatures, providing *E. coli* with a way to regulate acyl chain lengths in response to temperature (45) (17). The fact that *tmx* is regulated together with the genes coding for FabA and FabB, as well as the altered fatty acid profile of Δ*tmx*^{o} mutants suggests that TMX utilizes the fatty acid biosynthesis pathway to alter membrane fluidity. In an attempt to understand the specifics of the relationship between TMX and the fatty acid biosynthesis pathway, we probed potential interactions via bacterial two-hybrid assay and noted positive interactions with four enzymes. Two of these enzymes, FabG and FabI, are reductases, FabF is a synthase, and FabA is a dehydrase (3, 13). However, it is unknown whether these four enzymes share any structural similarity which may provide a binding site for TMX. We believe these to be true positive interactions due to the low instance of false positives with this assay and the lack of auto-activation reported between a protein's ability to interact with the vector itself (118). We also performed the two-hybrid assay on two site-directed mutants of TMX, H72F and H23F. This substitution, from a histidine to a phenylalanine, is generally unfavorable since histidines can function in binding sites and can often be found in the protein core (173). Though it is enticing to draw the conclusion that these conserved residues are important for the overall function of TMX, further experiments validating the functionality of these site-directed mutants should be performed. Though we also performed this assay with wild type and mutant *B. subtilis*, we were unable to detect any interactions between TMX_{bs} and FAB enzymes. This could be due to an actual lack of

interaction between these proteins or due to an inability of *B. subtilis* enzymes to function properly in this assay, which demands that *B. subtilis* genes are cloned into vectors and placed into an *E. coli* background.

Membrane fluidity can be altered from small changes in the fatty acid profile (3). Here we observe subtle changes in the profile of the Δ*tmx°* mutant as compared to the wild type including the presence of more long-chain fatty acids in the Δ*tmx°* mutant and the production of less cyclopropane fatty acids as compared to the wild type. The length of the acyl chains of fatty acids does impact the overall fluidity with longer chains adding to the viscosity of the phospholipid bilayer. Cyclopropane fatty acids are usually produced in the stationary phase (174) and their presence has been implicated in increasing membrane stability—through lipid packing—as well as decreasing permeability against antibiotics (174-178). The mutant responds to temperature by producing less cyclopropane fatty acids at 37ºC, however it maintains the same ratio as the wild type suggesting this may not contribute to the changes in fluidity between the wild type and mutant. In reference to the fatty acid profiles of *B. subtilis* and its mutant, we find the results of the branched chained fatty acid production quite interesting considering that the amount and type of branched chain fatty acids (iso- versus anteiso-) has been previously shown to drastically impact membrane fluidity as iso-chains decrease fluidity compared to anteiso-chains (169). These data suggest that *tmx* mutants respond to abiotic stressors by producing different amounts and/or types of fatty acids as compared to the wild type.

TMX is a member of the PAQR family which consists of 11 proteins shown to bind progestin (179) (membrane progesterone receptors), adiponectin (AdipoQ receptors) and a

third class of proteins which are hemolysin-III related proteins and have yet to be characterized. Membrane progesterone receptors play a significant role in the maturation of oocytes (180). Recent studies suggest they also regulate cAMP levels (181) and may have possible ceramidase activity. However, there is no structural data or direct experimental evidence for this function. In contrast, great strides have been taken in determining the structure of the AdipoQ receptors (PAQR 1, 2) in the PAQR family. These receptors bind adiponectin and crystal structures of AdipoR1 and AdipoR2 show these receptors possess seven membrane-spanning alpha helices surrounding a large internal space which with openings into the extracellular and intracellular regions. This internal region also houses a zinc binding site (182). Interestingly, AdipoR1 and AdipoR2 were crystallized with a C18:1 free fatty acid lodged in the internal cavity and were shown to possess ceramidase activity (182). They also hydrolyzed C6 fatty acids and C24 fatty acids although not as robustly (182). Two populations of AdipoR2 were crystallized leading to speculation that two forms may exist, an open and closed conformation which possibly aid in the hydrolysis reaction and subsequent release of the free fatty acid and sphingosine (182). The third category in the PAQR family incorporates hemolysin-III related proteins and is the least characterized. Phylogenetic analysis revealed that of the 11 human PAQR homologs, PAQR 10 and 11 are the most bacterial-like and are similar to the bacterial hemolysin-III related proteins (151).

Though we provide no evidence that TMX possesses enzymatic activity, we do note that the PAQR family is part of a larger superfamily called CREST (alkaline ceramidase, PAQR receptor, Per1, SID-1 and TMEM8) which unifies all membrane-bound proteins predicted

to have enzymatic activity as metal-dependent hydrolases (183). The enzymatic activity of all PAQR family members has yet to be experimentally determined, but AdipoR1 and AdipoR2 show ceramidase activity which is dependent upon zinc binding (182). Further experiments should be pursued to address the enzymatic activity of not only TMX but the remaining PAQR receptors.

The site-directed mutants used in this study are both mutations of strictly conserved histidine residues in the PAQR family. Sequence alignment of TMX with AdipoR2 shows that though both are conserved, His72 in TMX aligns with His202 in the AdipoR2 receptor (184) which is essential for mediating zinc binding, and therefore its enzymatic activity (182, 183). The results of the site-directed mutant staining suggest that perhaps both may contribute to structural integrity but perhaps His72 may be more important than His23 in terms of preserving the structure and/or function of the internal core which, as we know from structural work in AdipoQ receptors, is where zinc binding occurs (182, 184). However, we should ensure these mutants are fully functional.

In terms of physiology, changes in the ratios of fatty acids in gram negative bacteria—provoked by mutations in lipid metabolism genes—have previously been shown to change the amount of biofilm produced by bacteria (185). Biofilm production has been linked to increased immunity from antibiotics as well as increased survivability in harsh conditions (186). These results lead to the question of whether or not changes in membrane fluidity accompany all bacteria which are actively producing biofilm. Perhaps membrane fluidity contributes to the increased antibiotic resistance of biofilm-producing bacteria, but this remains to be experimentally determined.

CONCLUSION

The aim of this dissertation was to further characterize the complex nature of chemotaxis in the soil bacterium, *Azospirillum brasilense.* Previous work in the Alexandre lab demonstrated that two chemotaxis pathways, Che1 and Che4, were necessary for chemotaxis in this organism and that each of these pathways controlled a specific motility parameter, cell speed (Che1) or reversal frequency (Che4). We attempted to understand if there was any integration of these pathways, at the level of chemoreceptor baseplates.

The results presented in this dissertation conclude that interaction does exist between the proteins of the Che1 and Che4 pathways and hint at the probability of this phenomenon existing in other bacteria which encode more than one chemotaxis signaling pathway. We also concluded that *A. brasilense* produces two signaling clusters, one at 28 nm in length and one at 31 nm in length. However, this does not mean that *A. brasilense* encodes only two receptors. In fact, it is predicted to encode over 40 chemoreceptors (95); the reason only two clusters appeared in the cryo-EM images is due to the fact that those dozens of chemoreceptors are predicted to either be 28 nm or 31 nm in length. Receptors will only form signaling clusters with receptors of the same length, but each of these different receptors can bind different ligands. This is because chemoreceptors, though highly conserved in the signaling domain where CheA and CheW bind, are variable in their N-terminal cytoplasmic ligand-binding domain (70). Taken together with our data, this means that a bacterium can form extended arrays of receptors, of identical lengths, which can sense a variety of chemical cues but due to the high sequence conservation in the signaling domain, all chemoreceptors can form signaling clusters with CheA and CheW paralogs and

propagate a coordinated chemotaxis response. This level of integration would allow for a fine-tuned "hub" of receptors, present in large quantities, that are able to sense and respond to countless chemical cues in infinitesimally small concentrations, thereby providing the bacterium with a superior navigation system which does not invoke the complications of cross-talk but that can utilize chemotaxis baseplate paralogs similarly.

Results here allow us to build theoretical models of what these mixed based plates of paralogs, which propagate this coordinated response, may look like (Fig. 55). The figure presents two possible variations of baseplates (top), consisting of paralogs of both CheA and CheW, and interacting with trimers of Tlp1-dimers, although it is completely possible that baseplates consisting of proteins from just one pathway exist as well. While we have shown that paralogs can interact with either cluster, seen through positive interactions with Tlp1 and Tlp4a, we do note that more chemotaxis proteins interacted with Tlp1 than with Tlp4a. This could indicate a higher affinity of certain baseplate proteins with certain receptors, but this may be an unlikely conclusion seeing as how chemoreceptors are highly conserved on their signaling domain (where interaction with CheW and CheA occurs) (70). We believe these results are indicative of the limitations of the bacterial two-hybrid assay. Furthermore, receptors are known to dimerize and this assay was unable to detect positive interaction between two vectors, each containing Tlp4a. Further steps should be taken to address this, including cloning a truncated version of the receptor which has been shown in other two-hybrid assays to yield more conclusive results. These interactions should also be tested *in vivo* with co-immunoprecipitation experiments. The second project of this dissertation concluded that CheA1 of *A. brasilense* strain Sp7 contains an additional

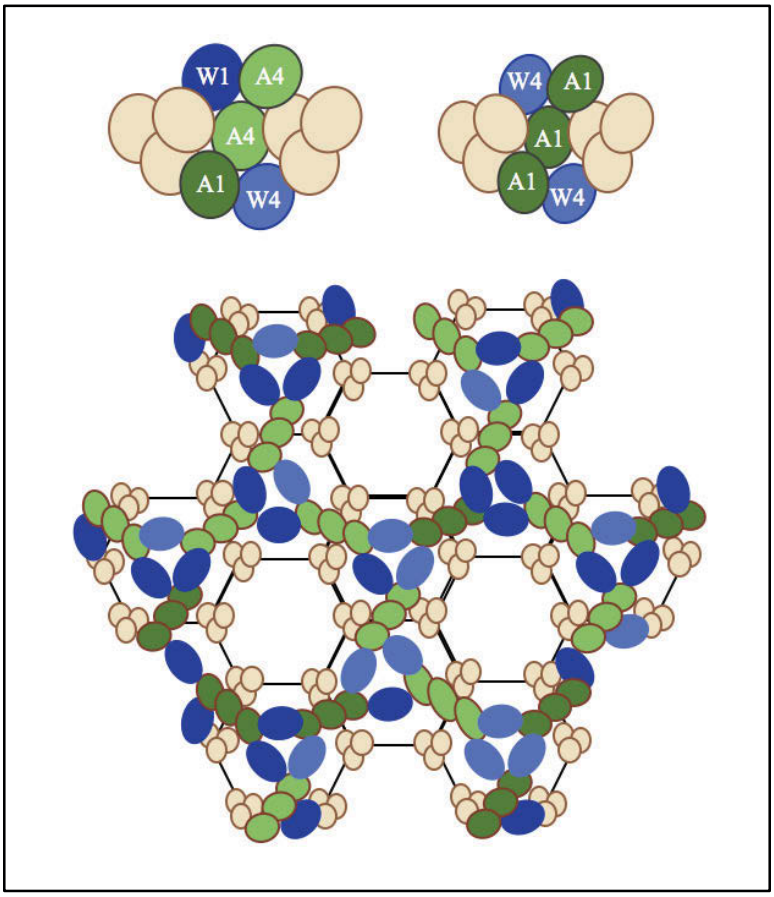

Figure 55. Model representation of mixed baseplates of paralogs (top) and an integrated extended receptor array (bottom).

The cartoon schematic represents a potential model of integration of paralogs as shown through an extended array. Top left, Tlp1 receptors (tan) form as a trimer of dimers and interacts with CheA1 (the soluble form) and CheA4, and the coupling proteins CheW1 and CheW4. Top right, Tlp1 interacting with CheA1 (the soluble form) and CheW4. Bottom, an extended array showing various interactions shown to positively occur with Tlp1 via the bacterial two-hybrid assay. Paralogs of proteins are shown as shades of the same color (CheA1, CheA4, green; CheW1, CheW4, blue). Though not shown, the potential for unmixed clusters containing only proteins from one pathway is also possible.

domain, TMX, which renders CheA1 as multifunctional. We conclude that there are two isoforms: a membrane-bound full length CheA1 and a soluble version, CheA1ΔTMX. This is an incredibly unique find amongst CheA proteins and though we begin to characterize it in these works, there is much more to investigate. CheA1 is produced as a full-length protein that it is somehow regulated by the phosphorylation of the aspartate in the REC domain. We have not yet teased apart this regulatory effect nor have we determined how the soluble isoform is produced. Few hints can be taken from *E. coli*, as no second translational start site is found in *A. brasilense*, but post-transcriptional and post-translational modifications should be considered as a potential avenue.

When considering the conclusions of the first project of the dissertation with the second project, the CheA1 story adds another layer of complexity to the chemotaxis picture in *A. brasilense*. CheA1ΔTMX is the only isoform that participates in chemotaxis behavior, and it is not very abundantly expressed in cells under the conditions we tested. It is curious that swimming speed is controlled by a pathway (Che1) which produces most of its CheA1 in an isoform which was determined not to contribute to chemotaxis. It would be interesting to compare the transcript and expression levels of the CheA1 in *A. brasilense* strains Sp7 and Sp245 and, furthermore, analyze swimming speeds of the two organisms to see if there are any drastic changes in the expression levels of the histidine kinase and whether or not those changes, if they exist, could be seen via changes in the swimming speeds. Considering these bacteria are present in the rhizosphere and must out-compete other bacteria to survive, a large difference in transient swimming speed may provide a distinct advantage. Also of interest would be exploring the potential evolutionary advantages to

having a chemotaxis protein fused to a domain which, as we determined later, functions in modulating the membrane.

The final project examines TMX, serendipitously found fused to the N-terminus of CheA1. This protein, in *E. coli* and *B. subtilis*, regulates membrane fluidity through controlling acyl chain length production. This project has only just begun and several questions remain about the overall role of TMX in the cell. We began by characterizing its role in modulating membrane properties and then linked TMX to controlling membrane fluidity. These are compelling experiments which can be expanded upon by seeing if the mutant can be complemented, or fluidized in response to temperature, if provided a plasmid with the *tmx* gene. We have not yet uncovered the mechanism of action for TMX. We have done bacterial two-hybrid assays which determined that TMX can interact with enzymes of the fatty acid biosynthesis pathway but we have no indication that this occurs *in vivo*.

Perhaps the most interesting focus of future study lies in the determination of whether or not TMX possesses enzymatic activity. The current state of the literature suggests that many members of the PAQR family possess hydrolase activity, including but not limited to the AdipoR1 and AdipoR2 receptors which were recently crystallized with a free fatty acid lodged in their core (182). Finding out the answers to this line of questioning would provide us with a more complete understanding of the remaining class of PAQR receptors which is the largely uncharacterized hemolysin-III related proteins. These proteins are the most ancient and our best chance at understanding characteristics of the last shared ancestral protein in this family. Another interesting question is whether TMX exerts its effects on *de novo* synthesis of fatty acids or by modulating the already existing

phospholipid bilayer during times where the cell is not actively growing. If it is the latter, hypothetically TMX would possess enzymatic activity and hydrolyze fatty acids in order to "recycle" them, creating a pool of free fatty acids to be fed into the lipid biosynthesis pathway and placed on different polar head groups. This would provide the cell with a different fatty acid profile which, in turn, could alter the fluidity of the membrane in the event of a temperature shift during a time where the cell is not actively growing. This would also provide an explanation to why we see very subtle changes in the fatty acid profile of the mutant as compared to the wild type even though the DPH results imply that the mutant membrane is drastically more rigid. If TMX remodels already-existing phospholipids, then the fatty acid analyses we performed would not result in drastic differences because the cells were actively growing up until the time they were collected for analysis. Perhaps re-doing the fatty acid analysis with cells that were grown in the presence of a fatty acid biosynthesis inhibitor, such as cerulenin, may lead to more conspicuous results. Cerulenin is an irreversible inhibitor of the FAB pathway (187, 188) which brings *de novo* synthesis to a halt; therefore, any changes seen would be directly linked to the "recycling" of the bilayer by TMX. We also acknowledge that these fatty acid analyses are representative of a steady-state analysis. Fatty acid biosynthesis and response of the cell to abiotic stresses likely happens very quickly, and the analyses presented here may have simply failed to detect the magnitude of what is really happening in the cell. Looking at the response to temperature of the wild type and mutant in flux, such as with a pulse-chase experiment, would be more comprehensive as it would allow for constant assessment of metabolism

and catabolism of a substrate, such as acetyl-coA, which feeds into the FAB pathway to make fatty acids.

REFERENCES

1. Sinensky M (1974) Homeoviscous adaptation--a homeostatic process that regulates the viscosity of membrane lipids in *Escherichia coli*. *Proceedings of the National Academy of Sciences of the United States of America* 71(2):522-525.

2. Silhavy TJ, Kahne D, & Walker S (2010) The bacterial cell envelope. *Cold Spring Harbor perspectives in biology* 2(5):a000414.

3. Cronan JE, Jr. & Rock CO (2008) Biosynthesis of Membrane Lipids. *EcoSal Plus* 3(1).

4. Lynen F (1969) [3] Yeast fatty acid synthase. *Methods in Enzymology*, (Academic Press), Vol 14, pp 17-33.

5. J J Volpe a & Vagelos PR (1973) Saturated fatty acid biosynthesis and its regulation. *Annual Review of Biochemistry* 42(1):21-60.

6. Roy Vagelos P, Alberts AW, & Majerus PW (1969) [5] Mechanism of saturated fatty acid biosynthesis in *Escherichia coli. Methods in Enzymology*, (Academic Press), Vol 14, pp 39-43.

7. Toomey RE & Wakil SJ (1966) Studies on the mechanism of fatty acid synthesis. XVI. Preparation and general properties of acyl-malonyl acyl carrier protein-condensing enzyme from *Escherichia coli*. *The Journal of biological chemistry* 241(5):1159-1165.

8. Schweizer E & Hofmann J (2004) Microbial Type I Fatty Acid Synthases (FAS): Major Players in a Network of Cellular FAS Systems. *Microbiology and Molecular Biology Reviews* 68(3):501-517.

9. Witkowski A, Joshi AK, & Smith S (2007) Coupling of the de novo fatty acid biosynthesis and lipoylation pathways in mammalian mitochondria. *The Journal of biological chemistry* 282(19):14178-14185.

10. Hiltunen JK*, et al.* (2009) Mitochondrial fatty acid synthesis type II: more than just fatty acids. *The Journal of biological chemistry* 284(14):9011-9015.

11. Moussaieff A*, et al.* (Glycolysis-mediated changes in acetyl-CoA and histone acetylation control the early differentiation of embryonic stem cells. *Cell Metabolism* 21(3):392-402.

12. Berg JM TJ, Stryer L. (2002) *Biochemistry* 5th edition Ed.

13. Janßen HJ & Steinbuchel A (2014) Fatty acid synthesis in *Escherichia coli* and its applications towards the production of fatty acid based biofuels. *Biotechnology for biofuels* 7(1):7.

14. Campbell JW & Cronan JE, Jr. (2001) Bacterial fatty acid biosynthesis: targets for antibacterial drug discovery. *Annu Rev Microbiol* 55:305-332.

15. Edwards P, Nelsen JS, Metz JG, & Dehesh K (1997) Cloning of the *fabF* gene in an expression vector and in vitro characterization of recombinant *fabF* and *fabB* encoded enzymes from Escherichia coli. *FEBS letters* 402(1):62-66.

16. Yoshimura M, Oshima T, & Ogasawara N (2007) Involvement of the YneS/YgiH and PlsX proteins in phospholipid biosynthesis in both *Bacillus subtilis* and *Escherichia coli*. *BMC microbiology* 7:69.

17. Lu YJ*, et al.* (2006) Acyl-phosphates initiate membrane phospholipid synthesis in Gram-positive pathogens. *Molecular cell* 23(5):765-772.

18. Coleman J (1990) Characterization of *Escherichia coli* cells deficient in 1-acyl-sn-glycerol-3- phosphate acyltransferase activity. *The Journal of biological chemistry* 265(28):17215-17221.

19. Coleman J (1992) Characterization of the *Escherichia coli* gene for 1-acyl-sn-glycerol-3-phosphate acyltransferase (*plsC*). *Molecular & general genetics : MGG* 232(2):295-303.

20. Fujita Y, Matsuoka H, & Hirooka K (2007) Regulation of fatty acid metabolism in bacteria. *Molecular microbiology* 66(4):829-839.

21. Feng Y & Cronan JE (2011) Complex binding of the FabR repressor of bacterial unsaturated fatty acid biosynthesis to its cognate promoters. *Molecular microbiology* 80(1):195-218.

22. Henry MF & Cronan JE, Jr. (1991) *Escherichia coli* transcription factor that both activates fatty acid synthesis and represses fatty acid degradation. *Journal of molecular biology* 222(4):843-849.

23. Henry MF & Cronan JE, Jr. (1992) A new mechanism of transcriptional regulation: release of an activator triggered by small molecule binding. *Cell* 70(4):671-679.

24. DiRusso CC, Heimert TL, & Metzger AK (1992) Characterization of FadR, a global transcriptional regulator of fatty acid metabolism in *Escherichia coli*.

Interaction with the fadB promoter is prevented by long chain fatty acyl coenzyme A. *The Journal of biological chemistry* 267(12):8685-8691.

25. Zhu K, Zhang YM, & Rock CO (2009) Transcriptional regulation of membrane lipid homeostasis in *Escherichia coli*. *The Journal of biological chemistry* 284(50):34880-34888.

26. Yao Z, Davis RM, Kishony R, Kahne D, & Ruiz N (2012) Regulation of cell size in response to nutrient availability by fatty acid biosynthesis in *Escherichia coli. Proceedings of the National Academy of Sciences of the United States of America* 109(38):E2561-2568.

27. Bremer H & Dennis PP (2008) Modulation of Chemical Composition and Other Parameters of the Cell at Different Exponential Growth Rates. *EcoSal Plus* 3(1).

28. Schneider DA & Gourse RL (2004) Relationship between growth rate and ATP concentration in *Escherichia coli*: a bioassay for available cellular ATP. *The Journal of biological chemistry* 279(9):8262-8268.

29. Sohlenkamp C, López-Lara IM, & Geiger O (2003) Biosynthesis of phosphatidylcholine in bacteria. *Progress in Lipid Research* 42(2):115-162.

30. Sohlenkamp C & Geiger O (2016) Bacterial membrane lipids: diversity in structures and pathways. *FEMS microbiology reviews* 40(1):133-159.

31. Los DA & Murata N (2004) Membrane fluidity and its roles in the perception of environmental signals. *Biochimica et biophysica acta* 1666(1-2):142-157.

32. Hasegawa Y, Kawada N, & Nosoh Y (1980) Change in chemical composition of membrane of *Bacillus caldotenax* after shifting the growth temperature. *Archives of microbiology* 126(2):103-108.

33. Suutari M & Laakso S (1994) Microbial fatty acids and thermal adaptation. *Critical reviews in microbiology* 20(4):285-328.

34. Denich TJ, Beaudette LA, Lee H, & Trevors JT (2003) Effect of selected environmental and physico-chemical factors on bacterial cytoplasmic membranes. *Journal of microbiological methods* 52(2):149-182.

35. Lenaz G (1987) Lipid fluidity and membrane protein dynamics. *Bioscience reports* 7(11):823-837.

36. Lande MB, Donovan JM, & Zeidel ML (1995) The relationship between membrane fluidity and permeabilities to water, solutes, ammonia, and protons. *The Journal of general physiology* 106(1):67-84.

37. Aguilar PS, Hernandez-Arriaga AM, Cybulski LE, Erazo AC, & de Mendoza D (2001) Molecular basis of thermosensing: a two-component signal transduction thermometer in *Bacillus subtilis. The EMBO journal* 20(7):1681-1691.

38. Albanesi D, Mansilla MC, & de Mendoza D (2004) The membrane fluidity sensor DesK of *Bacillus subtilis* controls the signal decay of its cognate response regulator. *Journal of bacteriology* 186(9):2655-2663.

39. Suzuki I, Los DA, Kanesaki Y, Mikami K, & Murata N (2000) The pathway for perception and transduction of low-temperature signals in *Synechocystis*. *The EMBO journal* 19(6):1327-1334.

40. Cossins AR & Macdonald AG (1989) The adaptation of biological membranes to temperature and pressure: fish from the deep and cold. *Journal of bioenergetics and biomembranes* 21(1):115-135.

41. Avery SV, Lloyd D, & Harwood JL (1995) Temperature-dependent changes in plasma-membrane lipid order and the phagocytotic activity of the amoeba *Acanthamoeba castellanii* are closely correlated. *The Biochemical journal* 312 (Pt 3):811-816.

42. Thompson GA, Jr. & Nozawa Y (1977) *Tetrahymena*: a system for studying dynamic membrane alterations within the eukaryotic cell. *Biochimica et biophysica acta* 472(1):55-92.

43. Glatz A, Vass I, Los DA, & Vígh L (1999) The *Synechocystis* model of stress: from molecular chaperones to membranes. *Plant Physiology and Biochemistry* 37(1):1-12.

44. Shivaji S & Prakash JS (2010) How do bacteria sense and respond to low temperature? *Archives of microbiology* 192(2):85-95.

45. Garwin JL, Klages AL, & Cronan JE (1980) Beta-ketoacyl-acyl carrier protein synthase II of *Escherichia coli.* Evidence for function in the thermal regulation of fatty acid synthesis. *Journal of Biological Chemistry* 255(8):3263-3265.

46. Bhakoo M & Herbert RA (1979) The effects of temperature on the fatty acid and phospholipid composition of four obligately psychrophilic *Vibrio* Spp. *Archives of microbiology* 121(2):121-127.

47. Kelkar DA & Chattopadhyay A (2007) The gramicidin ion channel: A model membrane protein. *Biochimica et Biophysica Acta (BBA) - Biomembranes* 1768(9):2011-2025.

48. Lundbaek JA, Birn P, Girshman J, Hansen AJ, & Andersen OS (1996) Membrane stiffness and channel function. *Biochemistry* 35(12):3825-3830.

49. Laloux G & Jacobs-Wagner C (2014) How do bacteria localize proteins to the cell pole? *Journal of cell science* 127(Pt 1):11-19.

50. Bonny M, Fischer-Friedrich E, Loose M, Schwille P, & Kruse K (2013) Membrane binding of MinE allows for a comprehensive description of Min-protein pattern formation. *PLoS computational biology* 9(12):e1003347.

51. Mazor S*, et al.* (2008) Mutual effects of MinD-membrane interaction: II. Domain structure of the membrane enhances MinD binding. *Biochimica et biophysica acta* 1778(11):2505-2511.

52. Mazor S*, et al.* (2008) Mutual effects of MinD-membrane interaction: I. Changes in the membrane properties induced by MinD binding. *Biochimica et biophysica acta* 1778(11):2496-2504.

53. Santos TM, Lin TY, Rajendran M, Anderson SM, & Weibel DB (2014) Polar localization of Escherichia coli chemoreceptors requires an intact Tol-Pal complex. *Molecular microbiology* 92(5):985-1004.

54. Mesibov R & Adler J (1972) Chemotaxis toward amino acids in *Escherichia coli. Journal of bacteriology* 112(1):315-326.

55. Adler J, Hazelbauer GL, & Dahl MM (1973) Chemotaxis toward sugars in *Escherichia coli. Journal of bacteriology* 115(3):824-847.

56. Adler J (1965) Chemotaxis in *Escherichia coli. Cold Spring Harb Symp Quant Biol* 30:289-292.

57. Silverman M & Simon M (1976) Operon controlling motility and chemotoxis in *E. coli. Nature* 264(5586):577-580.

58. Zhao R, Collins EJ, Bourret RB, & Silversmith RE (2002) Structure and catalytic mechanism of the *E. coli* chemotaxis phosphatase CheZ. *Nature structural biology* 9(8):570-575.

59. Segall JE, Block SM, & Berg HC (1986) Temporal comparisons in bacterial chemotaxis. *Proceedings of the National Academy of Sciences of the United States of America* 83(23):8987-8991.

60. Wadhams GH & Armitage JP (2004) Making sense of it all: bacterial chemotaxis. *Nat Rev Mol Cell Biol* 5(12):1024-1037.

61. Levit MN & Stock JB (2002) Receptor methylation controls the magnitude of stimulus-response coupling in bacterial chemotaxis. *The Journal of biological chemistry* 277(39):36760-36765.

62. Briegel A*, et al.* (2014) New Insights into Bacterial Chemoreceptor Array Structure and Assembly from Electron Cryotomography. *Biochemistry* 53(10):1575-1585.

63. Briegel A*, et al.* (2009) Universal architecture of bacterial chemoreceptor arrays. *Proceedings of the National Academy of Sciences of the United States of America* 106(40):17181-17186.

64. Briegel A*, et al.* (2012) Bacterial chemoreceptor arrays are hexagonally packed trimers of receptor dimers networked by rings of kinase and coupling proteins. *Proceedings of the National Academy of Sciences* 109(10):3766-3771.

65. Briegel A*, et al.* (2014) Structure of bacterial cytoplasmic chemoreceptor arrays and implications for chemotactic signaling. *eLife* 3:e02151.

66. Wang X, Vu A, Lee K, & Dahlquist FW (2012) CheA–Receptor Interaction Sites in Bacterial Chemotaxis. *Journal of molecular biology* 422(2):282-290.

67. Vu A, Wang X, Zhou H, & Dahlquist FW (2012) The receptor-CheW binding interface in bacterial chemotaxis. *Journal of molecular biology* 415(4):759-767.

68. Surette MG*, et al.* (1996) Dimerization Is Required for the Activity of the Protein Histidine Kinase CheA That Mediates Signal Transduction in Bacterial Chemotaxis. *Journal of Biological Chemistry* 271(2):939-945.

69. Jeon H*, et al.* (2009) Quantitative analysis of single bacterial chemotaxis using a linear concentration gradient microchannel. *Biomedical Microdevices* 11(5):1135-1143.

70. Alexander RP & Zhulin IB (2007) Evolutionary genomics reveals conserved structural determinants of signaling and adaptation in microbial chemoreceptors. *Proceedings of the National Academy of Sciences of the United States of America* 104(8):2885-2890.

71. Falke JJ & Hazelbauer GL (2001) Transmembrane signaling in bacterial chemoreceptors. *Trends in biochemical sciences* 26(4):257-265.

72. Zhulin IB (2001) The superfamily of chemotaxis transducers: from physiology to genomics and back. *Advances in microbial physiology* 45:157-198.

73. Hulko M*, et al.* (2006) The HAMP domain structure implies helix rotation in transmembrane signaling. *Cell* 126(5):929-940.

74. Aravind L & Ponting CP (1999) The cytoplasmic helical linker domain of receptor histidine kinase and methyl-accepting proteins is common to many prokaryotic signalling proteins. *FEMS microbiology letters* 176(1):111-116.

75. Herrera Seitz MK, Frank V, Massazza DA, Vaknin A, & Studdert CA (2014) Bacterial chemoreceptors of different length classes signal independently. *Molecular microbiology* 93(4):814-822.

76. Bilwes AM, Alex LA, Crane BR, & Simon MI (1999) Structure of CheA, a Signal-Transducing Histidine Kinase. *Cell* 96(1):131-141.

77. Sun H, Zusman DR, & Shi W (2000) Type IV pilus of *Myxococcus xanthus* is a motility apparatus controlled by the *frz* chemosensory system. *Current biology : CB* 10(18):1143-1146.

78. Guvener ZT & Harwood CS (2007) Subcellular location characteristics of the *Pseudomonas aeruginosa* GGDEF protein, WspR, indicate that it produces cyclic-di-GMP in response to growth on surfaces. *Molecular microbiology* 66(6):1459-1473.

79. Kirby JR & Zusman DR (2003) Chemosensory regulation of developmental gene expression in *Myxococcus xanthus*. *Proceedings of the National Academy of Sciences of the United States of America* 100(4):2008-2013.

80. Bible AN*, et al.* (2015) Metabolic adaptations of *Azospirillum brasilense* to oxygen stress by cell-to-cell clumping and flocculation. *Appl Environ Microbiol* 81(24):8346-8357.

81. Berleman JE & Bauer CE (2005) A che-like signal transduction cascade involved in controlling flagella biosynthesis in *Rhodospirillum centenum*. *Molecular microbiology* 55(5):1390-1402.

82. Berleman JE & Bauer CE (2005) Involvement of a Che-like signal transduction cascade in regulating cyst cell development in *Rhodospirillum centenum.* *Molecular microbiology* 56(6):1457-1466.

83. Mukherjee T, Kumar D, Burriss N, Xie Z, & Alexandre G (2016) *Azospirillum brasilense* chemotaxis depends on two signaling pathways regulating distinct motility parameters. *Journal of bacteriology*.

84. Hazelbauer GL, Falke JJ, & Parkinson JS (2008) Bacterial chemoreceptors: high-performance signaling in networked arrays. *Trends in biochemical sciences* 33(1):9-19.

85. Bray D, Levin MD, & Morton-Firth CJ (1998) Receptor clustering as a cellular mechanism to control sensitivity. *Nature* 393(6680):85-88.

86. Sourjik V & Armitage JP (2010) Spatial organization in bacterial chemotaxis. *The EMBO journal* 29(16):2724-2733.

87. Springer MS, Goy MF, & Adler J (1977) Sensory transduction in *Escherichia coli*: two complementary pathways of information processing that involve methylated proteins. *Proceedings of the National Academy of Sciences of the United States of America* 74(8):3312-3316.

88. Manson MD, Blank V, Brade G, & Higgins CF (1986) Peptide chemotaxis in *E. coli* involves the Tap signal transducer and the dipeptide permease. *Nature* 321(6067):253-256.

89. Liu X & Parales RE (2008) Chemotaxis of *Escherichia coli* to pyrimidines: a new role for the signal transducer tap. *Journal of bacteriology* 190(3):972-979.

90. Hazelbauer GL (1975) Maltose chemoreceptor of *Escherichia coli*. *Journal of bacteriology* 122(1):206-214.

91. Hegde M*, et al.* (2011) Chemotaxis to the quorum-sensing signal AI-2 requires the Tsr chemoreceptor and the periplasmic LsrB AI-2-binding protein. *Journal of bacteriology* 193(3):768-773.

92. Zhang P, Khursigara CM, Hartnell LM, & Subramaniam S (2007) Direct visualization of *Escherichia coli* chemotaxis receptor arrays using cryo-electron microscopy. *Proceedings of the National Academy of Sciences of the United States of America* 104(10):3777-3781.

93. Liu J*, et al.* (2012) Molecular architecture of chemoreceptor arrays revealed by cryoelectron tomography of *Escherichia coli* minicells. *Proceedings of the National Academy of Sciences* 109(23):E1481–E1488.

94. Wuichet K, Alexander RP, & Zhulin IB (2007) Comparative genomic and protein sequence analyses of a complex system controlling bacterial chemotaxis. *Methods Enzymol* 422:1-31.

95. Wisniewski-Dyé F*, et al.* (2011) *Azospirillum* Genomes Reveal Transition of Bacteria from Aquatic to Terrestrial Environments. *PLoS Genet* 7(12):e1002430.

96. Bible A, Russell MH, & Alexandre G (2012) The *Azospirillum brasilense* Che1 chemotaxis pathway controls swimming velocity, which affects transient cell-to-cell clumping. *Journal of bacteriology* 194(13):3343-3355.

97. Bible AN, Stephens BB, Ortega DR, Xie Z, & Alexandre G (2008) Function of a chemotaxis-like signal transduction pathway in modulating motility, cell clumping, and cell length in the alphaproteobacterium *Azospirillum brasilense*. *Journal of bacteriology* 190(19):6365-6375.

98. Stephens BB, Loar SN, & Alexandre G (2006) Role of CheB and CheR in the complex chemotactic and aerotactic pathway of *Azospirillum brasilense. Journal of bacteriology* 188(13):4759-4768.

99. Russell MH*, et al.* (2013) Integration of the second messenger c-di-GMP into the chemotactic signaling pathway. *MBio* 4(2):e00001-00013.

100. Karimova G, Pidoux J, Ullmann A, & Ladant D (1998) A bacterial two-hybrid system based on a reconstituted signal transduction pathway. *Proceedings of the National Academy of Sciences of the United States of America* 95(10):5752-5756.

101. Simon R, Priefer U, & Puhler A (1983) A Broad Host Range Mobilization System for In Vivo Genetic Engineering: Transposon Mutagenesis in Gram Negative Bacteria. *Nat Biotech* 1(9):784-791.

102. Amat F*, et al.* (2008) Markov random field based automatic image alignment for electron tomography. *Journal of structural biology* 161(3):260-275.

103. Ding HJ, Oikonomou CM, & Jensen GJ (2015) The Caltech Tomography Database and Automatic Processing Pipeline. *Journal of structural biology* 192(2):279-286.

104. Kremer JR, Mastronarde DN, & McIntosh JR (1996) Computer visualization of three-dimensional image data using IMOD. *Journal of structural biology* 116(1):71-76.

105. Hallez R, Letesson JJ, Vandenhaute J, & De Bolle X (2007) Gateway-based destination vectors for functional analyses of bacterial ORFeomes: application to the Min system in *Brucella abortus. Appl Environ Microbiol* 73(4):1375-1379.

106. Bible A (2012) Characterization of the Function of the *Azospirillum brasilense* Che1 Chemotaxis Pathway in the Regulation of Chemotaxis, Cell Length and Clumping. PhD (University of Tennessee, Knoxville).

107. Xie Z, Ulrich LE, Zhulin IB, & Alexandre G (2010) PAS domain containing chemoreceptor couples dynamic changes in metabolism with chemotaxis. *Proceedings of the National Academy of Sciences of the United States of America* 107(5):2235-2240.

108. Hauwaerts D, Alexandre G, Das SK, Vanderleyden J, & Zhulin IB (2002) A major chemotaxis gene cluster in *Azospirillum brasilense* and relationships between chemotaxis operons in α-proteobacteria. *FEMS microbiology letters* 208(1):61-67.

109. Bradford MM (1976) A rapid and sensitive method for the quantitation of microgram quantities of protein utilizing the principle of protein-dye binding. *Analytical Biochemistry* 72(1–2):248-254.

110. Ramsay JP*, et al.* (2013) A widely conserved molecular switch controls quorum sensing and symbiosis island transfer in Mesorhizobium loti through expression of a novel antiactivator. *Molecular microbiology* 87(1):1-13.

111. Martin AC, Wadhams GH, & Armitage JP (2001) The roles of the multiple CheW and CheA homologues in chemotaxis and in chemoreceptor localization in *Rhodobacter sphaeroides. Molecular microbiology* 40(6):1261-1272.

112. Gullett JM, Bible A, & Alexandre G (2017) Distinct Domains of CheA Confer Unique Functions in Chemotaxis and Cell Length in *Azospirillum brasilense* Sp7. *Journal of bacteriology* 199(13).

113. Ponting CP, Schultz J, Milpetz F, & Bork P (1999) SMART: identification and annotation of domains from signalling and extracellular protein sequences. *Nucleic acids research* 27(1):229-232.

114. Wadhams GH, Warren AV, Martin AC, & Armitage JP (2003) Targeting of two signal transduction pathways to different regions of the bacterial cell. *Molecular microbiology* 50(3):763-770.

115. Wadhams GH, Martin AC, Warren AV, & Armitage JP (2005) Requirements for chemotaxis protein localization in *Rhodobacter sphaeroides*. *Molecular microbiology* 58(3):895-902.

116. Wadhams GH*, et al.* (2002) TlpC, a novel chemotaxis protein in *Rhodobacter sphaeroides*, localizes to a discrete region in the cytoplasm. *Molecular microbiology* 46(5):1211-1221.

117. Porter SL & Armitage JP (2002) Phosphotransfer in *Rhodobacter sphaeroides* chemotaxis. *Journal of molecular biology* 324(1):35-45.

118. Battesti A & Bouveret E (2012) The bacterial two-hybrid system based on adenylate cyclase reconstitution in *Escherichia coli. Methods (San Diego, Calif.)* 58(4):325-334.

119. Li M & Hazelbauer GL (2011) Core unit of chemotaxis signaling complexes. *Proceedings of the National Academy of Sciences of the United States of America* 108(23):9390-9395.

120. Levit MN, Grebe TW, & Stock JB (2002) Organization of the receptor-kinase signaling array that regulates *Escherichia coli* chemotaxis. *The Journal of biological chemistry* 277(39):36748-36754.

121. Erbse AH & Falke JJ (2009) The core signaling proteins of bacterial chemotaxis assemble to form an ultrastable complex. *Biochemistry* 48(29):6975-6987.

122. Cannistraro VJ, Glekas GD, Rao CV, & Ordal GW (2011) Cellular stoichiometry of the chemotaxis proteins in *Bacillus subtilis*. *Journal of bacteriology* 193(13):3220-3227.

123. Wuichet K & Zhulin IB (2010) Origins and diversification of a complex signal transduction system in prokaryotes. *Sci Signal* 3(128):ra50.

124. Miller LD, Yost CK, Hynes MF, & Alexandre G (2007) The major chemotaxis gene cluster of *Rhizobium leguminosarum bv. viciae* is essential for competitive nodulation. *Molecular microbiology* 63(2):348-362.

125. Xu Q, Black WP, Cadieux CL, & Yang Z (2008) Independence and interdependence of Dif and Frz chemosensory pathways in *Myxococcus xanthus* chemotaxis. *Molecular microbiology* 69(3):714-723.

126. Black WP, Schubot FD, Li Z, & Yang Z (2010) Phosphorylation and dephosphorylation among Dif chemosensory proteins essential for

exopolysaccharide regulation in *Myxococcus xanthus*. *Journal of bacteriology* 192(17):4267-4274.

127. Campodonico EM & Zusman DR (2010) Developments in defining dif. *Journal of bacteriology* 192(17):4264-4266.

128. Howell A*, et al.* (2003) Genes controlled by the essential YycG/YycF two-component system of *Bacillus subtilis* revealed through a novel hybrid regulator approach. *Molecular microbiology* 49(6):1639-1655.

129. Laub MT & Goulian M (2007) Specificity in Two-Component Signal Transduction Pathways. *Annual Review of Genetics* 41(1):121-145.

130. Hoch JA & Varughese KI (2001) Keeping signals straight in phosphorelay signal transduction. *Journal of bacteriology* 183(17):4941-4949.

131. Kojadinovic M, Armitage JP, Tindall MJ, & Wadhams GH (2013) Response kinetics in the complex chemotaxis signalling pathway of *Rhodobacter sphaeroides*. *J R Soc Interface* 10(81):20121001.

132. Mukhopadhyay D & Varughese KI (2005) A computational analysis on the specificity of interactions between histidine kinases and response regulators. *Journal of biomolecular structure & dynamics* 22(5):555-562.

133. Rowland MA & Deeds EJ (2014) Crosstalk and the evolution of specificity in two-component signaling. *Proceedings of the National Academy of Sciences of the United States of America* 111(15):5550-5555.

134. Porter SL & Armitage JP (2004) Chemotaxis in *Rhodobacter sphaeroides* requires an atypical histidine protein kinase. *The Journal of biological chemistry* 279(52):54573-54580.

135. Alexander RP, Lowenthal AC, Harshey RM, & Ottemann KM (2010) CheV: CheW-like coupling proteins at the core of the chemotaxis signaling network. *Trends in microbiology* 18(11):494-503.

136. Ortega DR & Zhulin IB (2016) Evolutionary Genomics Suggests That CheV is an additional adaptor for accommodating specific chemoreceptors within the chemotaxis signaling complex. *PLoS computational biology* 12(2):e1004723.

137. Zhao J & Parkinson JS (2006) Mutational analysis of the chemoreceptor-Coupling domain of the *Escherichia coli* chemotaxis signaling kinase CheA. *Journal of bacteriology* 188(9):3299-3307.

138. Krell T*, et al.* (2011) Diversity at its best: bacterial taxis. *Environmental microbiology* 13(5):1115-1124.

139. Alexandre G (2010) Coupling metabolism and chemotaxis-dependent behaviours by energy taxis receptors. *Microbiology* 156(Pt 8):2283-2293.

140. Qi X*, et al.* (2013) Swimming motility plays a key role in the stochastic dynamics of cell clumping. *Physical biology* 10(2):026005.

141. Baldani VLD, Baldani JI, & Döbereiner J (1983) Effects of *Azospirillum* inoculation on root infection and nitrogen incorporation in wheat. *Canadian Journal of Microbiology* 29(8):924-929.

142. Vanstockem M, Michiels K, Vanderleyden J, & Van Gool AP (1987) Transposon mutagenesis of *Azospirillum brasilense* and *Azospirillum lipoferum*: Physical Analysis of Tn5 and Tn5-Mob Insertion Mutants. *Applied and Environmental Microbiology* 53(2):410-415.

143. Tomic-Canic M, Bernerd F, & Blumenberg M (1996) A simple method to introduce internal deletions or mutations into any position of a target DNA sequence. *In Vitro Mutagenesis Protocols,* Methods In Molecular Medicine™, ed Trower M (Humana Press), Vol 57, pp 249-257.

144. Kovach ME*, et al.* (1995) Four new derivatives of the broad-host-range cloning vector pBBR1MCS, carrying different antibiotic-resistance cassettes. *Gene* 166(1):175-176.

145. Katzen F, Becker A, Ielmini MV, Oddo CG, & Ielpi L (1999) New mobilizable vectors suitable for gene replacement in gram-negative bacteria and their use in mapping of the 3′ end of the *Xanthomonas campestris pv. campestris gum* operon. *Applied and Environmental Microbiology* 65(1):278-282.

146. Kentner D & Sourjik V (2006) Spatial organization of the bacterial chemotaxis system. *Current Opinion in Microbiology* 9(6):619-624.

147. Greer-Phillips SE, Stephens BB, & Alexandre G (2004) An energy taxis transducer promotes root colonization by *Azospirillum brasilense*. *Journal of bacteriology* 186(19):6595-6604.

148. Baida GE & Kuzmin NP (1995) Cloning and primary structure of a new hemolysin gene from *Bacillus cereus. Biochimica et biophysica acta* 1264(2):151-154.

149. Finn RD*, et al.* (2014) Pfam: the protein families database. *Nucleic acids research* 42(D1):D222-D230.

150. Chen Y-C, Chang M-C, Chuang Y-C, & Jeang C-L (2004) Characterization and virulence of hemolysin III from *Vibrio vulnificus*. *Current Microbiology* 49(3):175-179.

151. Tang YT*, et al.* (2005) PAQR proteins: a novel membrane receptor family defined by an ancient 7-transmembrane pass motif. *Journal of Molecular Evolution* 61(3):372-380.

152. Inclan YF, Laurent S, & Zusman DR (2008) The receiver domain of FrzE, a CheA-CheY fusion protein, regulates the CheA histidine kinase activity and downstream signalling to the A- and S-motility systems of *Myxococcus xanthus*. *Molecular microbiology* 68(5):1328-1339.

153. He K, Marden JN, Quardokus EM, & Bauer CE (2013) Phosphate flow between hybrid histidine kinases CheA(3) and CheS(3) controls *Rhodospirillum centenum* cyst formation. *PLoS Genet* 9(12):e1004002.

154. Kofoid EC & Parkinson JS (1991) Tandem translation starts in the *cheA* locus of *Escherichia coli*. *Journal of bacteriology* 173(6):2116-2119.

155. Smith RA & Parkinson JS (1980) Overlapping genes at the *cheA* locus of *Escherichia coli. Proceedings of the National Academy of Sciences of the United States of America* 77(9):5370-5374.

156. Kaneko T*, et al.* (2010) Complete genomic structure of the cultivated rice endophyte *Azospirillum* sp. B510. *DNA research : an international journal for rapid publication of reports on genes and genomes* 17(1):37-50.

157. Rivera D*, et al.* (2014) Complete genome sequence of the model rhizosphere strain *Azospirillum brasilense* Az39, successfully applied in agriculture. *Genome announcements* 2(4).

158. Kwak Y & Shin JH (2016) First *Azospirillum* genome from aquatic environments: Whole-genome sequence of *Azospirillum thiophilum* BV-S(T), a novel diazotroph harboring a capacity of sulfur-chemolithotrophy from a sulfide spring. *Marine genomics* 25:21-24.

159. Wisniewski-Dye F*, et al.* (2012) Genome sequence of *Azospirillum brasilense* CBG497 and comparative analyses of *Azospirillum* core and accessory genomes provide insight into niche adaptation. *Genes* 3(4):576-602.

160. Martin-Didonet CC*, et al.* (2000) Genome structure of the genus *Azospirillum*. *Journal of bacteriology* 182(14):4113-4116.

161. Pasek S, Risler JL, & Brezellec P (2006) Gene fusion/fission is a major contributor to evolution of multi-domain bacterial proteins. *Bioinformatics (Oxford, England)* 22(12):1418-1423.

162. Marcotte EM*, et al.* (1999) Detecting protein function and protein-protein interactions from genome sequences. *Science (New York, N.Y.)* 285(5428):751-753.

163. Vitrac H, Bogdanov M, Heacock P, & Dowhan W (2011) Lipids and topological rules of membrane protein assembly: balance between long- and short-range lipid-protein interactions. *Journal of Biological Chemistry*.

164. Vigh L, Maresca B, & Harwood JL (1998) Does the membrane's physical state control the expression of heat shock and other genes? *Trends in biochemical sciences* 23(10):369-374.

165. Mazzotta AS & Montville TJ (1997) Nisin induces changes in membrane fatty acid composition of *Listeria monocytogenes* nisin-resistant strains at 10°C and 30°C. *Journal of Applied Microbiology* 82(1):32-38.

166. Mishra NN*, et al.* (2011) Carotenoid-related alteration of cell membrane fluidity impacts *Staphylococcus aureus* susceptibility to host defense peptides. *Antimicrobial Agents and Chemotherapy* 55(2):526-531.

167. Bayer AS*, et al.* (2000) In vitro resistance of *Staphylococcus aureus* to thrombin-induced platelet microbicidal protein is associated with alterations in cytoplasmic membrane fluidity. *Infection and Immunity* 68(6):3548-3553.

168. Kumariya R, Sood SK, Rajput YS, Saini N, & Garsa AK (2015) Increased membrane surface positive charge and altered membrane fluidity leads to cationic antimicrobial peptide resistance in *Enterococcus faecalis. Biochimica et biophysica acta* 1848(6):1367-1375.

169. Zhang YM & Rock CO (2008) Membrane lipid homeostasis in bacteria. *Nature reviews. Microbiology* 6(3):222-233.

170. Blattner FR*, et al.* (1997) The complete genome sequence of *Escherichia coli* K-12. *Science (New York, N.Y.)* 277(5331):1453-1462.

171. Wang A & Ash GJ (2015) Whole genome phylogeny of *Bacillus* by feature frequency profiles (FFP). 5:13644.

172. Pace NR, Olsen GJ, & Woese CR (1986) Ribosomal RNA phylogeny and the primary lines of evolutionary descent. *Cell* 45(3):325-326.

173. Betts MJ & Russell RB (2003) Amino acid properties and consequences of substitutions. *Bioinformatics for Geneticists*, (John Wiley & Sons, Ltd), pp 289-316.

174. Muñoz-Rojas J*, et al.* (2006) Involvement of cyclopropane fatty acids in the response of *Pseudomonas putida* KT2440 to freeze-drying. *Applied and Environmental Microbiology* 72(1):472-477.

175. Hara H, Hyono A, Kuriyama S, Yano I, & Masui M (1980) ESR studies on the membrane properties of a moderately halophilic bacterium. II. Effect of extreme growth conditions on liposome properties. *Journal of biochemistry* 88(5):1275-1282.

176. Annous BA, Kozempel MF, & Kurantz MJ (1999) Changes in membrane fatty acid composition of *Pediococcus sp.* strain NRRL B-2354 in response to growth conditions and its effect on thermal resistance. *Appl Environ Microbiol* 65(7):2857-2862.

177. Guillot A, Obis D, & Mistou MY (2000) Fatty acid membrane composition and activation of glycine-betaine transport in *Lactococcus lactis* subjected to osmotic stress. *International journal of food microbiology* 55(1-3):47-51.

178. Asakura H*, et al.* (2012) Membrane topology of *Salmonella* invasion protein SipB confers osmotolerance. *Biochemical and biophysical research communications* 426(4):654-658.

179. Meyer C, Schmid R, Scriba PC, & Wehling M (1996) Purification and partial sequencing of high-affinity progesterone-binding site(s) from porcine liver membranes. *European journal of biochemistry* 239(3):726-731.

180. Thomas P, Zhu Y, & Pace M (2002) Progestin membrane receptors involved in the meiotic maturation of teleost oocytes: a review with some new findings. *Steroids* 67(6):511-517.

181. Karteris E*, et al.* (2006) Progesterone signaling in human myometrium through two novel membrane G protein-coupled receptors: potential role in functional progesterone withdrawal at term. *Molecular endocrinology (Baltimore, Md.)* 20(7):1519-1534.

182. Vasiliauskaite-Brooks I*, et al.* (2017) Structural insights into adiponectin receptors suggest ceramidase activity. *Nature* 544(7648):120-123.

183. Pei J, Millay DP, Olson EN, & Grishin NV (2011) CREST - a large and diverse superfamily of putative transmembrane hydrolases. *Biology Direct* 6:37-37.

184. Nosé S (1984) A molecular dynamics method for simulations in the canonical ensemble. *Molecular Physics* 52(2):255-268.

185. Shumilova E*, et al.* (2016) Changes in cell surface properties and biofilm formation efficiency in *Azospirillum brasilense* Sp245 mutants in the putative genes of lipid metabolism *mmsB1* and *fabG1*. *Mikrobiologiia* 85(2):162-170.

186. Lewis K (2001) Riddle of biofilm resistance. *Antimicrob Agents Chemother* 45(4):999-1007.

187. Omura S (1976) The antibiotic cerulenin, a novel tool for biochemistry as an inhibitor of fatty acid synthesis. *Bacteriological Reviews* 40(3):681-697.

188. Matsumae A, Nomura S, & Hata T (1964) Studies on cerulenin. IV. Biological characteistics of cerulenin. *The Journal of antibiotics* 17:1-7.

VITA

Jessica Marie Gullett was born on August 6, 1985, in the small town of Canadian, Texas. Through K-12, Jessica always considered herself more of an English student and won several awards for her literary prowess. It was not until her junior year at the University of Texas at Tyler that Jessica began to truly appreciate the beauty of biology. During her undergraduate studies, her biology focus was mainly on ecology, a major which involved a hefty amount of field work in addition to classwork. This experience taught her that biology was more than just words in a book or concepts to memorize for a test; it was real. She began doing undergraduate research with Dr. Neil Ford which proved to be an experience that changed the course of her life. She had the opportunity to move to Austin, Texas, and do a summer REU at The University of Texas, where she designed a testable research project and carried out the research under the supervision of a PhD candidate, Beth Dawson. It was at this time that Jessica realized that being a PhD provided the challenge she was looking for; a way to answer the questions she was asking. From here, she applied to graduate school at The University of Tennessee and had the opportunity to move away from ecology and into biochemistry. She joined the lab of Dr. Gladys Alexandre and has focused on signal transduction pathways in bacteria during her tenure as a graduate student. She has presented her work at several conferences including Bacterial Locomotion and Signal Transduction (BLAST) and the Gordon Research Seminar and has been the recipient of several awards including the Faculty Senate Research Council Summer Graduate Research Assistantship and the UTK Biochemistry Alumni Graduate Assistant Award.